NASA Contractor Report

CR-

AD

Illinois Institute of Technology, Chicago, Illinois 60616

EXPERIMENTS ON IDENTIFICATION AND CONTROL OF DISTURBANCES IN CONTRACTING STREAMS

by

A. H. Lee, H. M. Nagib, J. Tan-atichat and D. M. Wittwer

IIT Fluids & Heat Transfer Report R82-3

December, 1982

Supported under NASA Grant NSG-3220

TABLE OF CONTENTS

LIST OF TABLES

LIST OF FIGURES

LIST OF SYMBOLS

Symbol	Definition
A	On-center isolated disturbances
A'	Off-center isolated disturbances
1A,1A'	Cylindrical wake disturbance on- and off-center, respectively
2A,2A'	Spherical wake disturbance on- and off-center, respectively
3A	Longitudinal vortex disturbance
b	Half width of isolated disturbance
Bh	Small bellmouth-type fan intake with sharp edge
Bm	Small bellmouth-type fan intake with smooth edge
C	Contraction area ratio
Co	Large bellmouth-type fan intake assembled with the fifth order contraction FO4
C1, .., C6	Cylinders of various sizes, see Figure 7
d	Diameter of cylinder
D	Inside diameter of test section; inlet diameter of contraction MC4
Ep	Extended setup of fan intake mounted with porous backing
Es	Extended setup of fan intake mounted with solid backing
FO4	Fifth-order contraction, C=4, L/D=1
Fo	Flight-type fan intake
G2	Turbulence-generating grid

Symbol	Definition
H1, H4, H8	Controlled high disturbance conditions, see Figure 12
J1, J2, J3	Honeycomb positions, see Figures 2 and 12
K1, K2	Honeycomb positions, see Figure 12
ℓ	Length of various cylinders
L	Contraction length
L1	Controlled low disturbance condition
L_r	Radial integral scale of turbulence
MC4	Matched-cubic contraction C=4, L/D=1
N1	Hemispherical NASA honeycomb inflow control device, ICD#3
O1	No flow manipulator case
P1, P2	Honeycomb positions, see Figure 12
Q1, Q2	Honeycomb positions, see Figure 12
r	Distance from axis of symmetry
R(0)	Radius of the contraction at inlet
R(x)	Radius of the contraction at x
Sp	Flush setup of fan intake mounted with porous backing
Ss	Flush setup of fan intake mounted on impermeable backing
t, t', t"	Time
U	Streamwise velocity
$\overline{U}$	Streamwise mean velocity
u'	RMS of velocity fluctations in the streamwise direction
V	Radial velocity
$\overline{V}$	Radial mean velocity

Symbol	Definition
v'	RMS of velocity fluctations in the radial direction
Vg	Surface vorticity condition: ground plate generated
Vp	Surface vorticity condition: side panels generated
Vr	Surface vorticity condition: rear panel generated
W1, W2 ...	Positions of cylinder #5 oriented vertically upstream of fan intake
$\overline{W1}$, $\overline{W2}$ ...	Positions of cylinder #5 oriented horizontally upstream of fan intake
$\hat{W1}$, $\hat{W2}$ ...	Positions of cylinder #5 oriented obliquely upstream of fan intake
x	Direction parallel to axis of symmetry of test section and contraction with origin at inlet of contraction, positive downstream; or origin at ducted-fan intake, positive downstream
y	Vertical axis with origin on axis of symmetry, positive upward
z	Horizontal direction in a right-handed cartesian coordinate system with origin on the axis of symmetry
α	Pivot angle of oblique cylinder, see Figure 8
β	Half angle setting between airfoils, see Figure 27
ζ	Horizontal smoke-wire location
ξ	Vertical smoke-wire location, see Figure 14
σ	Grid solidity = closed area/total area

Subscript	Definition
e	Value at exit of contraction FO4
i	Value at inlet of contraction FO4

ABSTRACT

Persistent disturbances leading to blade-passing frequency noise in ground testing of jet engines for documentation of fan noise, and their control by passive flow manipulators, have been the subject of research in industry and government laboratories for many years. The goal of the present research is to identify the sources of these disturbances and the mechanisms for their development, as well as to establish effective means of controlling them. Vorticity from all surfaces and isolated objects in the vicinity of the fan intake, including the outside surfaces of the fan housing, have been identified as the major sources for these disturbances. The previously proposed mechanism based on "atmospheric turbulence" is refuted.

Flow visualization and hot-wire techniques are used in three different facilities to document the evolution of various types of disturbances, including the details of the mean flow and turbulence characteristics. The results suggest that special attention must be devoted to the design of the inlet and that geometric modeling may not lead to adequate simulation of the in-flight characteristics. While honeycomb-type flow manipulators appear to be effective in reducing some of the disturbances, higher pressure drop devices that generate adequate turbulence, for mixing of isolated

nonuniformities, may be necessary to suppress the remaining disturbances. The results are also applicable to the design of inlets of open-return wind tunnels and similar flow facilities.

CHAPTER I

INTRODUCTION

Background

In the past decade, the growth of the environmental movement has stimulated large research programs aimed at noise reduction. An industrial area in which the noise problem is particularly acute is the airplane industry. Both private manufacturers and governmental agencies have concentrated their efforts to reduce jet-engine noise. Such programs rely heavily on the frequent testing of jet engines. Two types of noise measurements have been used in the past. The first one consists of performing in-flight measurements, i.e., fly-over tests. The second approach is the static ground test. Difficulties encountered during in-flight tests and the high costs associated with them tend to favor ground testing. However, significant discrepancies in the noise levels between the two methods have been consistently reported (see Feiler and Groeneweg, 1977 and Chestnut. 1982).

The major difference resides in the noise spectra, with additional peaks appearing during static testing at the so-called blade-passing frequency. The source of such discrepancies has been traced to differences in the environment in which the measurements are performed. Many sources have been suggested for the disturbances leading to these discrepancies. The only item of general

agreement is that the noise generation mechanism of the blade-passing frequency is based on the presence, randomly in space and time, of very long concentrated vortical disturbances. The source of these disturbances remained a subject of controversy although several mechanisms had been proposed, such as atmospheric turbulence and the so-called ground vortex. Of these, atmospheric turbulence seemed to be the one that received most of the attention. Hence, the design of inflow control devices was generally undertaken in an attempt to reduce or eliminate undesirable turbulence rather than other "mean-flow" associated disturbances. However, numerous studies were encouraged by private industry and government laboratories (e.g., see Gedge, 1980, Atvars, 1980 and Peracchio et al., 1981), and the presence of various types of disturbances including boundary layers in ground tests has been suspected as a contributing factor to the higher noise levels.

Rogers et al. (1980) suggest that the suction of boundary layers on the inner wall of the fan duct, in addition to inflow control devices, seemed to reduce the radiated noise appreciably. Appropriate scaling of fan models in wind tunnels was also achieved successfully by Dietrich et al. (1977) and Shaw et al. (1977) among others. Kantola and Warren (1979) and numerous researchers investigated various types of inlet turbulence control techniques. Ganz (1980) indicates

that fan noise due to atmospheric turbulence is less in a ground test than in flight tests. He concluded that the control of atmospheric turbulence in the vicinity of the static test stand was not required. In general most of these attempts did not lead to a satisfactory or consistent solution. For a more complete review of the state of this subject, the reader is referred to the proceedings of a recent conference sponsored by NASA (Chestnut, 1982).

Objectives

Based on the results described above, it became clear that other sources of disturbances had to be identified. The control or suppression of these disturbances can only be achieved if their origin is clearly recognized and their behavior well characterized. In the meantime, at IIT we have always suspected tnat the role of "atmospheric turbulence" as originally proposed by Hanson, (1977) is not significant. In fact the long slender vortical disturbances that lead to the blade-passing frequency seemed to us as highly unlikely to result from the atmospheric boundary layer turbulence. The objectives of this work then emerged and evolved in two phases of experimentation:

- The first phase consists of identifying the disturbances. The knowledge of their nature would allow us to design a "clean" environment, in which controlled

disturbances can then be selectively introduced and parametric tests of their control conducted. By concentrating on one type of disturbance at a time, it becomes possible to describe its behavior and obtain their characteristics. In spite of the elimination of sources of disturbances other than the ones of interest, the flow field remains rather complex. This aspect is particularly enhanced by the unsteadiness and the three-dimensionality of some of these disturbances. The number of parameters, ranging from flow conditions to inlet geometry, is also a contributing factor. Hence, it was felt that conventional point measurement techniques would not permit accurate or complete description of the phenomena under investigation and at the same time cover the range of cases relevant to such a study. Therefore, global flow visualization was used to reach a significant part of the conclusions. Flow visualization allows one to quickly develop a qualitative understanding of the phenomena, hence becoming a valuable tool in diagnosing the various flow conditions. In the first phase of this investigation, the various disturbed and undisturbed flow conditions are thoroughly documented.

Careful review of the literature cited before reveals that the inlets being used in static ground tests might not be optimal for this type of testing. In fact, these flight-type inlets are designed to operate in totally different conditions, i.e., a different flowfield.

Hence, several types of inlet geometries are investigated here. Finally, various types of flow manipulators, including an actual NASA inflow control device were tested. From this phase of the study we concluded that vorticity generated at all surrounding surfaces (including the outside of the fan housing) and isolated disturbances such as wakes, that are ingested into the inlet, are the major contributors to the development of the disturbances. To quantitatively document the latter of these mechanisms the experiments of the second phase were designed and carried out.

- The second phase deals with the behavior of isolated disturbances through a contraction. Isolated disturbances (such as wakes, etc.) are always present in the vicinity of ground test facilities. It is therefore essential to analyze their behavior as they are convected by the mean flow through the inlet. It would be interesting to determine whether the infinite contraction imposed on the flow suppresses or enhances the various types of disturbances. Very little data are available in the literature on that topic. It was felt that the study of isolated disturbances through a contraction would provide valuable information to predict their behavior in an actual test configuration. It is indeed easier to follow and characterize an isolated disturbance in a confined stream undergoing a finite contraction. The results obtained from such a study should help in

predicting, at least qualitatively, the role of isolated disturbances in the flow of a real inlet. This phase of the study was conducted using standard hot-wire anemometry, rendered possible by the nonrandom position and occurrence of these artificially introduced disturbances.

The authors would like to express special thanks to Edward Nieman for his expert craftsmanship in building the facility. The authors are also grateful to Alain Marion for his help with various aspects of the instrumentation, and to all others whose contributions rendered this work possible, in particular Steve Bortz and Yann Guezennec. A special word of appreciation goes to Thelma Grymes for her careful typing of the manuscript.

The support of this research by NASA Grant NSG-3220 administered by the Lewis Research Center and monitored by John Groeneweg is also acknowledged.

CHAPTER II

FACILITIES AND TECHNIQUES FOR FLOW VISUALIZATION EXPERIMENTS

The facilities used for the flow visualization experiments will be described in this chapter. These facilities consist of a ducted fan drawing air from a low-disturbance environment through various types of inlets. The description of the low-disturbance chambers, as well as the various inlet geometries are given in the following paragraphs. Means of introducing controlled disturbances, as well as ways of suppressing them, are discussed next. Finally, the visualization techniques are introduced.

Inlet Characteristics

The characteristics of the four inlets used in this study are briefly mentioned here. The reader is referred to Appendix A for a complete description of their design and construction.

In order to model the real ground test conditions, a scaled-down version of a JTD-15 jet-engine inlet was first tested. This inlet, denoted Fo, is geometrically similar to the one used in actual testing by NASA. The results of the preliminary study led to the design and construction of a small bellmouth type inlet with a sharp edge, denoted "Bh". A modified version of this inlet was then tested. This modified inlet, abbreviated "Bm", is

characterized by a smooth edge. Finally, a large bellmouth-type inlet was constructed. This last one, "Co", was actually used in conjunction with a fifth-order contraction and provided controlled contraction of the stream prior to entering the test section.

Fan Ducts

The fan duct is made up of two sections of uniform plexiglass ducts, i.e., the fan and the exhaust ducts (see Figure 2). Air is drawn by a small axial fan powered by a 0.06 HP DC motor. Both the fan and the motor are suspended in the center of the duct by four 0.64 cm rods attached to the wall of the plexiglass duct. The rotational speed of the fan can be varied in a continuous manner up to a maximum speed of 3,800 rpm by connecting the motor to a variable DC power supply. In the present setup, this is achieved by means of a Variac and an AC/DC converter. The mean axial velocity in the test section can therefore be adjusted to any desired value in the range from 0 to 6 m/sec. The free-stream turbulence intensity, though not measured, was estimated from the visualization records to be very low when the facility is used in conjunction with the low-disturbance control chambers.

Flow visualization in the test section is achieved by installing a smoke wire 20 cm ahead of the fan, as shown in Figure 2. The details of the smoke wire

technique will be discussed later. A 30.5 cm long exhaust duct is located downstream of the fan, providing a uniform back pressure and thus increasing the efficiency of the fan.

Low-Disturbance Chambers

During the preliminary study, it became obvious that room disturbances have a considerable impact on the flow visualization results, and it is therefore necessary to control the environment in order to obtain consistent results and isolate the various ongoing phenomena.

Two low-disturbance chambers, "No.1" and "No.2", were set up in a large laboratory during the first and second part of the visualization study, respectively. These chambers were positioned ahead of the fan inlet to provide controlled flow conditions.

As shown in the upper portion of Figure 3, the low-disturbance chamber No.1 was like a small room. It was set up at the far left side of the laboratory, close to the end wall. During the first phase of this investigation, the laboratory served as a multipurpose working area as well as providing storage for a large amount of heavy equipment. Both the obstructions ahead of the chamber and the movements of persons in the room were found responsible for the undesirable flow condition ahead of the fan inlet (see Chapter III for more details).

Therefore, a second low-disturbance chamber, No.2, was established in the second part of this study. The chamber is shown schematically in the bottom of Figure 3. This low-disturbance chamber occupied a major area of the laboratory.

The same laboratory was then organized to provide adequate conditions for the experiment. Large pieces of equipment and obstructions were removed. In addition, a partition was raised to separate the rest of the room from the actual test area. As a result, undesirable flow disturbances were minimized.

Low-Disturbance Chamber No.1. Figure 4 is a schematic of the low-disturbance chamber No.1. It was used only during the preliminary study. The overall dimensions were 0.98 x 1.4 x 1.71 m. A number of 5.1 x 10.1 cm wooden studs were used to form a frame on which heavy weight black velvet material was attached. The position of the flow visualization apparatus is also shown in Figure 4. The initial camera position No.1 was set at an arbitary oblique angle with respect to the flow direction. However, the exact location of the camera was not recorded during this preliminary study. The fan intake was positioned approximately at the center of the front wall. The centerline of the fan duct was about one meter from the floor and 70 cm from the side walls. The wall opposite to the intake was removed to allow easy

access during the experiment. All fan inlets, except the large bellmouth-type, were documented by flow visualization in this facility during the preliminary study.

Low-Disturbance Chamber No.2. In view of the results of the preliminary experiment, room atmospheric conditions such as air conditioning and convection flow patterns seemed to affect the flow field upstream of the intake. In addition, neighboring objects, including the presence of the investigator during the experiment, contributed to the disturbance of the intake flow. Since one of the purposes of this experiment is to manage and control undesirable disturbances, it is necessary to have total control over the upstream flow field. Hence, a second low-disturbance chamber was set up to minimize all undesired effects. Once a "clean" environment is achieved, controlled disturbances can be introduced in the inlet flow field. This approach of decoupling the various sources of disturbance present in a real flow situation allows one to study specifically the effects of various disturbances such as wakes or surface vorticity and develop means of suppressing them effectively.

The overall dimensions of this chamber are 3.05 x 4.57 x 2.74 m. The setup used for flow visualization in the low-disturbance chamber No.2 is shown in Figure 5. Metal struts are used to construct the frame of the

chamber. Maximum spacing between both horizontal and vertical members was chosen in order to minimize flow obstructions. Porous black cloth (100% polyester) is tensioned across the top to form the ceiling. The four side walls are made out of overlapping cloth panels. This particular design allows easy modification of the geometry of the control chamber, while providing excellent isolation when all panels are down. Wooden beams are attached to the lower end of the cloth panels, providing the neccesary tension to prevent them from swaying during the experiment.

A right-handed cartesian coordinate system is used with its origin on the axis of symmetry at the inlet. The x-coordinate is aligned with the axis of symmetry, y is oriented vertically and z is in the horizontal direction. Therefore, positive x and y are in the upstream and upward directions, respectively. The fan inlet and duct assembly are positioned approximately at the center of the chamber's front wall (see Figure 5). The centerline of the assembly is 152 cm from the side walls and 130 cm above the ground.

The top view in Figure 5 indicates the camera positions No.2, No.3 and No.4 which correspond to the end view, side view and oblique view of the flow, respectively. It is clear from this figure that the end view and oblique view refer to the flow upstream of the inlet, while the side view refers to the flow inside the

test section (i.e., fan duct). Both cameras No.2 and No.4 were positioned as far as possible away from the inlet in order to avoid any undesirable disturbance due to their presence. The offset angle of camera No.4 was calculated to be 30 degrees, as shown in Figure 5. With the aid of this large chamber, it is possible for the experimentator to stay outside the control room and yet be fully capable of operating the cameras through remote control circuitry.

The details of the flow visualization instrumentation are presented at the end of this chapter. All four types of inlet configurations were documented inside the larger chamber No.2 and the results are discussed in Chapter IV.

In both low-disturbance chambers, the fan inlet assembly can be set up in two ways: a flush-mounted setup in which the backing material is touching the inlet, or an extended-mounted setup with the fan inlet protruding inside the chamber. These various configurations are illustrated in Figure 6.

Isolated-Disturbance Characteristics

Cylinders of various sizes placed in different positions were used to generate isolated disturbances upstream of the inlet. Figure 7 shows the characteristics of the wake-disturbance generators. A total number of six cylinders was studied. Their

diameters are 1.3 cm, 0.6 cm, 5.0 cm and 19.0 cm. The length of the cylinders ranges from 17 cm to 109 cm. As indicated in Figure 7, cylinder C5 was used for the extensive investigation.

Supports and clamps which are necessary to hold the cylinder were placed on the "false floor" (a large table placed ahead of the inlet; see next section for details). Hence, when cylindrical wakes were introduced upstream of the fan inlet, there existed also some disturbances generated by the supports and false floor.

Several vertical, horizontal and oblique orientations of the cylinders were investigated, as shown in Figure 8. The top view and side view are presented on the left and right side of the figure, respectively. Both the heavy dots and dash lines represent the locations of the wake-generating cylinder. Examples of typical cylinder orientations are highlighted by circles bearing a code. These codes used to describe the cylinder orientation are "W", "$\bar{W}$" and "$\hat{W}$", corresponding to the vertical, horizontal and oblique positions, respectively. A numeral following the letter "W" characterizes the actual x-y-z coordinate. For instance, "W3" is a vertical cylinder at x = 45.7 cm (upstream), and y = z = 0 (centerline of the fan duct). The following table is a summary of the different configurations.

Table 1. Characteristics of Wake-Generating Cylinders

CYLINDER ORIENTATION	NOTATION	CARTESIAN COORDINATE (cm)*		
		x	y	z
Vertical	W 1	0	0	0
	W 3	-45.7	0	0
	W 7	0	0	-22.9
Horizontal	$\bar{W}$ 1	0	0	0
	$\bar{W}$ 6	0	-30.5	0
	$\bar{W}$ 9	0	30.5	0
Oblique	$\hat{W}$ 1	-	0	0
	$\hat{W}$ 6	-	30.5	0
	$\hat{W}$ 9	-	-30.5	0
* x =	0;	-22.9;	-45.7;	-53.3;
y =	0;	±15.2;	±30.5;	
z =	0;	±22.9;	±45.7	

High-Disturbance Conditions

In both phases of the flow visualization experiments, the centerline of the fan duct was relatively high above the floor of the laboratory. The reader can refer back to Figures 4 and 5 showing the centerlines of the fan duct at 7 and 8.5 times the duct diameters above the ground in chamber No.1 and No.2,

respectively. One of the goals of the study is to verify that the ground serves as a vorticity source. A "false floor" is formed by placing a ground plate underneath the fan intake. In the preliminary study, a 90 x 120 cm plate was used for that purpose. The results indicated that the ground vortices are not energetic unless the ground plate is sufficiently close to the inlet. Therefore, in the second phase of the study, a 152 x 60 x 76 cm table is often positioned upstream of the fan inlet, as shown in Figure 9. The distance from the table top to the centerline of the fan duct is 3.5 times the duct diameter (i.e., 53.3 cm). When isolated disturbances are introduced upstream of the inlet, clamps and stands are placed on the ground plate to secure the wake-generating cylinder in place. Therefore, in addition to isolated disturbances, a small amount of surface vorticity was present. Figure 9(b) is a side view showing the relative position of a vertical cylinder placed on the ground plate, upstream of the fan intake.

Flow Manipulators

Five different flow control devices are used in the flow visualization experiment in an attempt to alter or suppress the incoming disturbances. Some of these flow manipulators have already been studied in detail (see Ahmed et al., 1976). The mesh size, thickness, diameter and geometry of the various honeycombs are tabulated in

Figure 10.

The IIT-type honeycombs are plane, with a circular cross-section. Four different combinations of diameter and thickness are coded by letters "J", "K", "P" and "O". The letter "N" is reserved to designate the dome-shaped honeycomb used at NASA Lewis Research Center (see Mc Ardle, et al., 1980). A number is added to the letter to encode the position of the flow control device with respect to the fan. The higher the number, the shorter the distance between the fan and the honeycomb, as illustrated in Figure 2. Figure 11 is a schematic drawing showing the positions of the flow control devices. The IIT-type honeycombs are usually placed inside the fan duct after the contraction. The distance between the flow manipulators and the fan can be varied (see Wigeland et al., 1979, for more detail on the positioning of honeycombs).

These flow control devices were documented with all four different inlet configurations. However, due to physical limitations, only the flight-type and the small bellmouth-type inlets were tested with the NASA ICD No.3.

Combinations of inlets, test flow conditions, flow manipulators and their arrangements are summarized in Figure 12. The codes corresponding to the different cases are described earlier in this chapter and are used consistently throughout the rest of the chapters. Details of the test flow conditions are discussed in

Chapter IV.

Smoke Visualization and Photographic Techniques

During the preliminary study, both conventional smoke visualization and the IIT smoke wire technique were employed. The former technique is described in Chapter III and the later one is discussed in this section. In the second phase of the investigation, extensive flow visualization was conducted using the IIT smoke wire technique which was introduced by Corke, Koga, Drubka and Nagib (1977). This technique allows the introduction of a sheet of discrete streaklines at any desirable location in the flow field of interest. A brief description of the principle and operation is given in the following paragraph.

The smoke-wire unit consists of two parts: the portable support for the 0.1 mm diameter wire and the control box. The wire can be coated with a series of oil droplets by various methods. For a vertical wire, pressure is applied to the oil reservoir to release a small drop of oil which slides along the wire due to gravity, leaving a string of minute droplets resulting from a capillary instability. In the case of a horizontal or any other shaped wire, a traversing mechanism can be used to wet the wire with a thin coat of oil. However, in an open facility coating the wire with oil manually is often more efficient in the later case.

A DC voltage is then applied to the wire. Due to the resistive heating, the oil droplets vaporize and a sheet of discrete smoke streaklines is emitted from the wire. The intensity of the smoke can be adjusted by varying the voltage across the wire. To ensure quality photographs of the visualized flow field, a control box is used in connection with the smoke wire. It allows the user to control accurately the time required for the smoke to be convected into the field of view before a picture is taken, and to disable the camera triggering circuitry once the sheet of smoke leaves the field of view. The proper sequencing of operations is performed by a cascade of timing-integrated circuits and solid-state logic circuitry. The outputs of the synchronization box allow direct interfacing with either a camera motor drive or the trigger of a strobe light or combination of these devices. The timing circuitry can also be bypassed to enable recording of the visualized flow field in continuous lighting through a video camera and recorder. This latter option is particularly useful for diagnostic purposes and was used extensively in the early stages of this study. It also presents the advantage of depicting clearly the dynamics of the unsteady flow field which are particularly hard to capture with instantaneous realizations.

Both the horizontal and vertical smoke wire orientations were used during the preliminary

investigations. Figure 13 shows the arrangement of the smoke wire with respect to the fan inlet which was set up in chamber No.1. The detailed descriptions of the low-disturbance chamber No.1 is presented earlier in this chapter. The horizontal smoke wire was placed parallel to the centerline of the fan duct, 2.5 cm below the inlet. At 1.5 cm upstream of the inlet, the vertical smoke wire was positioned off center, 2.5 cm to the right side of the inlet. Figure 14 describes the smoke wire orientations in low-disturbance chamber No.2. Only the vertical smoke wire is used in this case at various upstream positions, both on and off the centerline of the fan duct. In addition, a vertical smoke wire was installed in the fan duct, 19.8 cm upstream of the fan, see Figure 14(b).

Various camera positions are also shown in Figure 14. Cameras No.2 and No.4 were installed inside the low-disturbance chamber No.2 and are used simultaneously to obtain instantaneous end and oblique views of the upstream flow field. Camera No.3 is used to obtain side views of the flow in the test section upstream of the fan. In addition, a combination of camera No.2 and No.3 provides simultaneous recording of both end and side views in the test section.

CHAPTER III

PRELIMINARY VISUALIZATION STUDY

Flow visualization results of the preliminary investigation are presented in this chapter. In this phase of the study, qualitative information about the flow field of various fan inlets was obtained in the low-disturbance chamber No.1.

Two smoke visualization techniques are employed: the IIT smoke wire which is described in Chapter II and a conventional smoke visualization technique. The latter consisted of introducing quiescent, slightly heavier than air, smoke on a large tray placed upstream of the fan inlet in the absence of flow, i.e., before the fan was turned on. Once the experiment was initiated, the smoke was convected by the flow. Still photographs were used to record the smoke pattern marking the various flow features.

The fan inlets investigated in this experiment was the flight-type inlet, "Fo", and the small bellmouth-type inlets with sharp edge, "Bh", and with smooth edge, "Bm". Descriptions of the different inlet geometries are given in Chapter V (see Figure 1).

Flight-Type Inlet

Figure 15 shows different views of the flow field ahead of the flight-type inlet. The oblique view of a vertical smoke wire which is centered upstream of the

inlet is shown in Figure 15(a). The core of the flow appears to be free of disturbances. However, due to the smoke-wire orientation, it is difficult to determine whether or not the flow is separated from the surface at the inlet. In addition, wiggles of the streamlines near the walls tend to indicate the presence of a turbulent boundary layer "massaging" the core from underneath.

By offsetting the smoke wire to the right side of the inlet, it is possible to label the flow close to the inlet wall, as shown in Figure 15(b) from an oblique view. No clear evidence of flow separation at the lip is obtained. However, the development of the turbulent boundary layer shortly downstream of the lip is clearly visible and suggests the occurrence of flow separation. Localized streamwise vortices can also be observed in the upper part of the flow.

The presence of these localized streamwise vortices is clearly illustrated in a side view (see Figure 15(c)). They are characterized by the "crossing" of streaklines when visualized from the side, due to the helical motion associated with them. They are highly localized and elongated. These vortices appear before the flow enters the inlet and can be attributed to the presence of weak vortical disturbances in the environment of the inlet which are stretched by the flow acceleration and tilting. Due to accidental vibration of the horizontal smoke wire, the smoke sheet appears as a succession of

time lines. Valuable information concerning the kinematics of the velocity field can be gained from this interesting photograph.

Small Bellmouth-Type Inlet

As a sample of the conventional smoke visualization technique, the flow field upstream of the small bellmouth-type inlet with a sharp edge is depicted in Figure 16. Shown on the top (Figure 16(a)) is a side view of the inlet taken at an arbitary time after the fan motor was started. The time chosen was sufficient to allow the smoke to be convected throughout the field of view, and to reach steady state.

The smoke marks the air being drawn into the inlet. However, the technique does not yield detailed information about the entire core of the flow. One can also notice the complicated localized smoke pattern at the center of the photograph. This can be attributed to the existence of surface vorticity. The presence of any surface in the vicinity of the inlet represents a source of vorticity for this sink-like flow. Since the smoke was contained in a large tray positioned close to the inlet, the vortical structures marked by the smoke are most likely generated on the surface of the tray.

Shown in Figures 16(b) and (c) are two end views of the same inlet (Bh) taken in a time sequence. Information revealed in Figure 16(c) correlates well with

the phenomena observed in Figure 16(a). The differences in the smoke patterns exhibited in Figures 16(b) and (c) are likely due to two factors. First, the disturbances ahead of the inlet are unsteady. Secondly, the conventional smoke visualization technique requires a certain time for the smoke to mark a flow structure accurately.

As the disturbances of interest in this study are time-dependent, the conventional smoke visualization technique presents shortcomings. Consequently, the IIT smoke wire technique is employed throughout the rest of the visualization experiments, in an attempt to alleviate the problems described above.

To illustrate this concept, a similar case has been visualized using the smoke wire technique, as shown in Figure 17(a). By contrast to Figure 16(b), this picture reveals the instantaneous structure of the flow. In particular, an energetic streamwise vortex can be identified. Stretching and subsequent thinning are clearly taking place as the vortex enters the inlet. Other three-dimensional disturbances are also present, illustrating the complex nature of the neighboring environment.

Based on visualization results not shown here, flow separation at the lip is found to occur consistently for the small bellmouth-type inlet with sharp edge (Bh). To alleviate this problem, this inlet was modified into one

with a smooth edge (Bm). Results obtained from a smoke wire stretched across the upper part of this modified inlet are presented in Figure 17(b). Inspite of the difference in inlet geometries, similar flow modules can be identified. However, their intensity is lesser than that observed on the ground side of the inlet (see Figure 17(a)). This reinforcing of the disturbances by the presence of a surface in the neighborhood of the inlet was consistently observed throughout this preliminary study, regardless of the type of inlet being tested. This trend clearly demonstrates the importance of surface vorticity generation in the vicinity of an inlet and illustrates the difficulty encountered in designing the second low-disturbance chamber. The second chamber was planned to provide an environment in which surface vorticity generation can be kept to a minimum, and in turn can be introduced for controlled test conditions.

CHAPTER IV

CLASSIFICATION AND CONTROL OF VARIOUS DISTURBANCES IN FLOW OF DIFFERENT INLETS

The results presented in Chapter III led to the design of the low-disturbance chamber No.2. The description of this facility has been discussed in Chapter II. The study of various types of disturbances, as well as their control, in flow of different inlets was carried out in this controlled-environment chamber. The classification of flow conditions and the results of the flow visualization experiments are given in the following sections.

Classification of Flow Conditions

Due to the complexity of the flow field ahead of a real fan inlet, it is necessary to identify and segregate the various basic flow disturbances. This is made possible by placing the inlet in a clean environment in which controlled disturbances can then be introduced. Three classes of disturbances were identified from the preliminary study:

(1) isolated two-dimensional mean velocity nonuniformities, or localized shear layers, e.g., wakes, jets, or separted shear layers.

(2) surface-generated vorticity, including the ground, chamber walls and the external surface of the fan setup.

(3) three-dimensional high intensity vortical disturbances, made of concentrated streamwise vortices.

In addition to these three classes, a "clean" case is always used as a reference. The specified cases investigated are summarized in Figure 12, under test flow conditions. All of these flow conditions were tested with all four types of inlets. Descriptions of the inlet geometries and arrangements are discussed in detail in Chapter II and Appendix A.

In an attempt to suppress or attenuate these specific disturbances, various flow control devices were tested. (A general description of the flow control devices is given in Chapter II). Figure 12 summarizes the combinations of flow inlets, test flow conditions, flow manipulators and their arrangements.

The total number of cases renders a discussion of all of the results impossible. Hence, only selected samples of the representative cases are presented here. These sample photographs are identified by an eight-letter-code system. The first two letters refer to the type of inlet. The second group of two letters indicates the attachment setup. Test flow conditions are identified by the third group. Finally, the flow manipulators are characterized by the last group of letters. All codes are explained in Figure 12.

Results

To illustrate the trends exhibited in this study, the results of selected cases are presented in the following:

Flight-Type Inlet. Figure 18 shows side views of the test-section ahead of the fan for this type of inlet. Photographs (a) and (b) correspond to the extended and flush attachment setups, respectively, in the presence of sources of surface vorticity. The surface vorticity is generated by positioning a large table in the vicinity of the inlet. The walls of the chamber do not contribute significant surface vorticity unless some of them are left partially open. The floor of the chamber is also sufficiently far from the inlet. Under a controlled low-disturbance environment, the air is supplied to the chamber through the porous material of the walls by the pressure difference created by the fan.

In both setups of Figure 18, the flow is characterized by a thick turbulent boundary layer on the side wall. These boundary layers, which can be attributed to the flow separation at the lip, have been considered as significant noise sources (see Hanson, 1980). This is in agreement with the results obtained from the preliminary study. However, the flush setup seems to minimize this phenomenon. Elongated streamwise vortices can be observed in the core region of the flow.

The absence of other types of disturbances confirms that these vortices originate from the upstream surface vorticity source.

For the flush setup in a similar flow condition, two types of flow control devices were tested. Figure 18(c) corresponds to the IIT plane honeycomb with 0.318 cm mesh size, placed between the inlet and the test section. The flow obtained with the NASA hemispherical honeycomb is shown in Figure 18(d). This flow control device was placed upstream of the inlet.

Both honeycombs suppress the stretched longitudinal vortices in the core of the flow. Some reduction of the boundary layer is obtained with the IIT honeycomb due to its position downstream of the reattachment region. It is not surprising, however, that no such reduction is observed with the NASA honeycomb. The fact that the separation took place downstream of the device, was expected.

Small Bellmouth-Type Inlet. Selected results obtained with the small bellmouth-type inlet are presented in Figures 19, 20 and 21. All three figures consist of visualization results in the test section viewed from the side (see camera No3 in Figure 5(a)). The effects of the inlet mounting arrangement are illustrated in Figure 19. The left column ((a), (c) and (e)) corresponds to the flush mounted setup, and the

right column ((b), (d) and (f)) corresponds to the extended setup. Each row characterizes a different flow condition. The low-disturbance case (reference case) is shown on the top ((a) and (b)). The flow appears undisturbed for both types of setup and no anomalous behavior is observed.

Surface vorticity is introduced upstream by placing a large table in the vicinity of the inlet. The results obtained in this case are depicted in the middle row ((c) and (d)). The presence of the elongated streamwise vortices is consistent with the results obtained in the preliminary study for a similar test flow condition. The extended setup might be slightly "cleaner", but this trend would have to be confirmed by quantitative measurements. For the flush setup case, the NASA hemispherical honeycomb was tested. Photograph (e) shows its ability in suppressing the longitudinal vortices.

Figure 20 illustrates the effectiveness of various flow control devices in removing two- and three-dimensional wakes introduced upstream of the inlet. All photographs are taken with the flush mounted setup. The left column ((a), (c) and (e)), corresponds to the wake of a horizontal cylinder placed immediately upstream of the inlet. The right column ((b), (d) and (f)), corresponds to the presence of a person in front of the inlet. In this figure, we try to model cases of isolated nonuniform flow disturbances including complex

three-dimensional wakes such as the ones commonly present in actual fan-testing stands. The photographs shown in the top row ((a) and (b)) illustrate the resulting flow fields. Two of the flow control devices tested are presented in the next photographs to highlight the main trends exhibited by the results.

In the middle row ((c) and (d)) an IIT 0.32-cm mesh size honeycomb is used. The suppression of large-scale vortical motions is completed, but small-scale quasi-homogeneous turbulence generated by the honeycomb is still present in the test section. This latter effect could be alleviated by allowing a larger distance for the turbulence decay, by a better choice of the mesh size, or by the introduction of screens.

The results obtained with the NASA honeycomb are shown in the bottom row ((e) and (f)). The disturbances are equally suppressed and the large distance between the NASA honeycomb and the test section is reflected in the absence of small scales. In addition, the free contraction of the flow past the NASA honeycomb helps in further reducing the homogenous turbulence.

The performance of the various flow control devices was also evaluated in the presence of other high-intensity disturbances. These results are summarized in Figure 21. All photographs were taken in the extended setup configuration and the high-level disturbances were created by a large household fan blowing in the back of

the control chamber (approximately four meters from the inlet).

The disturbed case is shown in (a) and the flow obtained with the NASA hemispherical honeycomb is shown in (b). The large-scale disturbances have only been partially suppressed. By contrast, the results achieved with the IIT plane honeycomb are shown in (c) and (d). These two photographs correspond to 0.64 and 0.32 cm mesh sizes respectively. The large-scale vorticity is clearly inhibited by these devices. The presence of the remaining fine scales has been already explained, and it does not constitute a potential problem for blade-passing frequency generation.

Large Bellmouth-Type Inlet Assembled with a Fifth-Order Contraction. Figures 22 to 26 show the visualization results of the large bellmouth-type inlet assembled with a fifth-order contraction. The end and the oblique views of the fan inlet are recorded by cameras No.2 and No.4 Camera No 3 is used to record side views of the test section ahead of the fan. The reader can refer to Figure 5(a) for the camera orientations.

The end view and the oblique view shown in the same column in Figure 22 were recorded simultaneously (i.e., (a) and (b), (c) and (d), as well as (e) and (f)). More precise information can be drawn from simultanecus multi-view pictures, since the flow field ahead of the

inlet is three-dimensional and unsteady.

Figures 22 (a), (b), (c) and (d) were obtained in the presence of surface vorticity. A vertical smoke wire was placed at the center of the inlet in the first two photographs and at z = 10.2 cm (offset to the right of the inlet) in the latter case. Figures 22 (e) and (f) are in presence of surface vorticity and a vertical cylinder, C5, at position z = 10.2 cm (offset to the left of the inlet). A smoke-wire was placed at z = 10.2 cm (offset to the right of the inlet).

Simultaneous end view ahead of the inlet and side view of the test section ahead of the fan are shown in Figure 23. The inlet is flush-mounted in all the cases here. Figures 23 (a) and (b) were recorded in the presence of surface vorticity sources. A vertical cylinder, C5, was placed on a large table at z = -10.2 cm (off set to the left of the inlet) in Figures 23 (c) and (d).

Side views of the test section ahead of the fan are shown in Figure 24 for various types of disturbances. The low-disturbance condition shown in Figure 24(a) is a typical "clean" flow. The streak lines are evenly spaced throughout the flow field. Stretched longitudinal vortices of various intensities can be observed in presence of different sources of surface vorticity such as: a large table in the vicinity of the inlet (Figure 24(b)), and open panels of the control chamber (Figures

24 (c) and (d)). Distortion of the streaklines is observed in the core of the flow not only when the nearby panels of the control chamber are removed (see Figure 24(c)), but also when the far end panels are open, as shown in Figure 24 (d).

Figures 24 (e) and (f) show the flow conditions resulting from the presence of a complicated structure (a chair) in the vicinity of the inlet. Complex flow modules are displayed in Figure 24(e). The effect of the IIT honeycomb (M = 0.635 cm) positioned downstream of the inlet under the same flow condition is demonstrated in Figure 24(f). The resulting flow condition is as "clean" as that obtained in the low-disturbance condition (Figure 24(a)).

Figures 25 and 26 are sample photographs showing the flow conditions corresponding to various cylinder wakes introduced upstream of the inlet. These wakes are typical of two-dimensional isolated disturbances. In Figure 25, a vertical cylinder, C5, was placed at two different positions along the diameter of the fan duct, (W1 and W3, as shown in Figure 8). The intensity of the disturbance appears to be proportional to the relative distance between the vertical cylinder and the inlet (compare Figures 25 (a) and (b)). Under flow conditions identical to those of Figure 25(a), IIT honeycombs with mesh sizes of 0.635 cm and 0.318 cm were placed downstream of the inlet. The results are shown in

Figures 25 (c) and (d), respectively. One can easily conclude that both honeycombs are equally efficient in suppressing the vortical motions.

Two different orientations of a horizontal cylinder, C5, positioned ahead of the fan inlet and the effects of a flow control device are shown in Figure 26. For the cylinder orientations W6, W9, W6 and W9, the reader is referred to the illustration in Figure 8. The left and right column in Figure 26 correspond to a horizontal cylinder placed near the bottom and the top of the inlet, respectively. Figures 26(a) and (b) correspond to a flow condition in which a horizontal cylinder was placed parallel to the z-axis. An oblique cylinder, pivoted at an angle of 10 degrees off the z-axis is the same as the disturbance observed in Figures 26(c) and (d). The randomness of the positions of these stretched streamwise vortices confirms the unsteadiness of this nominally steady flow. Under flow conditions similar to those of Figures 26(c) and (d), an IIT honeycomb with a mesh size of 0.635 cm was inserted in the flow. J2 and J4 refer to the two different locations for it between the inlet and the fan (see Figure 1 for honeycomb positions). Figures 26(e) and (f) indicate that the disturbance suppression is rather insensitive to these honeycomb positions.

CHAPTER V

FACILITY AND INSTRUMENTATION FOR VELOCITY MEASUREMENTS

In this chapter, the facility used in the second phase of the investigation is described. The wind-tunnel characteristics as well as the means of introducing selected disturbances are also, examined. Finally, a description of the instrumentation used for the velocity measurements, as well as a description of the experimental procedure is given.

Facility

Wind-Tunnel Characteristics. The experimental study of the behavior of isolated disturbances through a contraction was conducted in an open-circuit wind tunnel. This tunnel is connected to an 180-psi compressed air line through a series of valves and filters. All the connecting pressure lines and filters are acoustically insulated. The air first enters a large settling chamber lined with acoustic foam. This chamber is equipped with a series of flow manipulators (screens, grids, etc.). Their arrangement ensures good flow uniformity and a low disturbance level. The design of the settling chamber is based on the results of Loehrke and Nagib (1972). The actual construction and optimization of this settling chamber has been reported by Ahmed et al. (1976). The flow then passes through a 25:1 contraction before

entering the test section. The test section consists of a versatile arrangement of 15.4 cm diameter plexiglass ducts. The particular configuration used in this study consists of two straight sections and a 4:1 contraction. A turbulence-generating grid was inserted at the junction between the two pieces of straight ducts. A schematic diagram of the test section is given in Figure 27. Also shown in this figure is the coordinate system used in this part of the investigation. Its origin is located along the axis of symmetry of the contraction. The x-axis is parallel to the test section axis, pointing downstream. The y- and z-axes are defined in the cross-sectional plane, y pointing upwards and z defined to form a right-handed coordinate system.

The measurements were taken with a hot-wire probe. The probe is supported by a three-dimensional traversing mechanism, located downstream of the test section. The reader is refered to Ahmed et al. (1976) for its detailed description. This traversing mechanism allows the movement of the probe along the three axes, and its positioning within 0.2 mm of any desired location. Built-in electrical circuitry permits accurate determination of the probe location. The velocity measurements inside the test section were obtained by inserting the probe through the downstream end of the tunnel. Hence, a low-obstruction probe is used to minimize the flow blockage.

Contraction Characteristics. The contraction used to study the behavior of the disturbances in contracting streams has a matched-cubic profile. This contraction, denoted MC4-100, has an area ratio of 4:1 and a length-to-inlet diameter ratio equal to unity. The matched-cubic profile is actually made out of two cubic polynomials matched at the inflection point. In a regular cubic profile, the position of the inflection point is fixed at the mid point between the inlet and the outlet of the contraction. The use of a matched-cubic profile gives extra flexibility in choosing the location of the inflection point, resulting in a better performance of the contraction. The design, construction and testing of such contraction is given by Tan-atichat (1980).

Grid Characteristics. A turbulence generating grid is used throughout the study to provide a uniform, quasi-homogeneous turbulence background. The grid, denoted G2, consists of a 0.84-mm thick steel plate punched with square holes forming a regular square array. The grid has a 2.5-cm mesh size and is characterized by a low solidity (σ = 0.37). To ensure quasi-isotropy and homogeneity of the turbulence at the inlet of the contraction, a grid-to-contraction distance of 25.4 cm was chosen, based on the results of Tan-atichat (1980) and Marion (1982).

Disturbance Generators

Three types of disturbances are investigated in this phase of the study: wake of a cylinder, wake of a sphere and longitudinal vortex. The two- and three-dimensional wakes were studied both on-center and off-center.

Two 0.71-cm diameter cylinders were fabricated out of plexiglass. For the typical velocity used in the experiment (3 m/s), the Reynolds number based on the diameter is approximately equal to 1500. This size was chosen large enough to ensure a turbulent wake, yet not too large in order to minimize the flow obstruction in the test section. Cylinder 1A has a length of 15.4 cm and can be mounted along the diameter of the test section. The second one, denoted 1B, has a length of 12.4 cm, and was machined to fit off-center, approximately 3.9 cm above the diameter of the test section (i.e., r/R(0) = 0.52).

A 0.73 cm diameter sphere was fabricated out of wood. It can be mounted on a 0.1 mm stainless steel wire that suspended it either on-center or off-center (r/R(0) = 0.52).

Longitudinal Vortex Generator. A vortex generator is to introduce a longitudinal vortex in the center of the flow. It consists of a pair of identical NACA-0012 airfoils, hinged at the quarter-chord position. The chord length and span of these airfoils are 7.62 cm

and 6.99 cm, respectively. These airfoils are mounted next to each other in the spanwise direction inside a 15.4 cm long plexiglass duct. Each airfoil can be adjusted individually to any angle of attack. Two gear-reducing mechanisms allow the positioning of the airfoils within ten seconds of arc. For the details of the design and the construction of this swirl generator, the reader is referred to Ahmed et al. (1976). The apparatus generates a strong solid-body rotation vortex core with an approximately potential outer part. The determination of the optimal angles of attack for symmetry and stability of the vortex is necessary. A full description of these preliminary measurements is given in Appendix B.

Instrumentation

Analog instrumentation is used throughout this investigation. A schematic of the instrumentation is shown in Figure 28. Two velocity components can be simultaneously measured using an x-wire probe. The hot wires are operated in a constant-temperature mode at an overheat ratio of 1.7, using two DISA CTA anemometers. The anemometer's output are then fed to a pair of exponential-type DISA linearizers. The value of the exponent used was determined after calibration of the hot wires, and was found close to 2.2. The velocity signals are low-pass filtered at 10 kHz using DISA auxilary

units, to reduce the electronic noise. Operational amplifier sum-and-difference circuitry is then used to separate the two velocity components. The output signals are constantly monitored on a dual-trace oscilloscope. Depending on the type of measurements desired, a digital voltmeter or a DISA true-rms-meter are used in conjunction with either channel of anemometry. Another voltmeter is dedicated to the traversing mechanism, indicating either the reference voltage supply or any of the outputs of the triaxial position indicator. Velocity or rms profiles can be recorded on an H.P. X-Y plotter.

Experimental Procedure

All the measurements pertaining to this phase of the study were obtained at a constant free-stream velocity of 3 m/s. In addition, the turbulence-generating grid was always placed upstream of the test section, as described in the beginning of this chapter.

Velocity measurements were obtained for six different cases. The first one, denoted 0A, is a reference case, corresponding to the absence of isolated disturbances in the flow. The other cases correspond to the various types of disturbances. They have been denoted 1A, 2A, 3A, 1A' and 2A' to simplify the referencing. The numerals 1, 2 and 3 are attributed to the cylinder wake, the spherical wake and the longitudinal vortex, respectively. The suffixes, A and

A', refer to the on- and off-center disturbance positions. Figure 29 summarizes the various cases and their labeling.

For each of these six cases, sets of data were taken for both the uniform duct case (C = 1) and the contraction case (C = 4). In the first case, a section of straight duct was mounted in place of the contraction. Data acquired in absence of any stream contraction were taken in order to clearly discriminate the effects due to the presence of the contraction from those due to the natural decay of turbulence and the disturbance through viscosity.

Each set of data consists of mean and rms velocity profiles of the axial and radial velocity components. For each of these quantities, radial profiles were obtained at six axial locations, corresponding to x/L of -0.33, 0., 0.33, 0.67, 1. and 1.33, where L represents the length of the contraction and x is the downstream distance measured from the inlet of the contraction. The actual measurement stations are shown schematically in Figure 27. In addition, two axial profiles were obtained, one on-center (r/R(0) = 0), and one off-center (r/R(0) = 0.52). Following the acquisition, all data were non-dimensionalized by the axial velocity at that particular downstream location. The data were also compensated for possible drift of the free-stream velocity of the tunnel.

CHAPTER VI

DOCUMENTATION OF VELOCITY FIELD OF ISOLATED DISTURBANCES THROUGH A CONTRACTION

In this chapter, the results from the second phase of the investigation are reported, starting with the presentation of the data for the reference case obtained in absence of any isolated disturbances. The disturbance cases are then analyzed. Axial measurements are then interpreted and a brief discussion of the lateral ones closes the chapter. Analysis of on-center disturbances, i.e., cylindrical wake, spherical wake and longitudinal vortex, is delivered prior to the off-center cases, i.e., cylindrical and spherical wakes. Figures 30 to 69 summarize the large volume of data for the reference case and each different test flow condition. Both the contraction (C = 4) and the straight duct (C = 1) values are depicted on each of the graphs.

Uniform-Flow Reference Condition

A reference condition has been established in the absence of any isolated disturbances. The uniform duct data were taken to provide a good comparison basis when evaluating the other cases.

For a free-stream velocity of 3 m/s, the turbulence level at the inlet of the contraction is approximately 2.5%. The radial distributions of normalized axial velocity, $U/\overline{U}_i$; axial turbulence intensity, $u'/\overline{U}_i$; and

radial turbulence intensity, $v'/\overline{U}_i$, obtained at all six measurement stations, are uniform. No cross-flow (V = 0) or anomalous behavior of the turbulence was noticed, as expected (see Figures 37 and 38 of Loehrke and Nagib, 1972). These reference profiles appear in dotted lines in Figures 30 to 39 for the axial traverses, and Figures 40 to 69 for the radial traverses.

Axial Surveys

In this section, axial measurements, recorded at two radial positions for all test flow conditions, are examined. The streamwise and radial velocities and their corresponding root-mean-square values are normalized by the streamwise velocity at the inlet of the contraction ($\overline{U}_i$). These velocity quantities are plotted against the axial measurement locations, x/L, where L is the length of the contraction. The on-center isolated disturbances (i.e., flow conditions 1A' and 2A') are shown in Figures 36 to 39. Five groups of two consecutive figures (starting from Figures 30 to 39) illustrate five flow conditions at two radial locations along the streamwise direction. Therefore, it is possible to compare the turbulence decay for various types of isolated disturbances at a certain radial location.

On the left top corner of Figures 30 and 31, one notices that the mean velocity increases monotonically through the contraction. These curves show that the

stream starts to contract before the solid wall does and that it overshoots slightly at the outlet. Hence, the behavior of this contraction is in agreement with Marion-Moulin (1982) and Tan-atichat (1980).

The on-axis measurements of on-center isolated disturbances, i.e., test flow conditions 1A, 2A and 3A shown in Figures 30, 32 and 34, display some decays of turbulence intensities. Figures 31, 33 and 35 exhibit the off-axis data for test flow conditions 1A, 2A and 3A, respectively. However, the longitudinal and radial turbulence intensities remain constant and start to increase at two-thirds and one-third of the contraction length for the two former disturbance cases and the later case, respectively. The off-center isolated disturbances i.e., test flow conditions 1A' and 2A', shown in Figures 36 to 39, do not reveal much information for the on-axis measurements. It appears to be a difficult task to record any off-axis data and obtain meaningful interpretation (see Marion-Moulin (1982) and Tan-atichat (1980)).

Lateral Surveys

Lateral measurements, recorded at six axial locations with isolated disturbances, both on-center and off-center, are discussed in this section. The streamwise and transverse profiles of the two components of mean and fluctuating velocities are normalized by the

local mean velocity, $\bar{U}(x)$. The radial distances are nondimensionalized by the local radius of the contraction to accentuate the flow contraction. Plots of the normalized velocity quantities versus the normalized radial distance are shown in Figures 40 to 57 for the on-axis isolated disturbances and Figures 58 to 69 for the off-axis cases. The horizontal axes across the top of the graphs are the normalized radial distance of the straight duct and those across the bottom of the graphs represent the normalized radial distance of the contraction. Since there are five test flow conditions investigated, each group of six figures, starting from Figure 40 to Figure 69, pertaining to a given test condition, corresponds to six different measurement stations. Hence, the reader can observe the evolution of the velocity profiles in the test section by flipping through a sequence of six graphs.

One can notice that all the quantities have a higher value for the uniform-duct cases compared to the contraction cases. This observation implies that the contraction does suppress the streamwise and transverse mean velocity defects associated with the disturbances, as well as the turbulence intensity. More discussion on the effects of contraction on isolated disturbances is presented in Chapter VII.

CHAPTER VII

DISCUSSION

The results from the preliminary and final stages of this investigation, as well as from the first and second phases of the study, are presented separately in Chapters III, IV and VI. In this chapter, integration of the findings from these results is achieved through discussion of the various important ingredients of the problem in order to draw the conclusions summarized in the next chapter.

Intake Geometry

From the various experiments one finds several consistent patterns. The flight-type inlet tends to encourage flow separation at the lip. Thick boundary layers near the walls can be decreased by placing a plane honeycomb downstream of the inlet. However, a hemispherical-type honeycomb upstream of the inlet does not correct such a phenomenon since the flow separation occurs after the inflow control device.

The boundary layer of the fan duct can be minimized and incipient separation prevented by altering the geometry of the fan intake. All the bellmouth-type inlets (i.e. Bh, Bm and Co) have demonstrated such ability. The extended setup of the fan inlets appears to provide a velocity field near the inlet slightly better than a flush mounted case.

In any case, inlet design for static testing facilities, where no forward velocity is present can be carried out in a straight-forward manner using potential flow theory with boundary layer corrections, including some separation criterion. Such codes are now available and used in industry to design many internal flow problems, e.g., rotating machinary intakes or wind-tunnel contractions. Simple empirical approaches can even be used in many cases. Anyway, it appears quite obvious that flight-inlet configurations should be avoided in ground-testing facilities. In fact, proper modeling of the ducted fan flow is being violated from the fluid mechanics point of view when they are used.

Surface Vorticity Sources

By having entire control on the incoming flow condition ahead of the fan inlet in the low-disturbance chamber No.2, it was possible to establish a "clean flow" reference condition. However, stretched streamwise vortices are observed whenever a surface is introduced in the vicinity of the inlet. As illustrated in many sample photographs in Chapter IV, the distance between the surface and the inlet is proportional to the intensity of the vortex. One of the effective means to control the undesirable flow conditions is to minimize the number of obstacles and surfaces upstream of the fan inlet. Such obstacles include any structures, large surfaces, even

the experimentaters. The study suggests that a plane honeycomb installed downstream of the inlet is more effective in removing the intense longitudinal vorticity and high-level disturbances than the external control devices, at least at the present low Reynolds numbers of operation.

As it is pointed out several times in earlier chapters, all surfaces near this sink-like flow field may act as sources of vorticity. These surfaces include the "ground", the chamber walls, laboratory walls, neighboring buildings in outdoor test facilities, and the outside surfaces of the fan and its test stand. Recently, De Siervi et al. (1982) concluded that two mechanisms are responsible for inlet-vortex formation: the amplification of ambient vortivity as the vortex lines are stretched and drawn into the inlet, and in an upstream irrotational flow for an inlet in cross wind, a vortex is developed due to the variation of circulation (or lift) along the axial length of the inlet. They claim that these two mechanisms are substantially different and that the latter had not been recognized before. They suggest that the inlet and its potential image on the ground develop this vortex during the startup process. They do not explain sources of ambient vorticity other than the ground boundary layer developed by the approaching mean flow.

De Siervi et al. (1982) proceed to state "In this

second mechanism of vortex formation, ambient vorticity does not play a role. The vorticity in the core of the vortices is produced initially by the action of viscosity in the boundary layers on the outer surfaces of the inlet. Once the vortex is formed, however, there is no longer any vorticity convected into the core; the vorticity needed to maintain this is produced by the extension of the vortex filaments in the core. Thus the presence of a ground boundary layer (or ambient vorticity) is not necessary for the formation of an inlet vortex."

We believe that in practical applications, some vorticity from the surfaces of the inlet may continue to convect into the core of the vortex. In any case, for our application, pure and steady cross flow is not the most likely operating condition. It is therefore preferable to think in terms of all surfaces near the aerodynamic inlet as sources of vorticity. This vorticity is generated and convected away from these surfaces by the mean flow established by the sink-like action of the fan setup.

Both in outdoor and indoor test facilities, without substantial forward speed, the flow external to the sink is very slow compared to the inlet flow and often slowly unsteady. The outdoor wind direction and the flow patterns and direction inside a chamber are rarely steady. Wherever the vorticity is generated from surface

sources, it is convected and the vertex lines pile up as demonstrated by Figure 11 of De Siervi et al. (1982). The lower branch of the vortex loop is always more concentrated and stronger. This is why it can be easily identified and mislabelled the "ground" vortex. The presence of a separate boundary layer on the ground due to wind, i.e., the atmospheric surface layer is not an essential ingredient to this mechanism as has been incorrectly proposed many times. In fact, we have been able to record both legs of the same vortex loop, with their opposite sense of rotation, in several photographs like those of Figure 22. The two simultaneous views provide us with the adequate information to make this conclusion. It is also important to recognize, as we have from many such photographs, that the coexistence of several such vortex loops is often the case because of the several surfaces of different orientations available as sources of vorticity.

Appreciating this major mechanism for the introducton of the most undesirable element into the flow field of the fan, one may try to select the type of flow manipulators required. With the external flow control devices used most often in this application, the development of these vortices from the mean flow and the mean vorticity field is not inhibited. At best, the evolution of such vortices is slightly modified by the inflow control device where a substantial part of the

contraction of the flow is achieved freely downstream of it.

The only inlet which prevents and controls this most important mechanism is the one which has a controlled and confined slight contraction (say 4:1) of the stream past the flow manipulators. We recognize the severe limitation of such an arrangement from the point of view of the radiated sound field. As Nagib pointed out (Chestnut, 1982), the best design for static testing of jet engines is likely to be a compromise for both the acoustic as well as the fluid dynamics modeling, i.e., a design optimization approach.

Isolated Disturbances

Isolated disturbances such as cylindrical wakes, introduced upstream of a fan inlet were also investigated. Depending on the inlet geometries, dimensions of the cylinder and fan duct, flow distortions can develop into either a stretched longitudinal vortex or other complicated flow modules. Plane honeycombs with proper mesh size arranged at an optimal distance downstream of the fan inlet can suppress such flow disturbances.

External inflow control devices can also contribute to their suppression. However, one must realize that, becuase of the difference in flow velocity, the internal manipulators are likely to work more effectively when the

same type of manipulator is used, e.g., honeycomb of similar mesh. As was given in the flow management recipes of Loehrke and Nagib (1972), different manipulators are more efficient for the control of mean flow nonuniformities, as compared to those used for turbulence management. The bulk of the inflow control devices that have been used, including the ones tested in this investigation, are of the honeycomb type and are ineffective in reducing such isolated disturbances.

It is therefore obvious that for future applications when localized mean flow nonuniformities, such as wakes, jets, and separated shear layers, are likely to exist, the design of the flow manipulators must account for them. As outlined in the proceedings edited by Chestnut (1982), some recent improvement in inflow control device performance was achieved by the introduction of grid (or perforated-plate) like manipulators ahead of the honeycomb. The most important ingredients to satisfy such an isolated disturbances manipulator are highlighted by Tan-atichat et al. (1982) and Loehrke and Nagib (1972). The solidity has to be no more than 0.40 and the mesh Reynolds number [illegible] to be sufficiently large (more than 10,000) to p[illegible] homogeneous turbulence that can mix the flow and dissipate the nonuniformities. Some of the uniformization is of course achieved by the pressure drop provided by the less than 0.40 and larger than 0.30 solidity.

In the second phase of the investigation, quantitative measurements on various cases of such isolated disturbances, including an already developed concentrated streamwise vortex was carried out through a finite ratio contraction. The discussion of those results follows.

Effects of Contraction on Isolated Disturbances

The contraction used in the velocity measurements has a matched-cubic contour MC4, with an area ratio of four to one and a length-to-inlet-diameter ratio equal to unity. Effects of this contraction on various types of isolated disturbances are studied and the results are compared with a uniform duct in order to separate the effects due to stream contraction. Two- and three-dimensional wakes, developing along and off the centerline, as well as a concentrated streamwise vortex on the axis represent the five disturbances used here.

The detailed measurements are presented in Chapter VI. Here, the summary of the results is condensed in Figures 70 to 72. Figure 70 is a plot of the normalized mean and transverse velocity deficits versus the normalized distance along the contraction. All three types of isolated disturbances (cylindrical wake, spherical wake and longitudinal vortex) are suppressed through the contraction. This is true for both on-center and off-center data. Normalized mean and transverse

velocity fluctuation are plotted against the normalized distance along the contraction in Figure 71. All cylindrical and spherical wakes are suppressed through a contraction. However, the ratio of the longitudinal vortex transverse velocity fluctuation in a contraction to that in a uniform duct is unity. In other words, the contraction has no effect on the transverse velocity fluctuations of the longitudinal vortex.

The above two figures suggest that isolated disturbances, except for the longitudinal vorticity and its tranverse fluctuations, are suppressed by even a mild contraction. It appears, therefore, that the main mechanism of the amplification of the various disturbances in a contracting stream must depend on the potential tilting and accumulation of the vortex lines associated with these disturbances, and their streamwise stretching into the contraction as loops. This can be highlighted by the next figure.

Figure 72 shows the normalized characteristic length scales based on mean and radial velocity fluctuations. Generally speaking, these quantities decrease with the geometric scale of the contraction. While the integral scales of the turbulence increase through a contraction (for more details, see Tan-atichat (1980), Marion (1982), and Marion-Moulin (1982), all isolated disturbances representing nonhomogeneity in the flow are squeezed by the contraction. (The integral scale data shown here are

reproduced from Marion-Moulin (1982) for the same flow condition through the same contraction). The shrinking of the transverse scales of the isolated disturbances leads to the concentration of vorticity and the development of longitudinal vortices through the tilting, thereby contributing to the blade-passing frequency generation.

Figure 72 presents clear evidence that atmospheric turbulence or any homogeneous or semihomogeneous turbulent field ahead of a contraction cannot lead to the development of the undesirable long concentrated vortical structures. The integral and other characteristic scales of such turbulence increase not only in the streamwise direction but also in the transverse direction; see Marion-Moulin (1982) for more details. This completely refutes the mechanism based on atmospheric turbulence originally proposed by Hanson (1977).

Comparison of Various Types of Isolated Disturbances

Three types of isolated disturbances were investigated: cylindrical wake, spherical wake and longitudinal vortex. The relative velocity deficits for the cylindrical wake are the lowest. Figure 70 shows also that the spherical wake has lower relative velocity deficits than the longitudinal vortex. On the other hand, the cylindrical wake has higher relative velocity fluctuation than the spherical one (see Figure 71). The

longitudinal vortex has the highest relative velocity fluctuations. From Figure 72, the characteristic length scales for the cylindrical wake seem to be larger than those for the spherical wake. However, the characteristic length scales for the longitudinal vortex do not show a definite trend. The above observation can be due to the fact that the cylindrical wake is two-dimensional and the spherical wake is three-dimensional. The two-dimensional wake, where the vortex lines are all aligned in one transverse direction, has lower velocity deficits, higher velocity fluctuations and larger characteristic length scales than the three-dimensional one.

Correlation Between On-Axis and Off-Axis Data

When comparing the velocity deficits, velocity fluctuation and the characteristic length scales, the on-center data usually has a higher value than the off-center cases. It is important to compare the characteristic length scales for the isolated disturbances and the homogenous disturbances (see Figure 72) undergoing the same contraction. The characteristic scales of the isolated disturbances decrease along the geometric scale of the contraction, while that for the grid-generated turbulence increase.

CHAPTER VIII

CONCLUSIONS

The conclusions have been reached by a thorough and systematic review of the results presented in the previous chapters, as well as a large volume of flow visualization data not included here for lack of space. Some recommendations concerning the design of better static-test facilities are made along with the conclusions. The objectives of this investigation are to identify, and possibly develop methods for effective control, of the various sources of disturbances present in static jet-engine test facilities. The second phase of the study included the additional objective of analyzing the behavior of isolated disturbances through a finite axisymmetric contraction. The interrelation between these two aspects is highlighted in the following.

In view of the preliminary results presented in Chapter III, as well as the final visualization study described in Chapter IV, it is quite clear that the inlet design plays a very important role in the quality of the flow inside the fan duct. It is not surprising that a geometrical similarity principle does not hold in the design of inlets for static testing of jet engines. The primary difference between static and in-flight conditions resides in the drastic change in the

streamline patterns approaching the inlet in flight conditions from those encountered in static-test stands. The differences between the two cases render the flight-type inlet, which was designed for flight conditions, unsuitable for static ground testing. In fact, the visualization records clearly illustrate that the flight-type inlet leads to incipient flow separation resulting in thick boundary layers inside the fan duct. This may partly explain why noise measurements in the far field of the jet in static ground tests still exhibit anomalous differences from fly-over data, despite the use of flow manipulators upstream of the inlet. The efficiency of such manipulators in "cleaning" the flow cannot be blamed for this effect because thick turbulent boundary layers are created by the unsteady separation/reattachment flow module at the inlet, past the point of action of the manipulators.

The various smooth bellmouth-type inlets used in this study proved themselves successful in controlling this problem. However, the large difference in velocity and Reynolds number between the present simulation and actual test facilities does not guarantee that the present design is an optimum one. A complete potential flow calculation, matched with a good boundary layer code with an empirical separation criterion, would have to be carried out to determine the external flow field.

All of the manipulators tested in this study are

reasonably effective in suppressing most of the artificially introduced disturbances. Their efficiency in "cleaning" the flow is found rather insensitive to their position ahead of the fan. However, enough distance has to be allowed between them and the fan for the turbulence they generate to decay to a low enough level. This distance will vary with the mesh size and to a lesser degree with the velocity of the flow. Hence, no specific values can be recommended from the present study due to the difference in Reynolds number between the experiment and the actual case. However, Loehrke and Nagib (1972, 1976), Tan-atichat et al. (1982), Marion (1982) and Ahmed et al. (1976) provide ample information for these design criteria.

It is worthwhile pointing out that the hemispherical honeycomb-type inflow control device is not totally effective in suppressing the highest intensity disturbances used here. This fact highlights one of the key factors related to the design of flow control devices. The disturbance suppression is obtained at the expense of a pressure drop across the device, i.e., the local velocity. The design of a flow manipulator is a compromise between flow quality and pressure drop arguments. The precise knowledge of the type of disturbances, as well as their behavior in the flow of an inlet, can lead to a more appropriate design of the inflow control device.

Based on the results of Chapters IV and VI and the discussion of Chapter VII, it is concluded that the main two mechanisms for the development of the most undesirable flow module for the generation of the blade-passing frequency, i.e., the long slender vortical disturbances appearing "randomly" in time and space in the fan duct, are:

1) The generation and convection of the vorticity from the many surfaces surrounding the sink-like flow of the inlet, including the external surface of the fan housing.
2) The convection of vorticity from isolated disturbances into the inlet of the duct.

Both of these sources of vorticity lead to the undesirable flow module through the tilting and piling-up of vorticity lines just upstream of an inlet due to the action of the mean flow, i.e., the potential contraction of the stream. These concentrated vortex lines develop into vortex loops inside the duct, as pointed out in Chapter VII, with the "lower" branch being more intense. The isolated disturbances appear to contribute only through the tilting mechanism, and the subsequent amplification of the streamwise vorticity and the shrinking of its lateral characteristic scale.

These mechanisms are particularly acute and aggravated when the contraction is achieved freely

downstream of the inflow control device or in its absence. Such free and rapid contraction of the stream is extremely sensitive to small external disturbances that lead to its unsteadiness, i.e., causing it to appear "randomly" in time and space inside the duct.

A detailed discussion which leads to this conclusion is contained in Chapter VII. When a controlled and confined contraction of the stream is introduced downstream of the inflow control device, such as in the cases of the large bellmouth-type inlet, it is possible to suppress the most undesirable flow modules substantially. Even a smaller area ratio confined contraction of two to one downstream of the inflow control device is likely to achieve the desired effect. While we recognise the problems with the acoustic modeling of such an arrangment, it is obviously a closer modeling from the fluid mechanics point of view. In any case, the results completely refute the mechanism based on atmospheric turbulence originally proposed by Hanson (1977).

In summary, the results of this study, though obtained at low velocity, are considered qualitatively applicable, to more realistic conditions. The identification of the various flow modules, in particular the generalized surface vorticity sources, is a key factor in understanding the environment surrounding the actual test facilities. The flight-type inlet should not

be used for static ground tests, in view of the undesirable flow separation associated with it. The design of a bellmouth-type inlet is, therefore, strongly recommended. A compromise between the two main aspects of the problem, namely the acoustics and the fluid dynamics, is necessary. Acoustical compromises, such as the modification of the inlet geometry or the insertion of an inflow control device, may be accounted for properly. For example, a far-field calibration of the modified facility may be performed with a known sound source replacing the fan inside the engine assembly. An approach incorporating the various suggestions made here may lead to a significant improvement in the quality of the results obtained in static ground tests.

APPENDIX A

DESIGN AND CONSTRUCTION OF FAN INLETS

DESIGN AND CONSTRUCTION OF FAN INLETS

Several ducted-fan inlets are used in the present investigation. A brief description of their design is given in the following parts. Earlier chapters detail how these inlets were used in the parametric tests.

Flight-Type Inlet, Fo

This inlet is a scaled-down version of the JDT-15 jet engine inlet tested at NASA Lewis Research Center. The scaling ratio is 1.4 to 1. It consists of a straight duct on which a blunt edge of constant radius equal to 1.52 cm was glued. A flange is attached to the other end to allow easy handling and assembling to the rest of the facility. The whole assembly is made out of plexiglass. The inlet is shown schematically in Figure 73. Also included on that figure are the various dimensions of the IIT model and the NASA JDT-15 inlet.

Small Bellmouth-Type Inlets, Bh and Bm

These two inlets differ from each other by the type of edge. "Bh" has a sharp edge and "Bm" is a modified version on which a smooth lip section has been attached. The common part to both inlets is shaped like a horn spun out of sheet metal. A flange is secured to one end for easy assembly to the rest of the facility.

The smooth lip attached to the modified version, Bm, consists of a wooden ring machined to a proper profile.

This ring is glued to the back of the lip. The joint between the wood and the metal was filled with body filler and sanded smooth. Schematics of both small bellmouth-type inlets are given in Figure 74, showing the various dimensions.

Large Bellmouth-Type Inlet, Co

This inlet consists of three components assembled together: a large bellmouth, a straight duct and a contraction. The schematic of all three parts is given in Figure 75, along with the design specifications. An assembly drawing is given in Figure 76.

The bellmouth part was machined out of styrofoam. Its profile is a combination of two ellipses. Each of the ellipses has a major to minor axis ratio of 1.5. The minor axis of the larger of the two ellipses (outer) matches the major axis of the smaller (inner) one. The surface of the styrofoam was coated with epoxy resin to provide a smooth surface and prevent accidental clipping of the styrofoam. All striations and corrugations were filled with polyester filler (body filler), sanded smooth and recoated with expoxy. Finally, the bellmouth was sprayed with matt-black paint to provide a dark background for the visualization study. A wooden backing and studs were glued to the back of the bellmouth to facilitate its assembly to the rest of the facility.

The center portion of the inlet is a 15 cm diameter

ght duct with flanges at both ends. It provides adequate space for housing various types of flow manipulators.

The contraction part was fabricated using the same materials and techniques as the large bellmouth. A fifth-order polynomial profile was chosen based on the work of Tan-atichat (1980). To add rigidity to the assembly, eight equally spaced ribs are secured around the outer circumference of the contraction. Flanges and studs were also glued to both ends. The contraction gradually reduces the large diameter of the bellmouth to the standard diameter of the other inlets and the fan duct.

APPENDIX B

ADJUSTMENT OF THE VORTEX GENERATOR

ADJUSTMENT OF THE VORTEX GENERATOR

The airfoil vortex generator has been used in the past by several experimenters to produce controlled longitudinal vortex disturbances. It is always a good practice to adjust such a device against some reference conditions before using it. The procedure is described in this appendix.

It is necessary to determine the actual reading on the dial and vernier corresponding to the zero angle of attack of the airfoils. In this exercise, the airfoils were pitched as a single wing inside the test section. If the initial nominal setting is truly zero, the mean-velocity profile in the wake of the airfoil must be symmetric. Positioning a hot-wire probe about 25.4 mm downstream of the airfoil's trailing edge, the velocity profile was mapped. Although the velocity profiles are not shown here, they suggested that a symmetric profile lies between 2.0 and 2.5 degrees nominal setting. Ahmed et al. (1976) showed that this method of determining the zero angle of attack is not sensitive to any angle changes less than 0.04 degrees. However, further trials indicated that there was an offset between the dial readings of the two airfoil parts. Finally, the zero angles of attack for the top and bottom airfoil were found to be a reading of 1.8 and 2.2 degrees, respectively.

According to Ahmed et al. (1976), the behavior of the trailing vortex varies with the combination of the half-angle, α, and the free-stream velocity. In order to establish a satisfactory test condition, i.e., 3A, an x-wire probe was placed 1.27 cm downstream of the trailing edge of the airfoil to survey the velocity profiles for different half-angles. Prior to each survey, the above-mentioned basic procedure in checking for symmetry was repeated. Once the desired angle was set, two transverse measurements were recorded both at $x/L = 0.24$ and $x/L = 1.33$ inside the straight duct. The attempts for 8 and 12 degrees suggested an intermediate angle may serve as a good test condition that would permit measurement of the half width of the velocity profiles through the contraction. Hence, a half-angle, α, of 10 degrees was the final choice

APPENDIX C

FIGURES

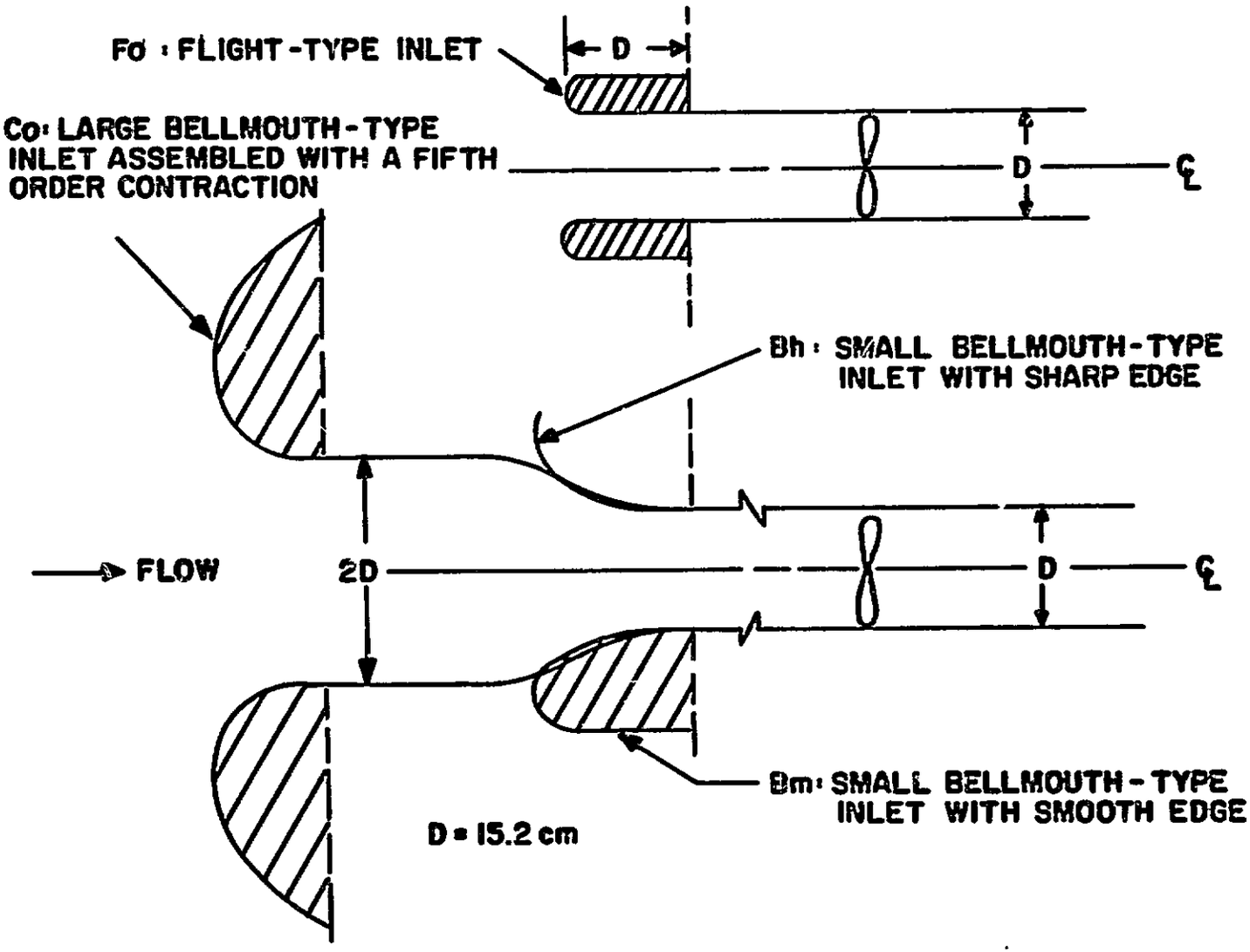

Figure 1. Schematic of Ducted-Fan Inlet Configurations

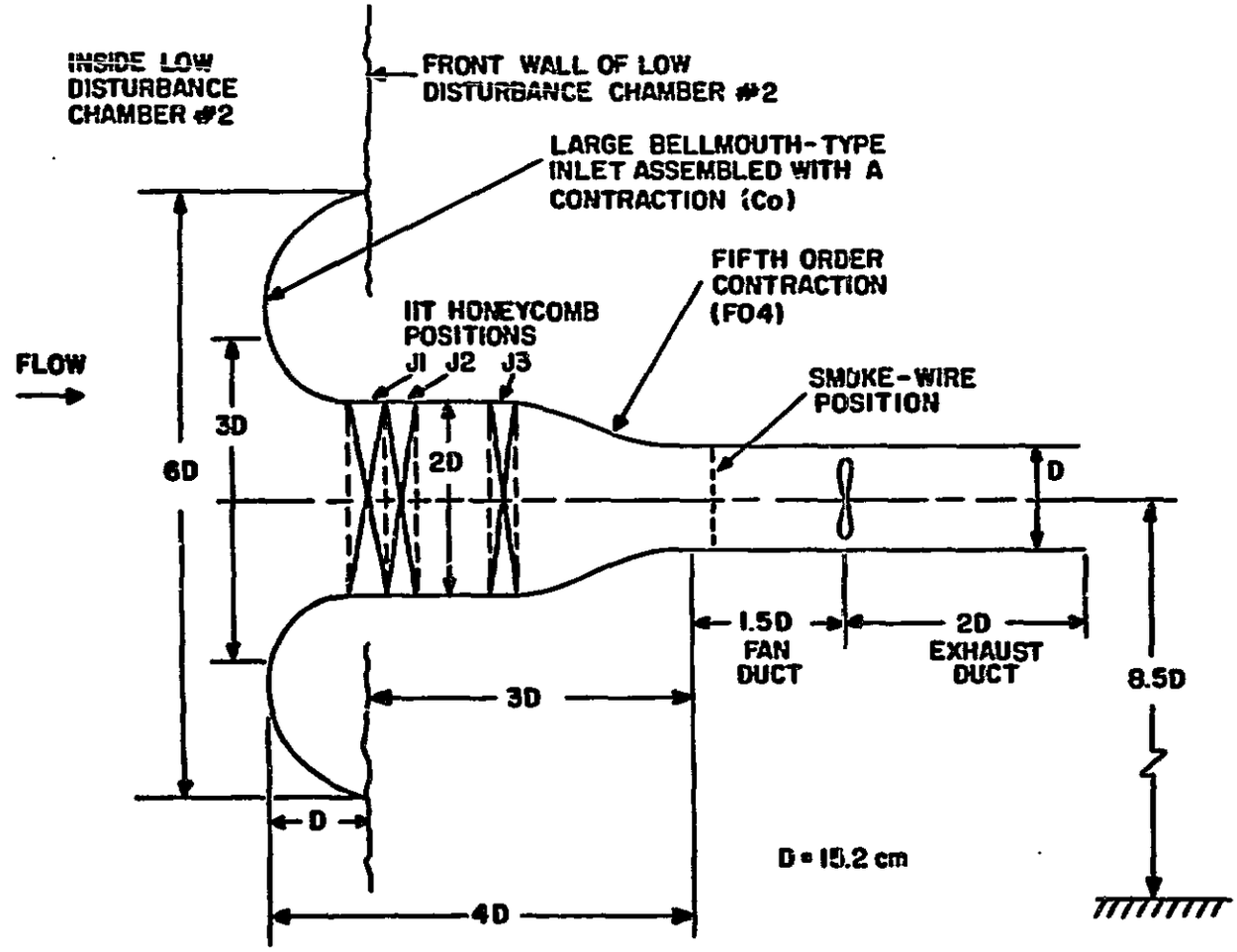

Figure 2. Typical Arrangement of Inlet, Ducted-Fan and Flow Manipulators

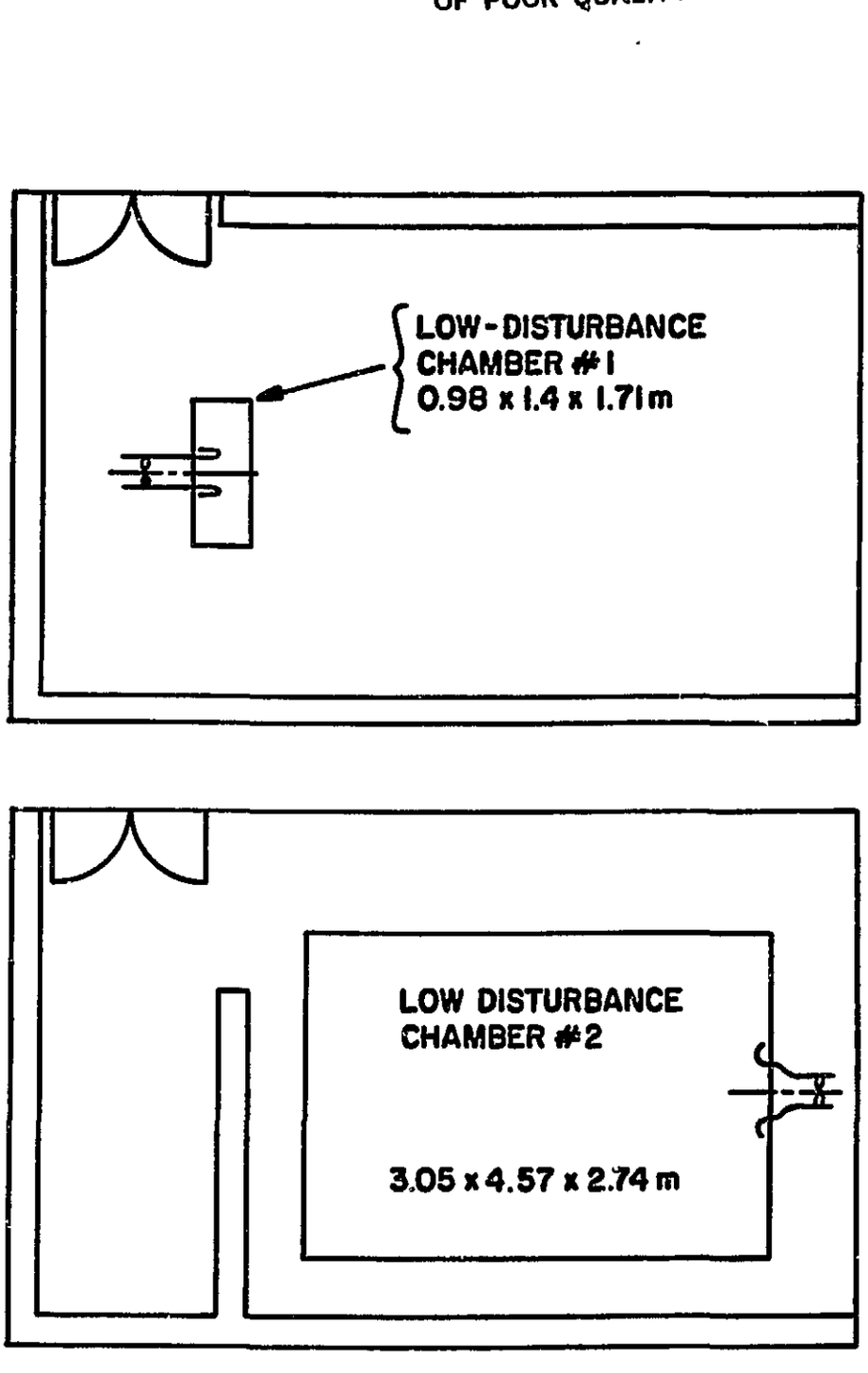

Figure 3. Location of Low-Disturbance Chambers #1 and #2 in Laboratory

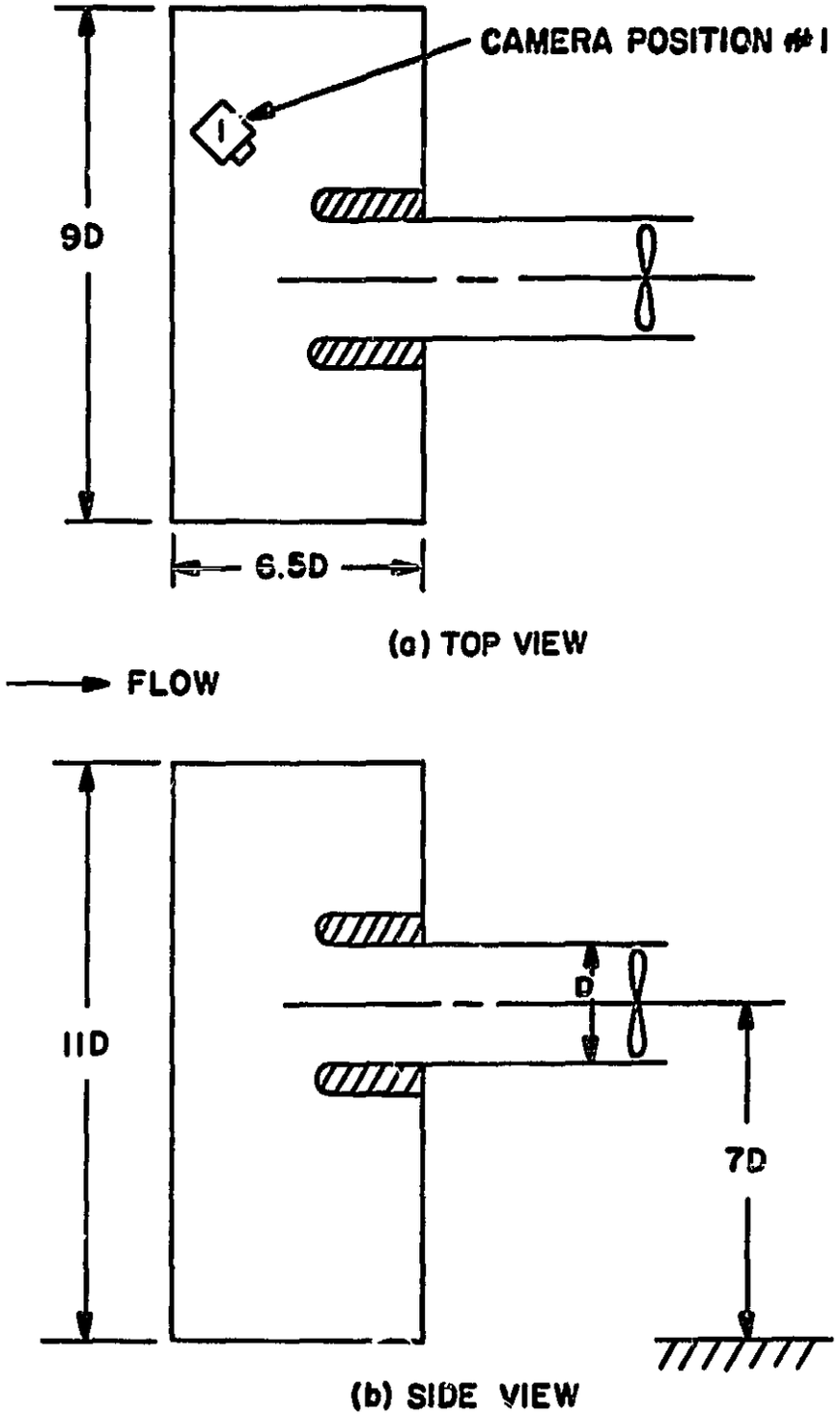

Figure 4. Schematic of Low-Disturbance Chamber #1 for Flow Visualization Facility

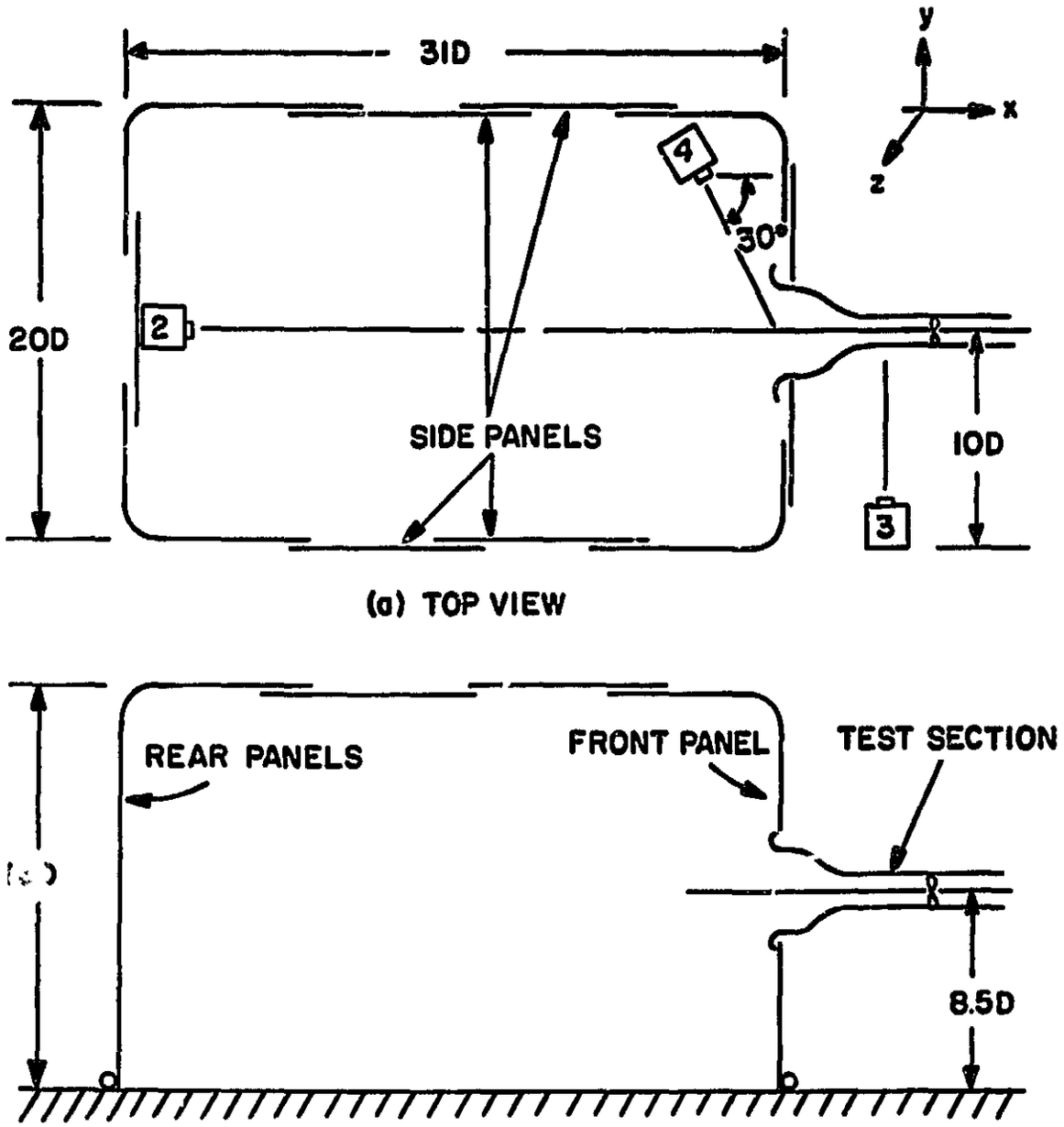

Figure 5. Schematic of Low-Disturbance Chamber #2 for Flow Visualization Facility

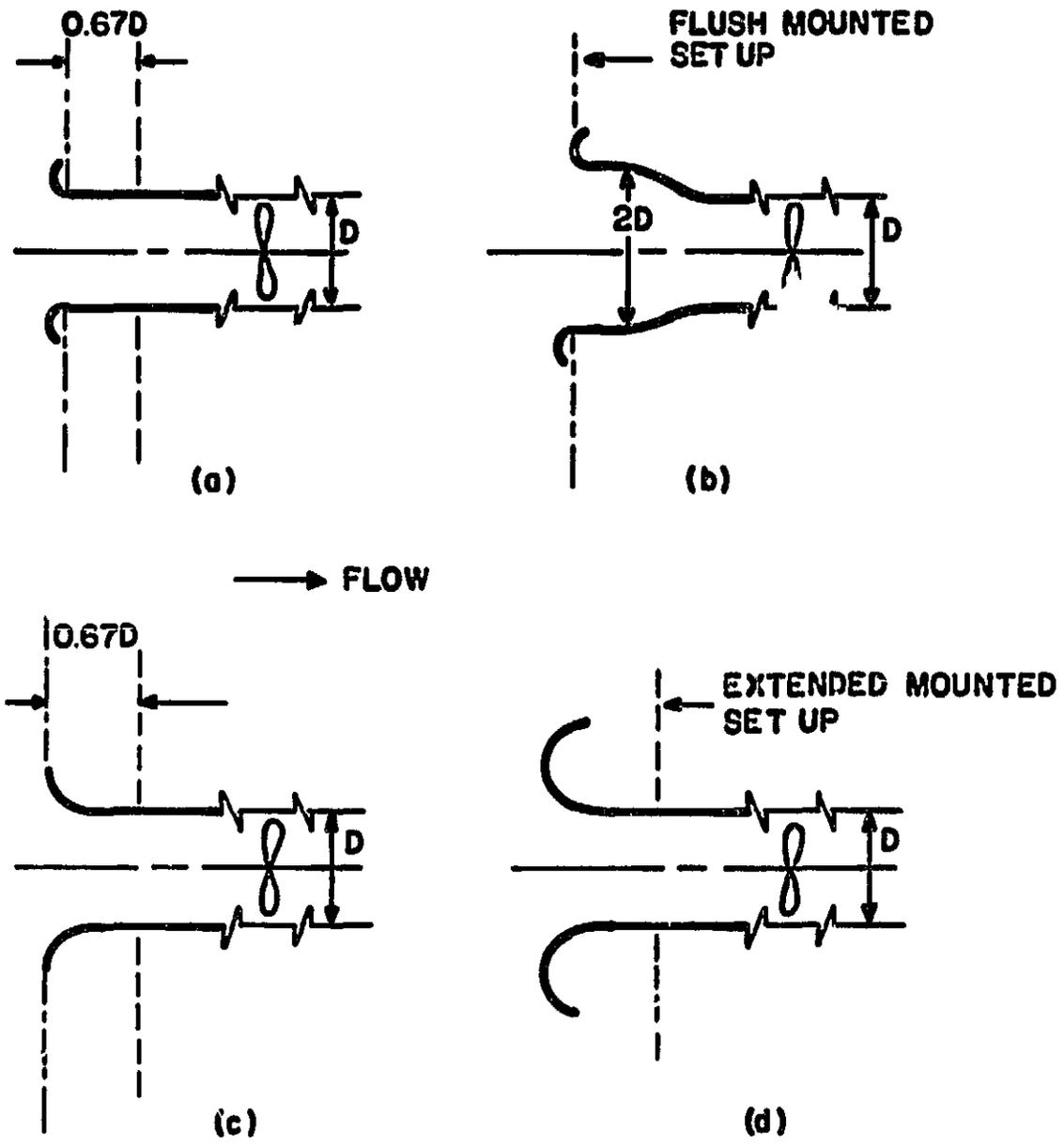

D = 15.2 cm

TYPES OF FAN INLET

(a) FLIGHT - TYPE (b) LARGE BELLMOUTH WITH CONTRACTION

(c) SHARP - EDGE BELLMOUTH

(d) SMOOTH EDGE BELLMOUTH

Figure 6. Schematic of Ducted-Fan Inlet Arrangements

CYLINDER	DIAMETER (cm)	LENGTH (cm)
C1	1.3	90
C2	0.6	104
C3	5.0	17
C4	5.0	35
* C5	5.0	140
C6	19.0	109

*USED FOR EXTENSIVE INVESTIGATIONS

Figure 7. Characteristics of Wake-Disturbance Generators

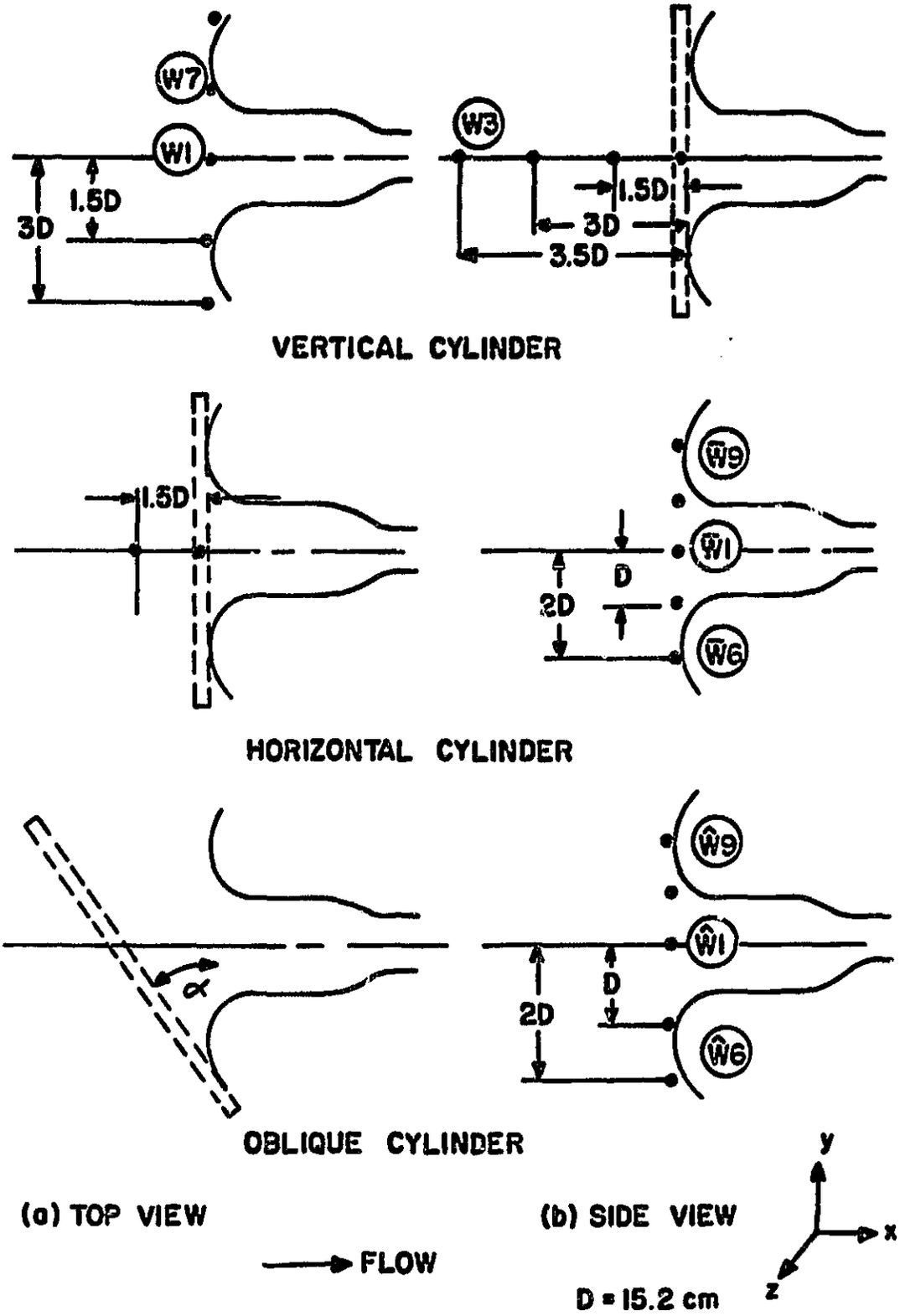

Figure 8. Orientation of Wake-Generating Cylinder (C5; d=5.08 cm, l=1.40 m) Upstream of Inlet

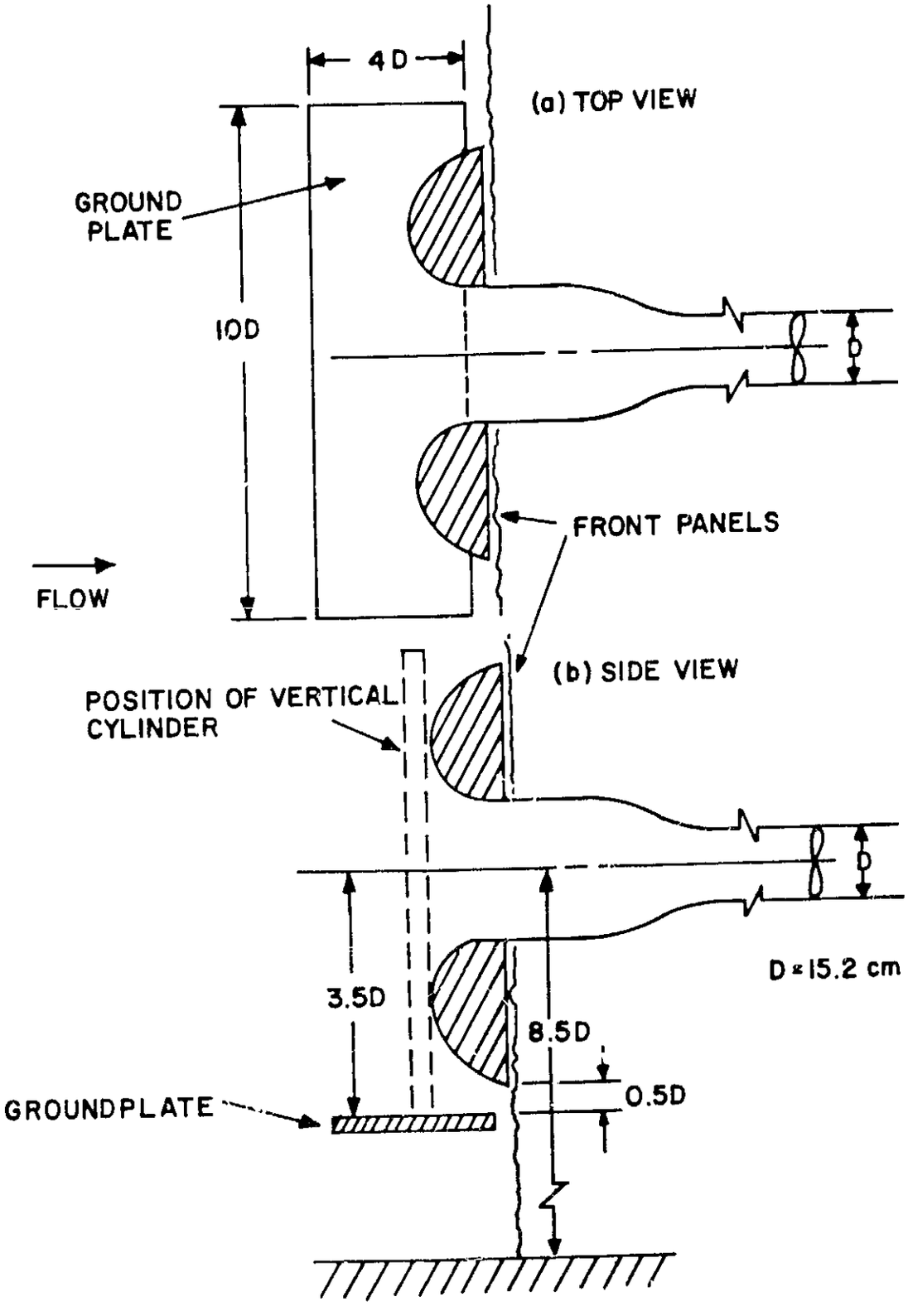

Figure 9. Schematic of Ground Plate

INFLOW CONTROL DEVICE		MESH SIZE M (cm)	THICKNESS (cm)	DIAMETER (cm)
IIT	J	.64	5.1	30.5
	K	.32	3.8	30.5
	P	.64	2.5	15.2
	Q	.32	3.8	15.2
NASA	N	1.0	5.1	90.0

Figure 10. Characteristics of Flow Control Devices

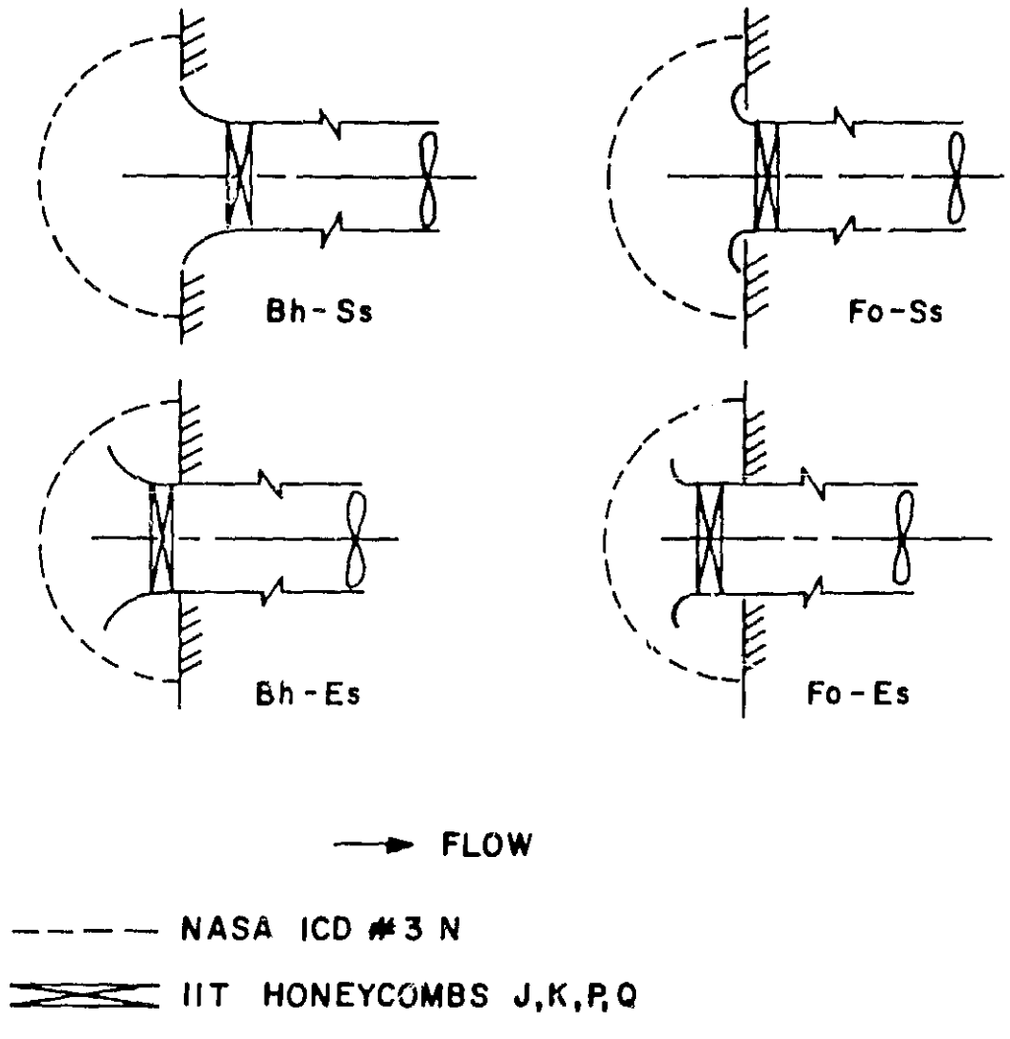

Figure 11. Schematic of Flow Control Device Arrangements

ARRANGEMENT FLOW PASSAGE	ATTACHMENT SET UP	TEST FLOW CONDITION	MANIPULATOR ARRANGEMENT
Fo: FLIGHT-TYPE INLET	Sp: FLUSH SET UP POROUS BACKING	Ll: CONTROLLED DISTURBANCE CONDITION	Ol: NO MANIPULATOR
Bl: SMALL BELL-MOUTH TYPE INLET WITH SHARP EDGE	Ss: FLUSH SET UP SOLID BACKING	CONTROLLED HIGH DISTURBANCE COND. HI: PERSON H4: CHAIR & SIDE PANELS H8: FAN BLOWING INSIDE	30.5 cm DIAMETER HONEYCOMB J1, J2, J3, K1, K2
Bm: SMALL BELL-MOUTH TYPE INLET WITH SMOOTH EDGE	Ep: EXTENDED SETUP POROUS BACKING	SURFACE VORTICITY SOURCE CONDITION Vg: GROUND PLATE Vp: SIDE PANELS Vr: REAR PANELS	15.2 cm DIAMETER HONEYCOMB P1, P2, Q1, Q2
Co: LARGE BELL-MOUTH TYPE INLET WITH A CONTRACTION	Es: EXTENDED SET UP SOLID BACKING	WAKE DISTURBANCE CONDITION W1: VERTICAL CYLINDER $\bar{W}$9: HORIZONTAL CYLINDER $\hat{W}$6: INCLINED CYLINDER	NASA INFLOW CONTROL DEVICE (ICD #3) N1: HEMISPHERICAL HONEYCOMB

Figure 12. Combinations of Flow Inlets, Test Flow Conditions, Flow Manipulators and Their Arrangements

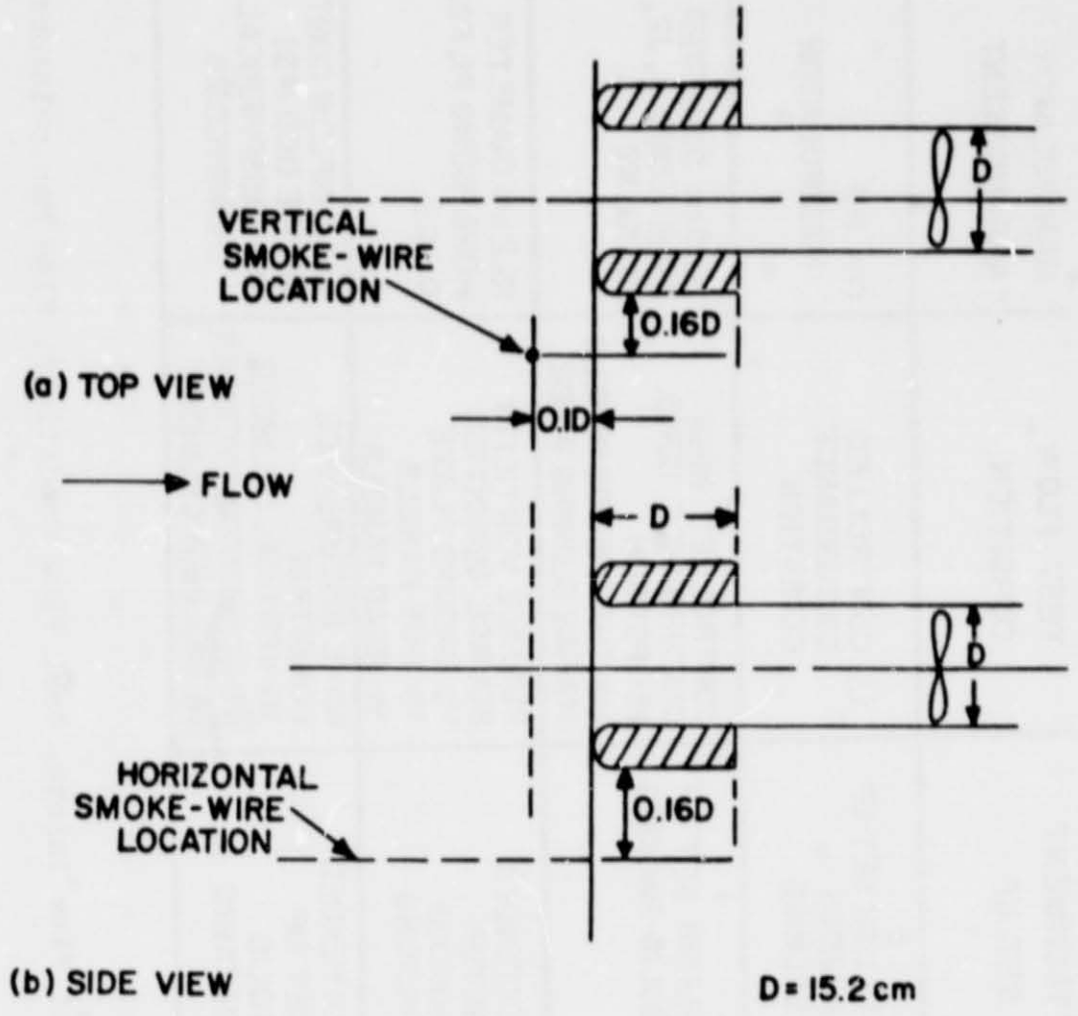

Figure 13. Smoke-Wire Orientations in Low-Disturbance Chamber #1

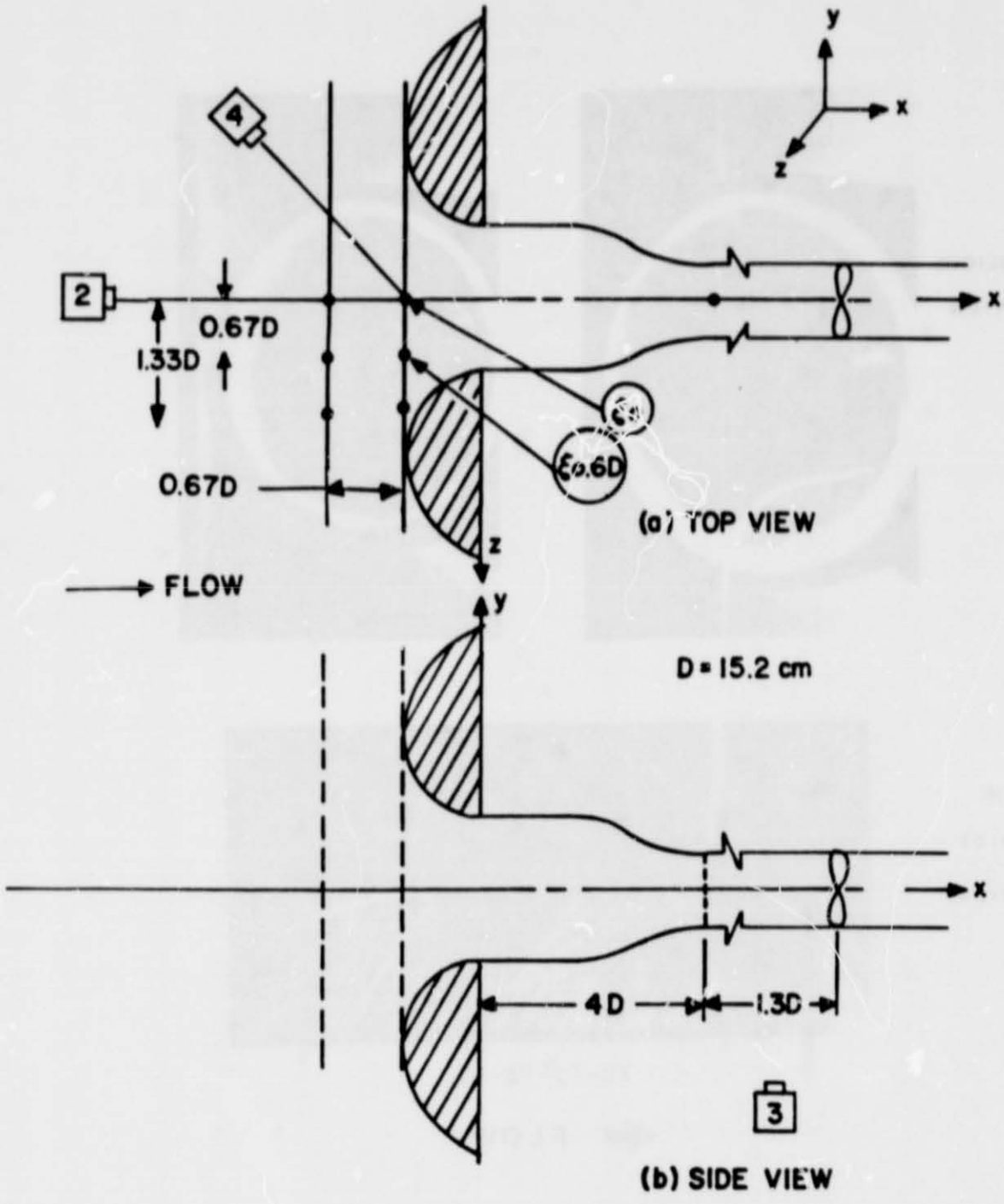

Figure 14. Smoke-Wire Orientations in Low-Disturbance Chamber #2

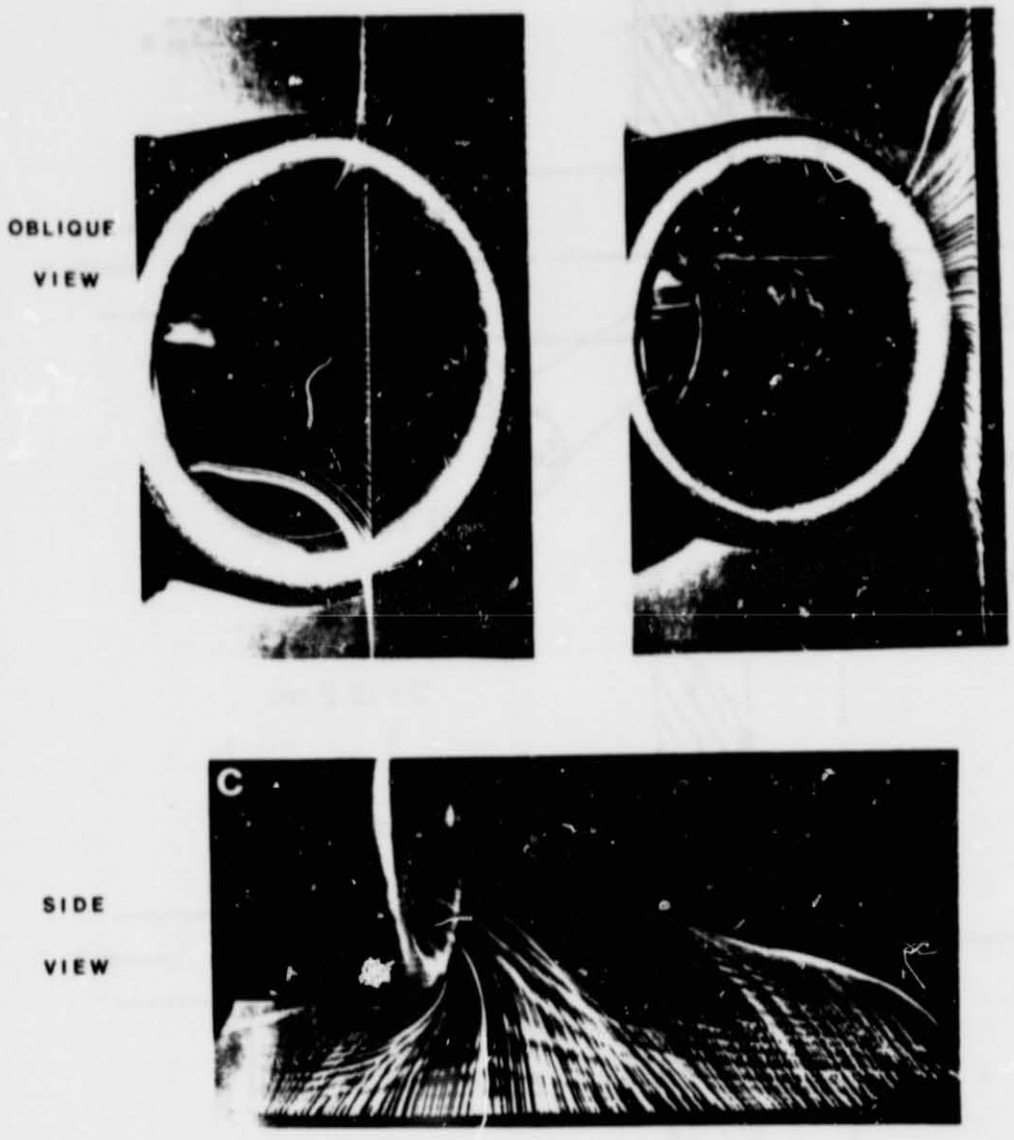

Figure 15. Oblique and Side-View Visualization of Incoming Flow Into a Flight-Type Inlet

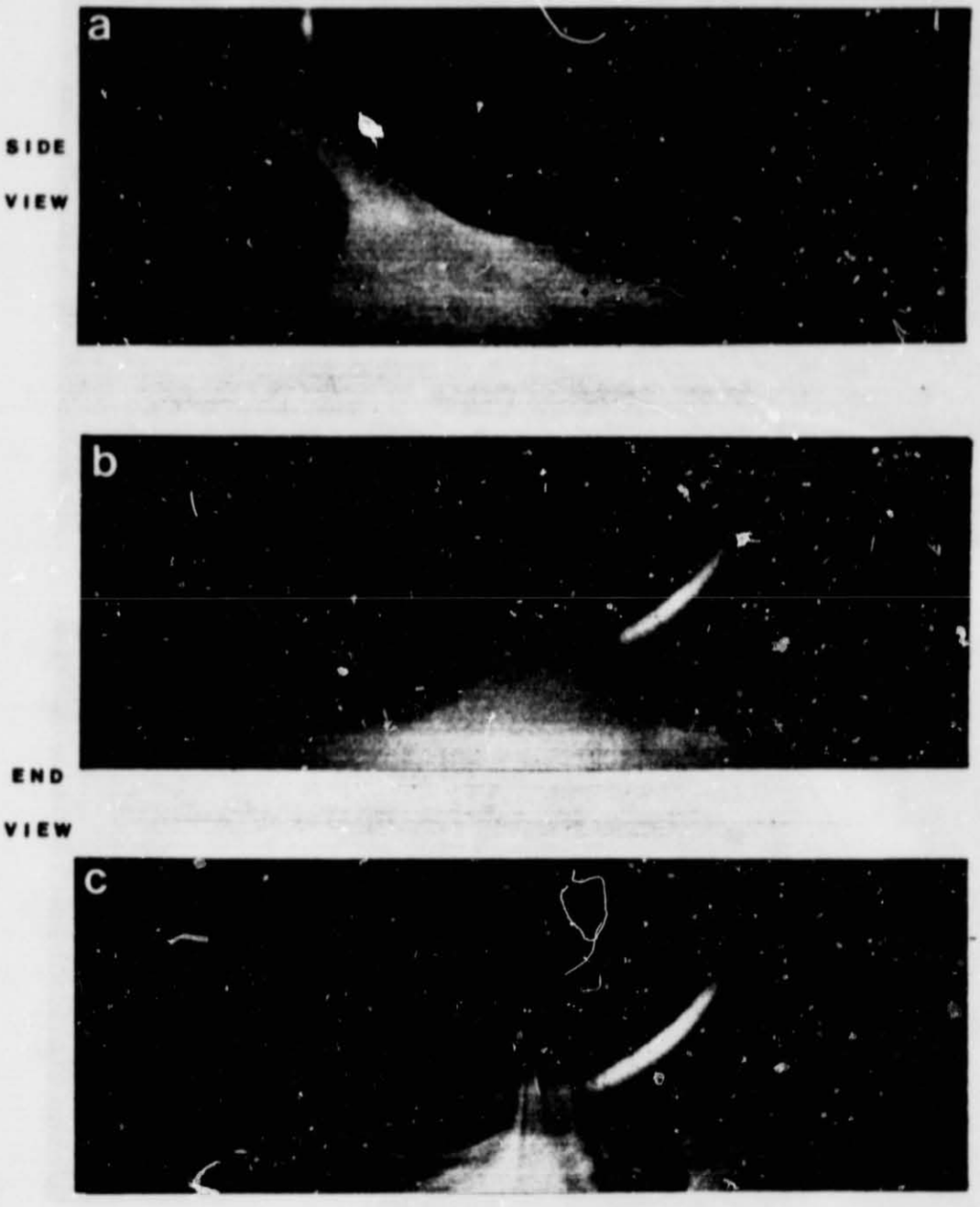

Figure 16. Ingestion of Smoke-Labeled Surface Vorticity Into a Bellmouth-Type Inlet

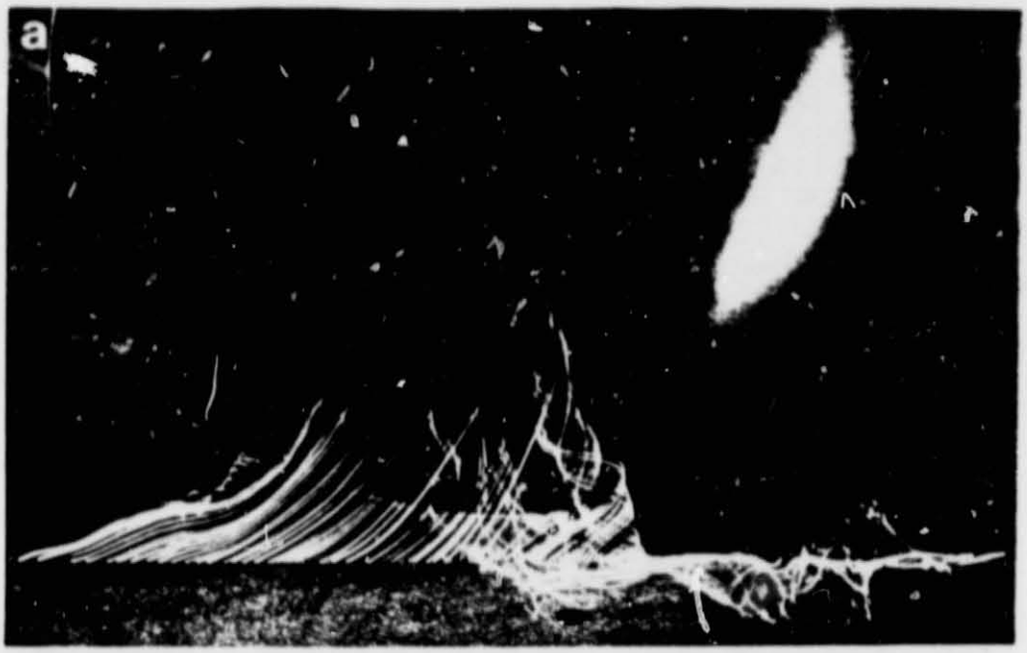

END VIEW

Bh-Ep-Vg-01

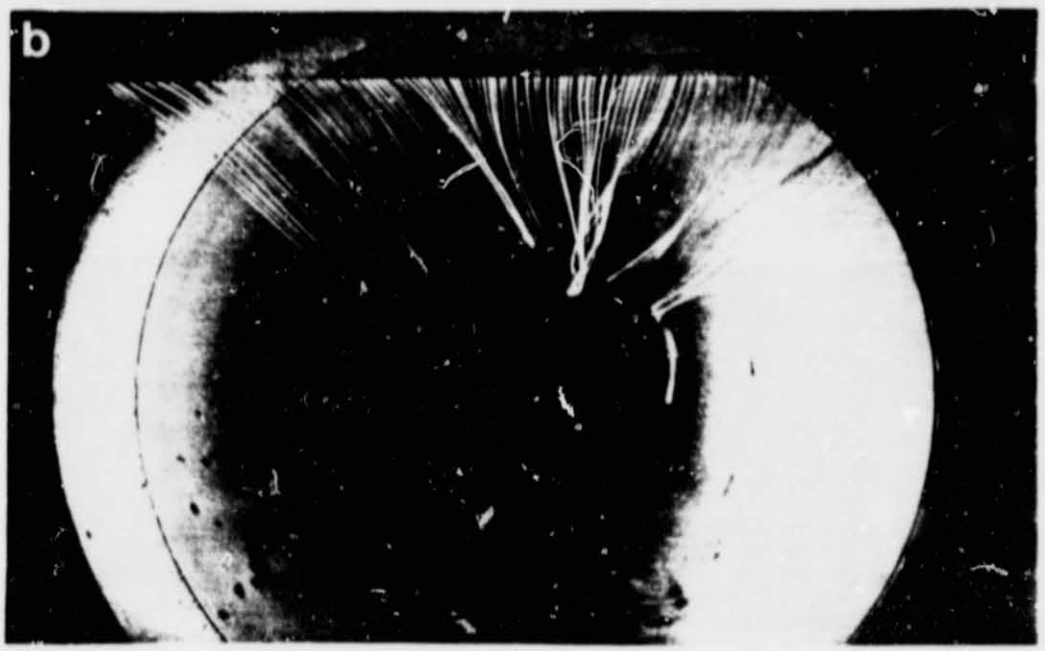

Bm-Ep-Vg-01

Figure 17. End-View Visualization of Stretched Longitudinal Vortex Entering Bellmouth-Type Inlet With (a) Sharp Edge, and (b) Smooth Edge

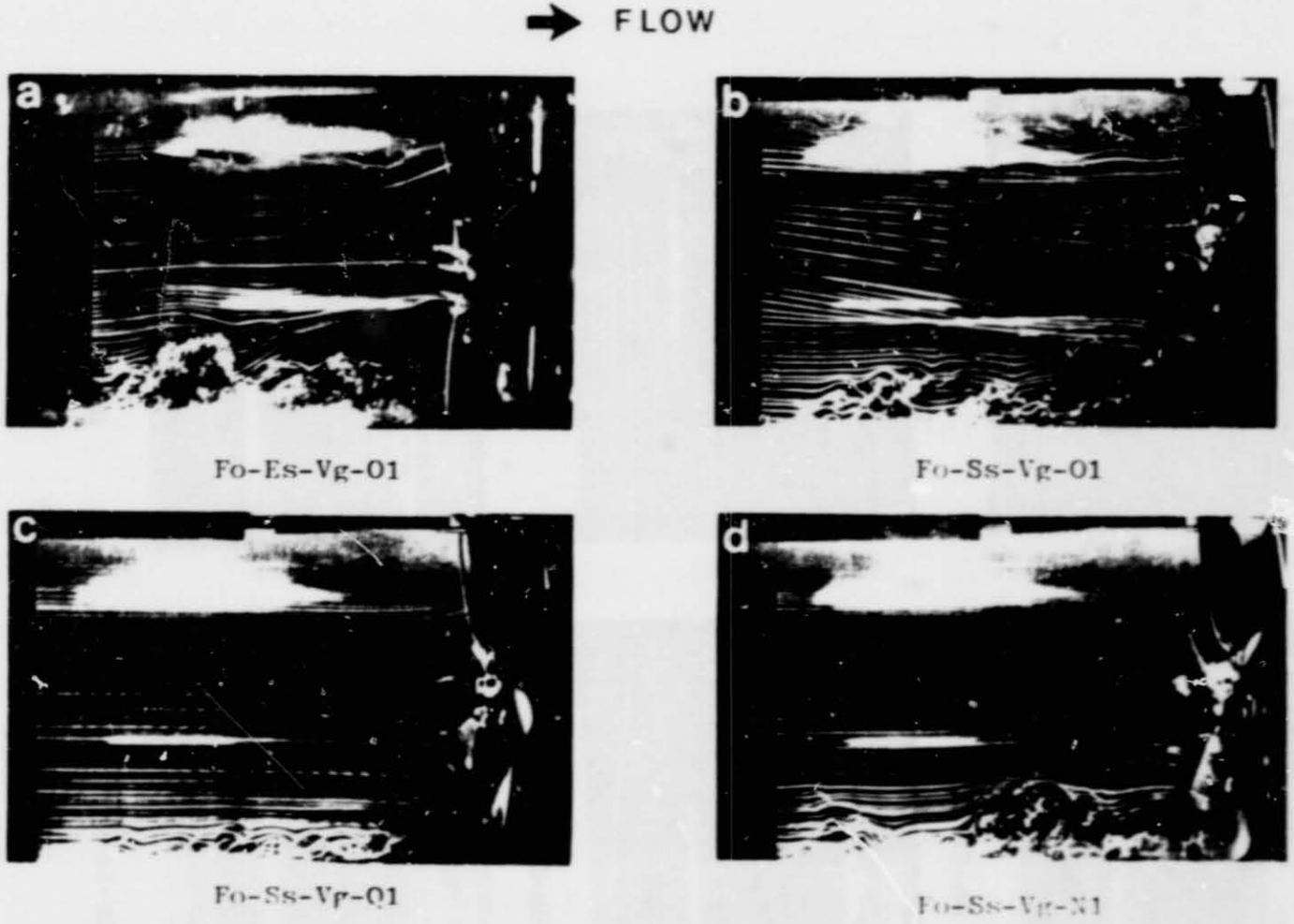

Fo-Es-Vg-01

Fo-Ss-Vg-01

Fo-Ss-Vg-01

Fo-Ss-Vg-X1

Figure 18. Side-View Visualization of Flow Inside Flight-Type Inlet for both Extended- and Flush-Mounted Setup With and Without Flow Control Devices

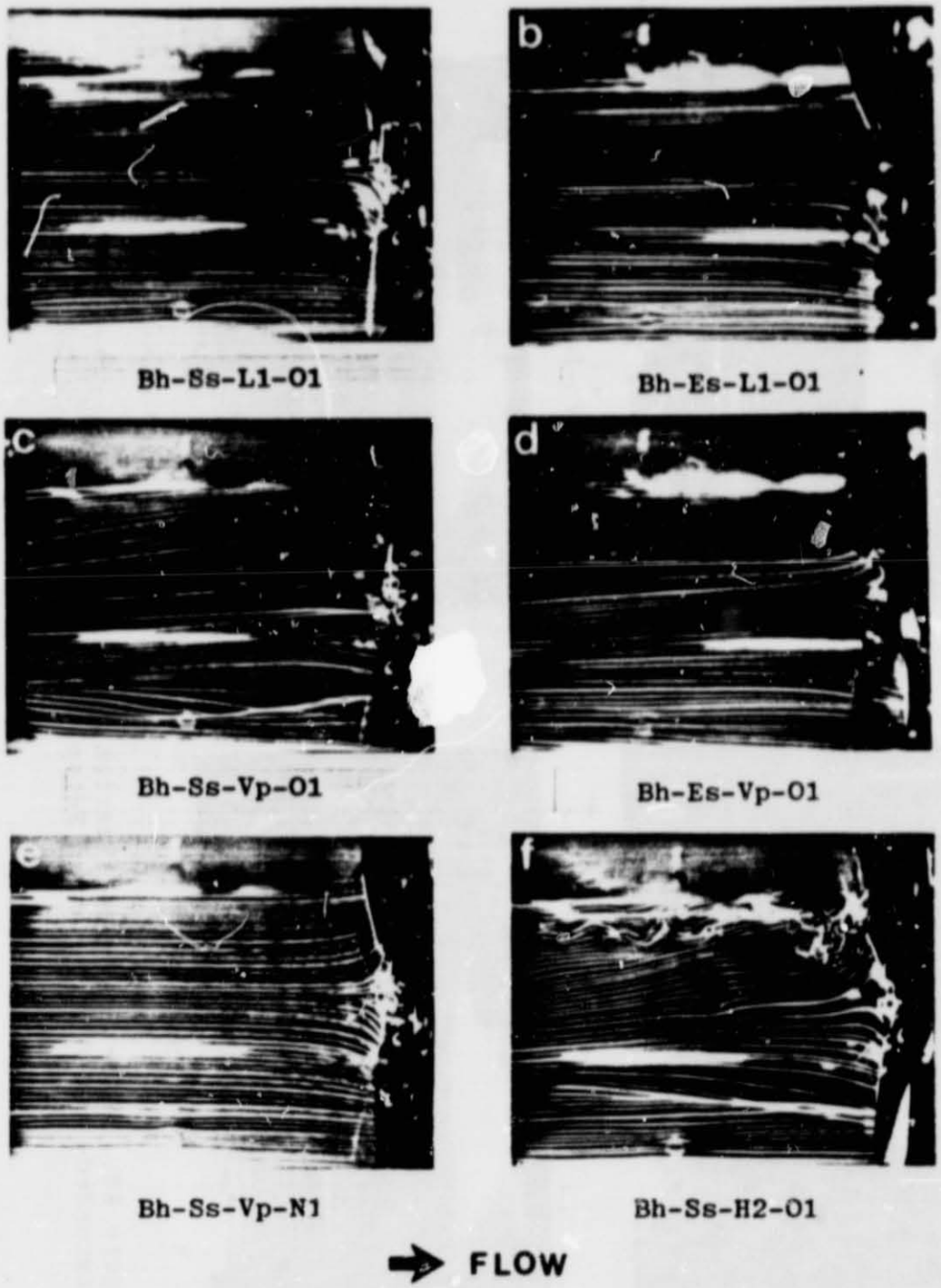

Figure 19. Side-View Visualization Comparing Both Extended- and Flush-Mounted Setup for Bellmouth-Type Inlet for Various Test Flow Conditions.

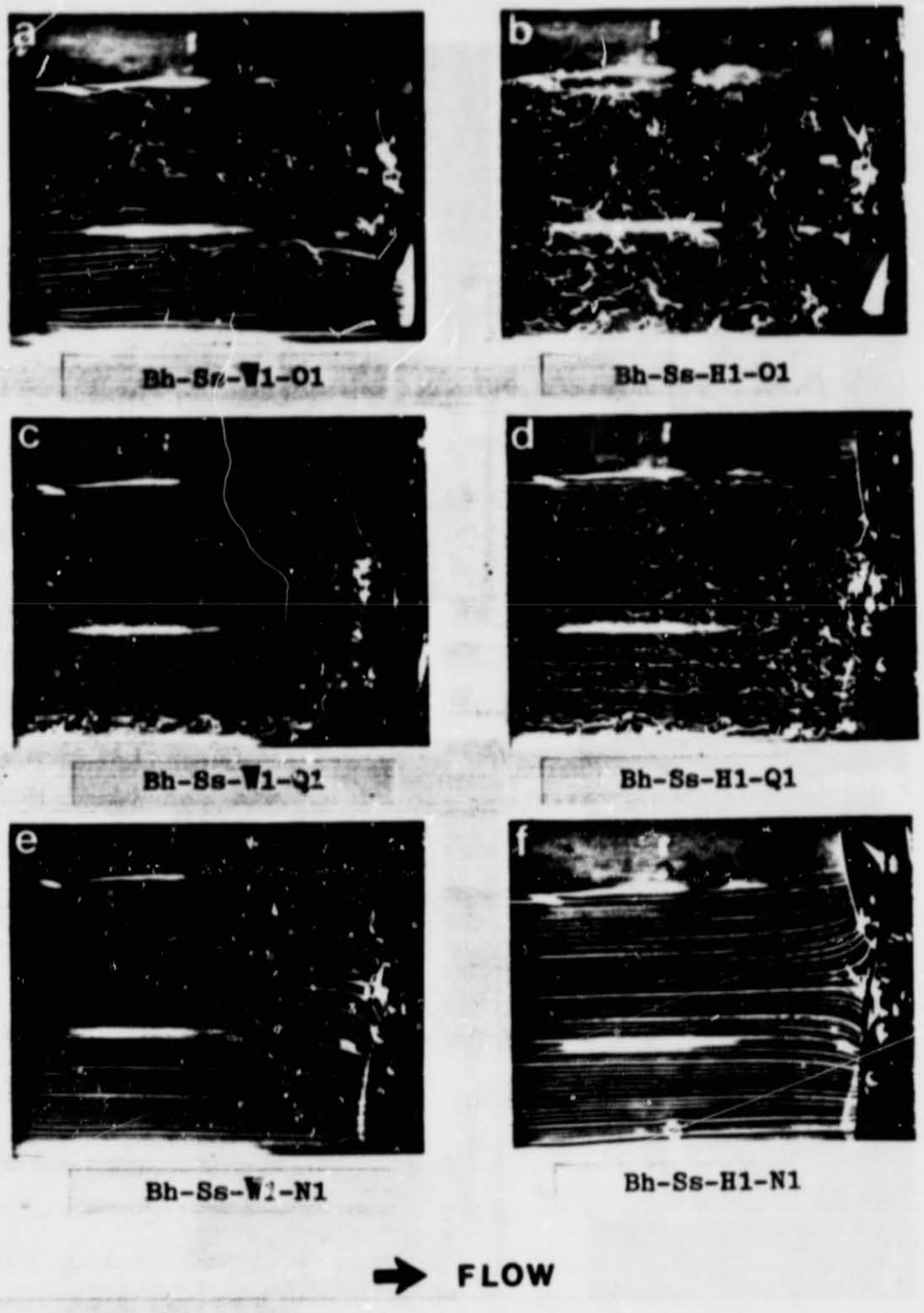

Figure 20. Side-View Visualization of Flush-Mounted, Bellmouth-Type Inlet With Sharp Edge for Various Test Flow Conditions With and Without Inflow Control Devices

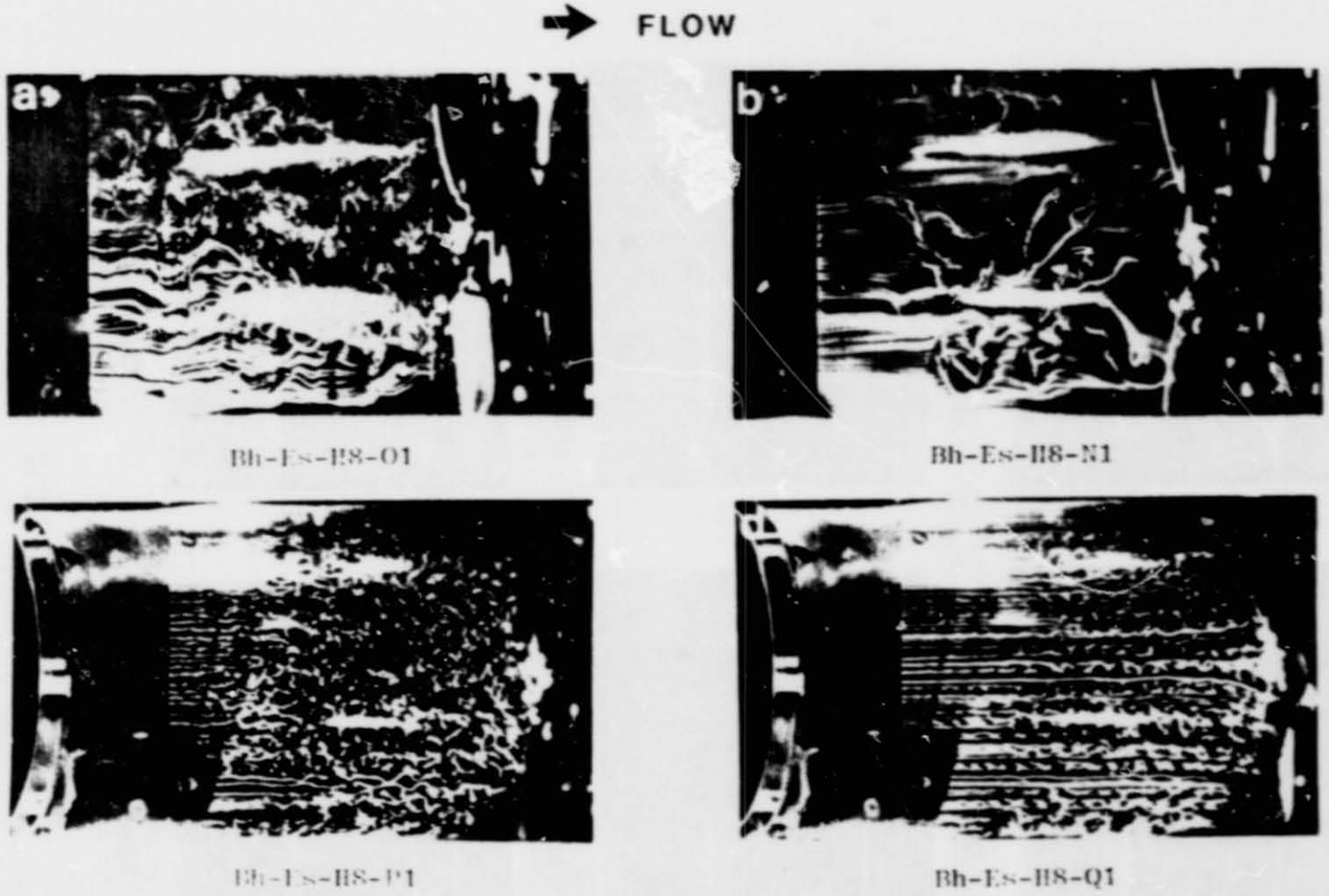

Figure 21. Side-View Visualization of Extended-Mounted Bellmouth-Type Inlet With Sharp Edge for Highly Disturbed Test Conditions With Various Inflow Control Devices

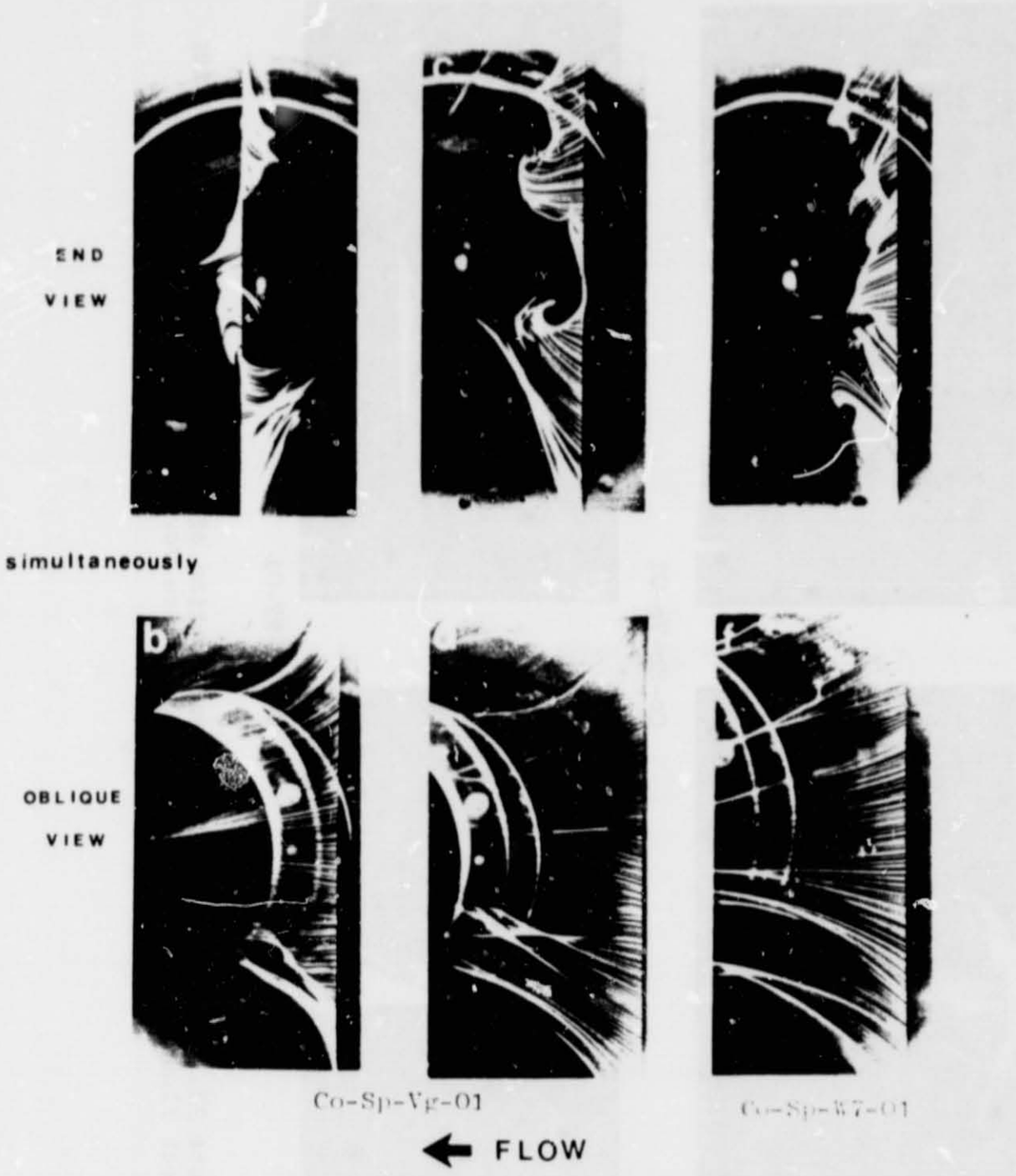

Figure 22. Simultaneous Oblique and End-View Visualization of Large Bellmouth-Type Inlet for Test Flow Conditions Introducing Surface Vorticity and Wake Disturbances

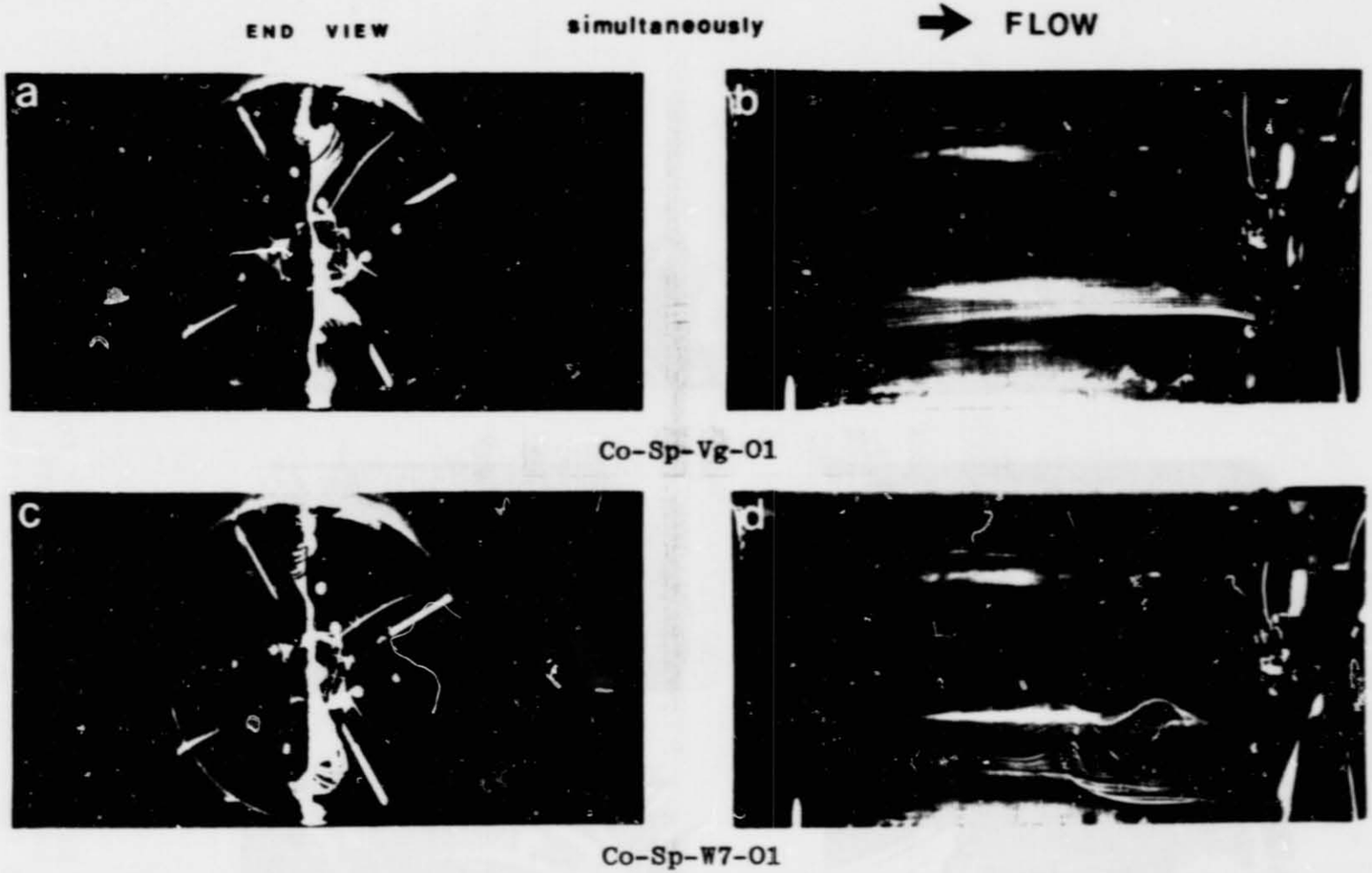

Figure 23. End and Side-View Visualization of Large Bellmouth-Type Inlet for Test Flow Conditions Introducing Surface Vorticity and Wake Disturbance

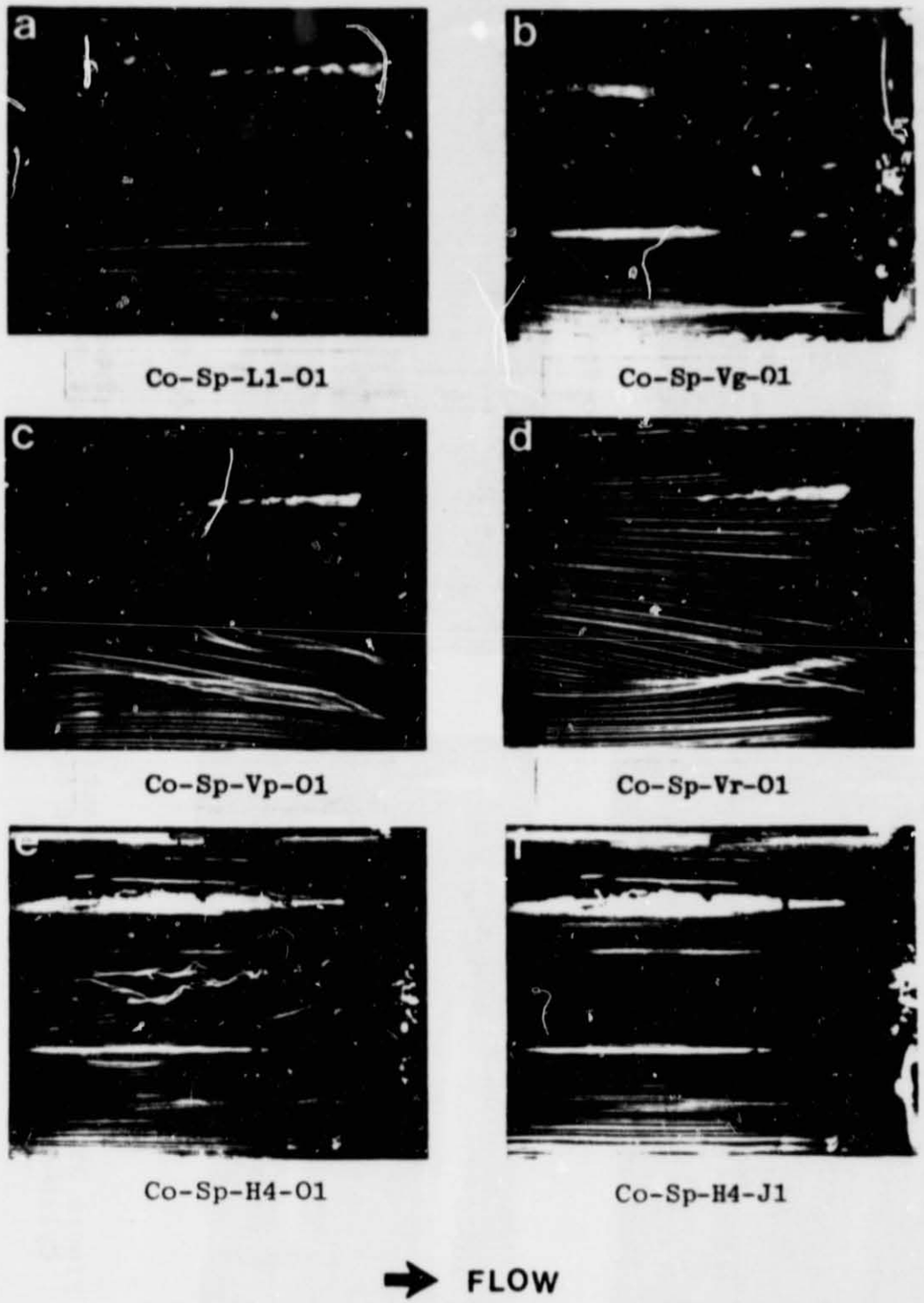

Figure 24. Side-View Visualization of Large Bellmouth-Type Inlet for Various Test Flow Conditions With and Without Inflow Control Devices

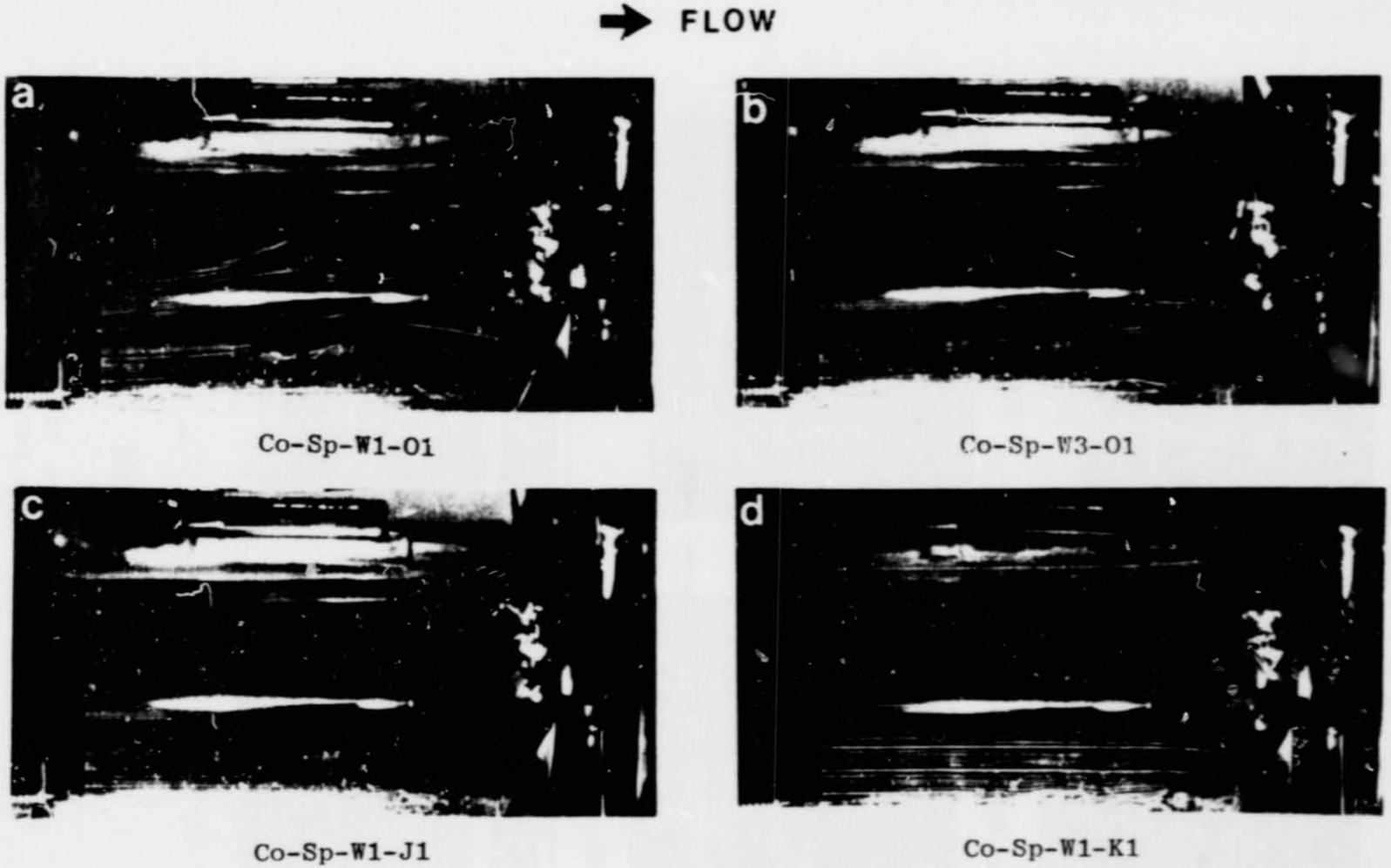

Figure 25. Side-View Visualization of Large Bellmouth-Type Inlet for Cylinder-Wake Test Flow Condition With and Without Inflow Control Devices

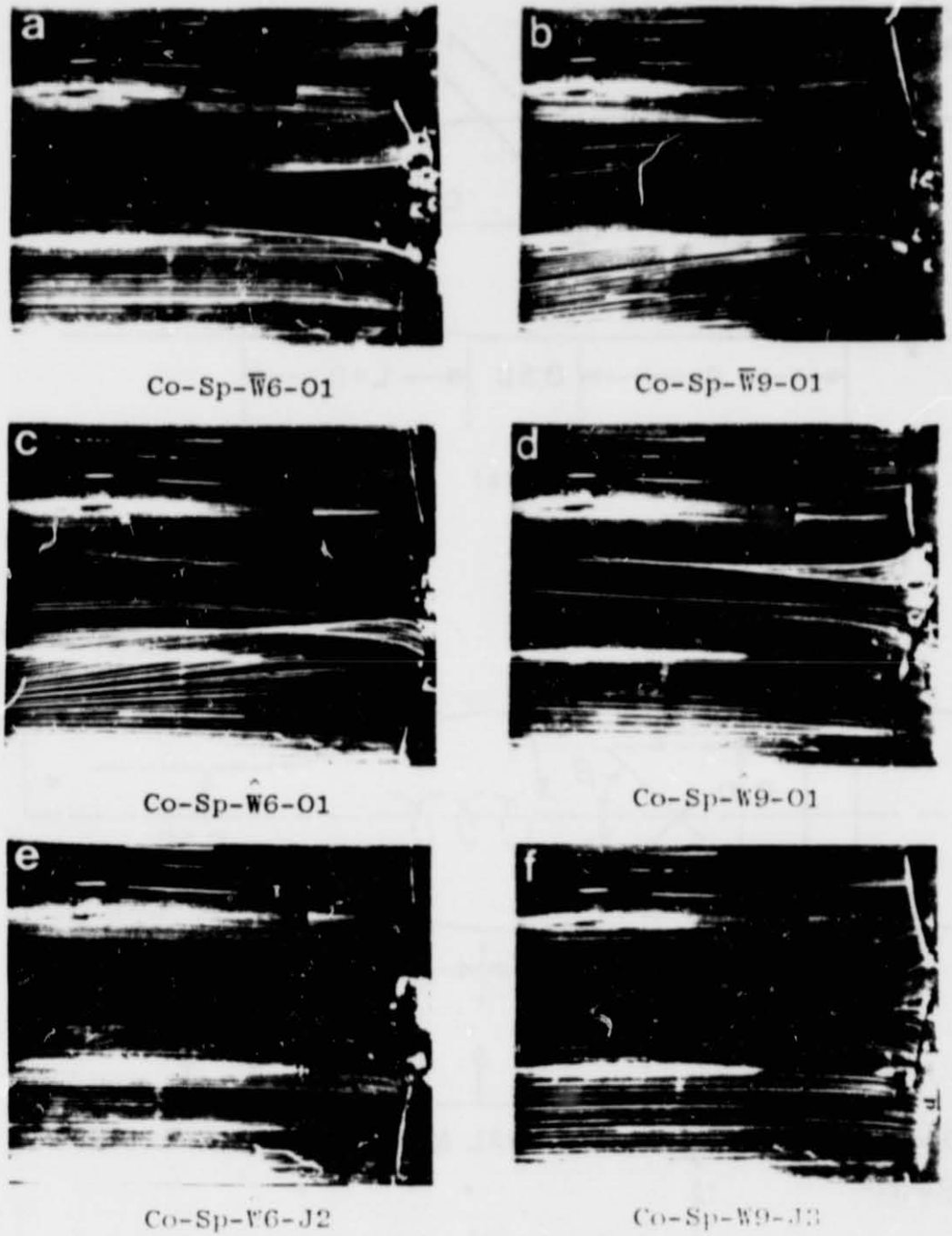

Figure 26. Side-View Visualization of Large Bellmouth-Type Inlet For Flush-Mounted Flow Conditions With and Without Inflow Control Devices

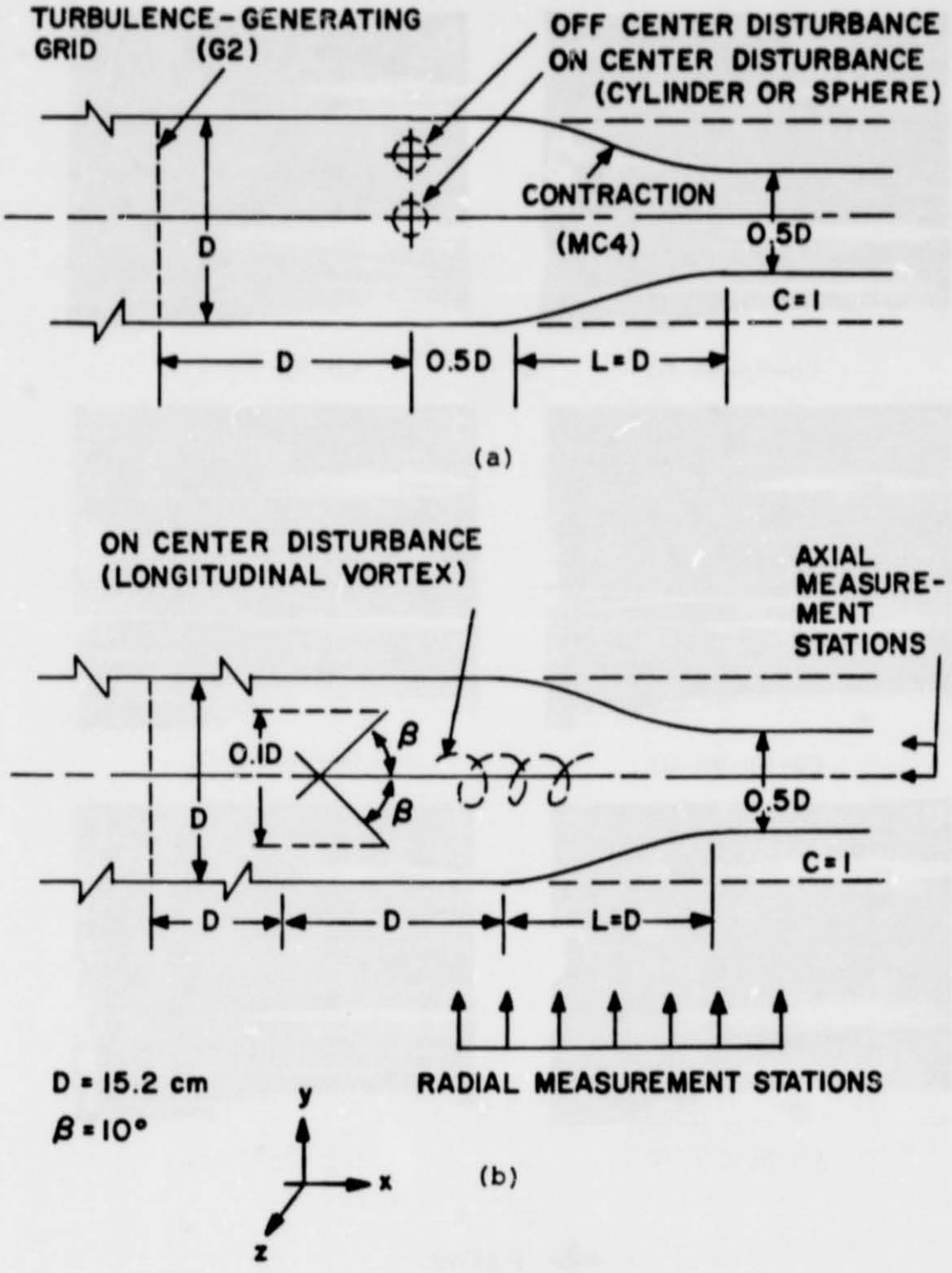

Figure 27. Setup for Investigation of Isolated Disturbance Through a Contraction

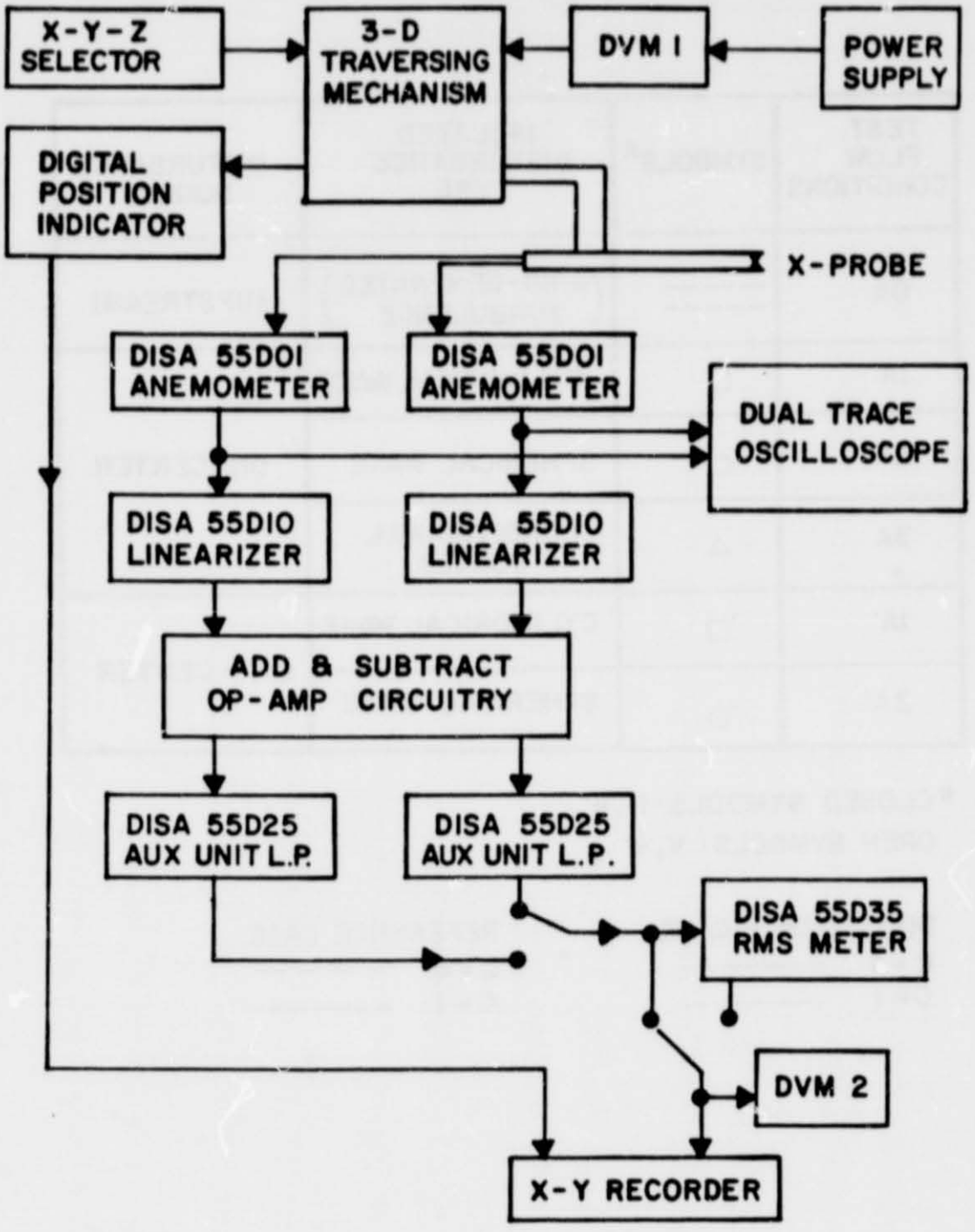

Figure 28. Circuit Diagram for Analog Measurement of Velocity

TEST FLOW CONDITIONS	SYMBOLS*	ISOLATED DISTURBANCE TYPE	DISTURBANCE SOURCE
OA	— — — / - - - - -	(GRID-GENERATED TURBULENCE)	(UPSTREAM)
IA	□	CYLINDRICAL WAKE	ON-CENTER
2A	○	SPHERICAL WAKE	
3A	△	LONGITUDINAL VORTEX	
IA'	□	CYLINDRICAL WAKE	OFF-CENTER
2A'	○	SPHERICAL WAKE	

*CLOSED SYMBOLS: U, u'
OPEN SYMBOLS: V, v'

DISTURBANCE CASE		REFERENCE CASE	
C = 4	————	C = 4	— — — —
C = 1	—·—·—	C = 1	- - - - - - -

Figure 29. Summary of Test Flow Conditions for Isolated Disturbances

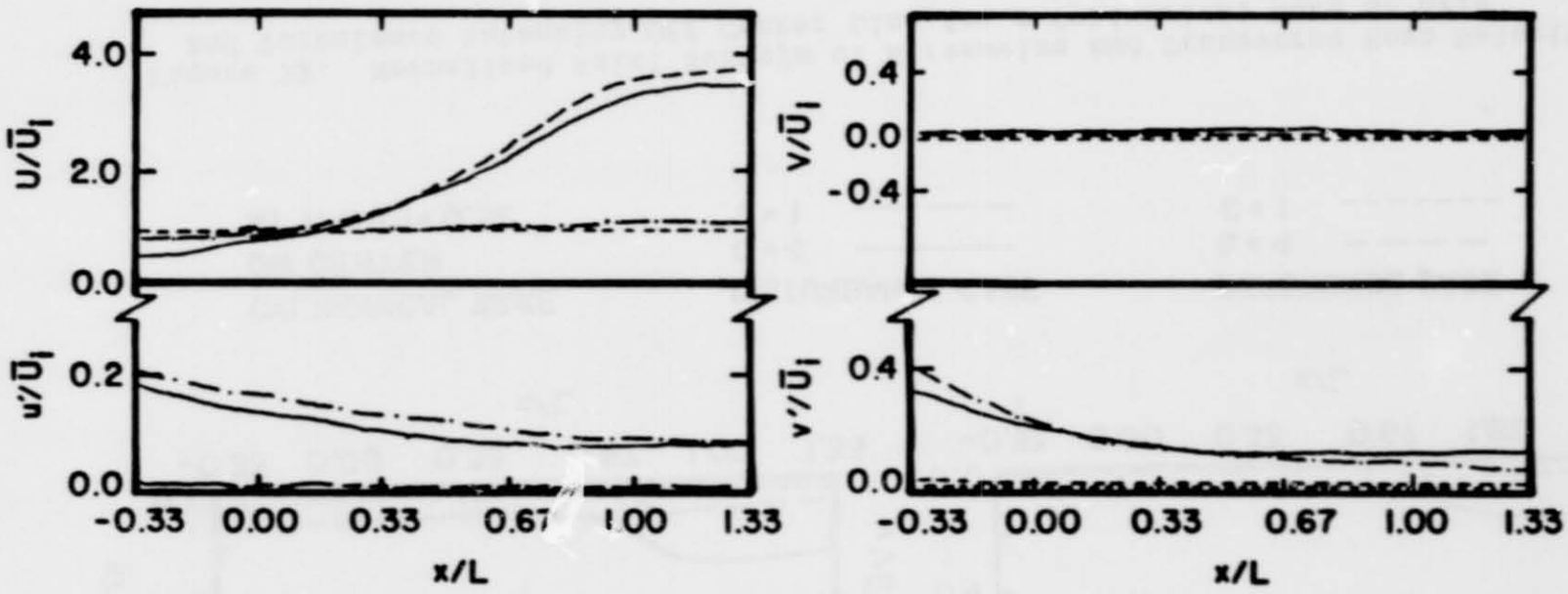

CYLINDRICAL WAKE ON CENTER AT r/R(0) = 0.	DISTURBANCE CASE	REFERENCE CASE
	C = 4 ————	C = 4 – – – –
	C = 1 —·—·—	C = 1 -------

Figure 30. Normalized Axial Surveys of Streamwise and Transverse Mean Velocity and Turbulence Intensity Along Center Line for a Cylindrical Wake on Axis

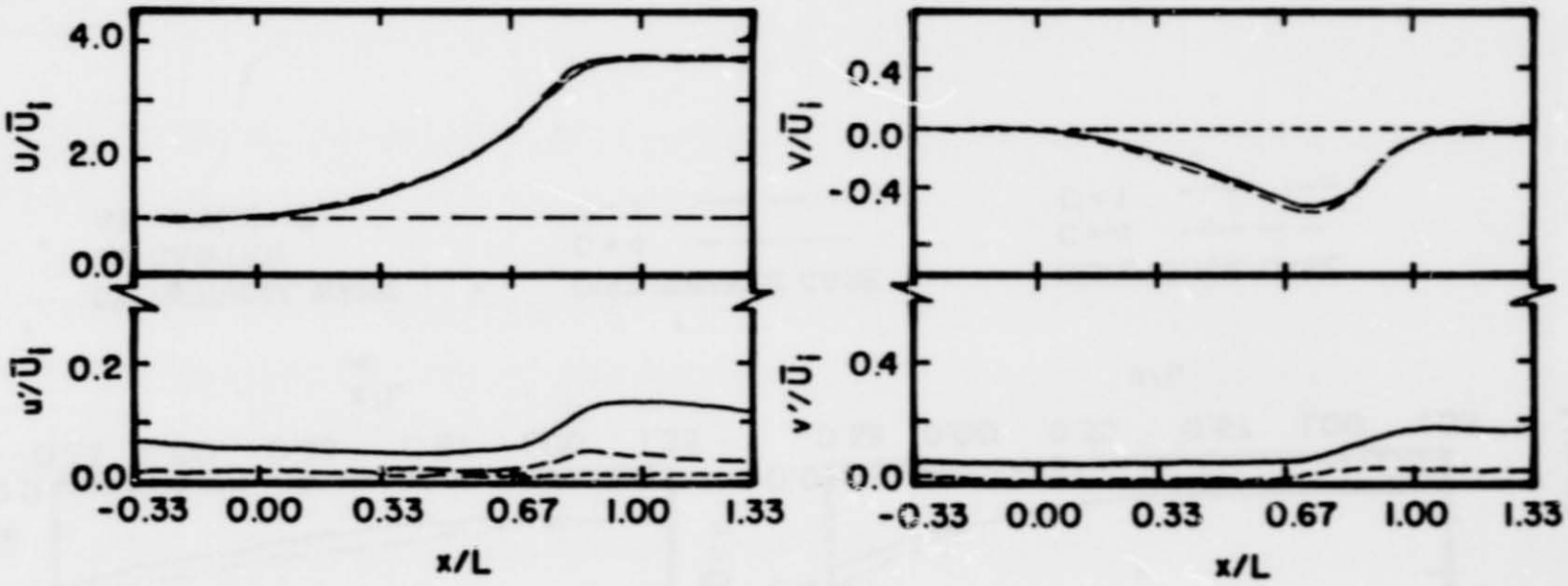

Figure 31. Normalized Axial Surveys of Streamwise and Transverse Mean Velocity and Turbulence Intensity Off Center Line for a Cylindrical Wake on Axis

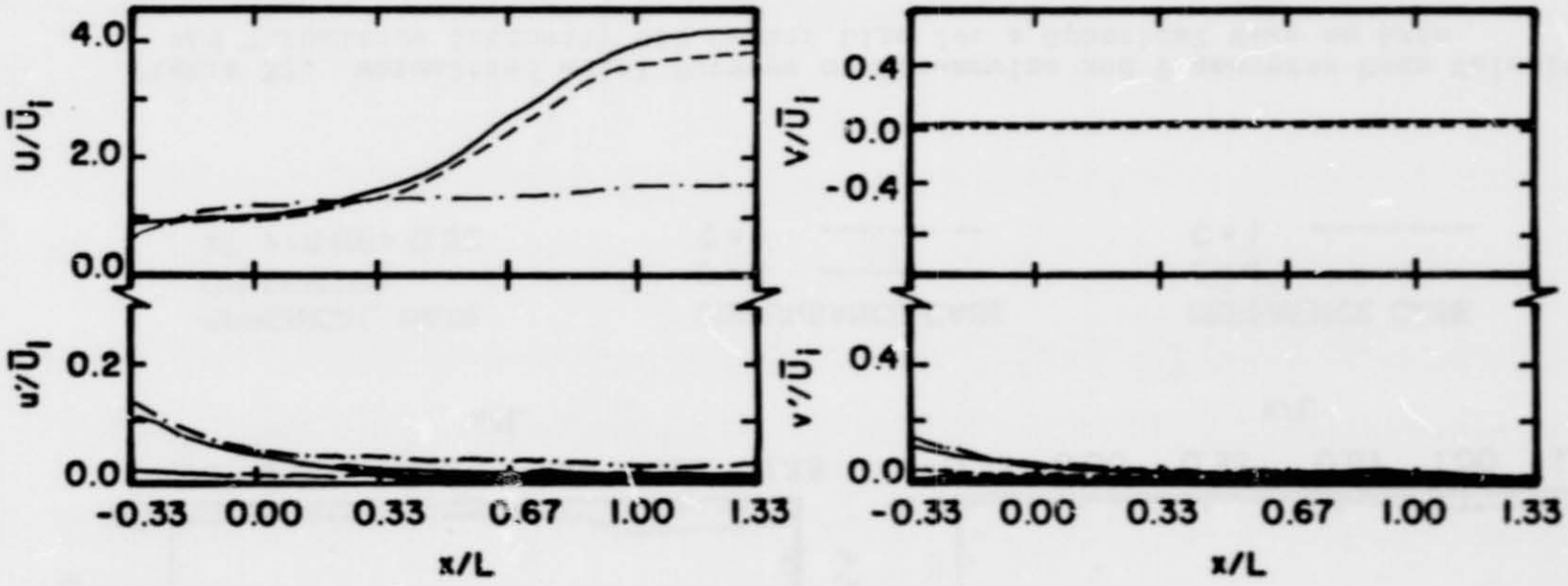

SPHERICAL WAKE ON CENTER AT r/R(0) = 0	DISTURBANCE CASE	REFERENCE CASE
	C = 4 ———	C = 4 – – – –
	C = 1 —·—·—	C = 1 -------

Figure 32. Normalized Axial Surveys of Streamwise and Transverse Mean Velocity and Turbulence Intensity Along Center Line for a Spherical Wake on Axis

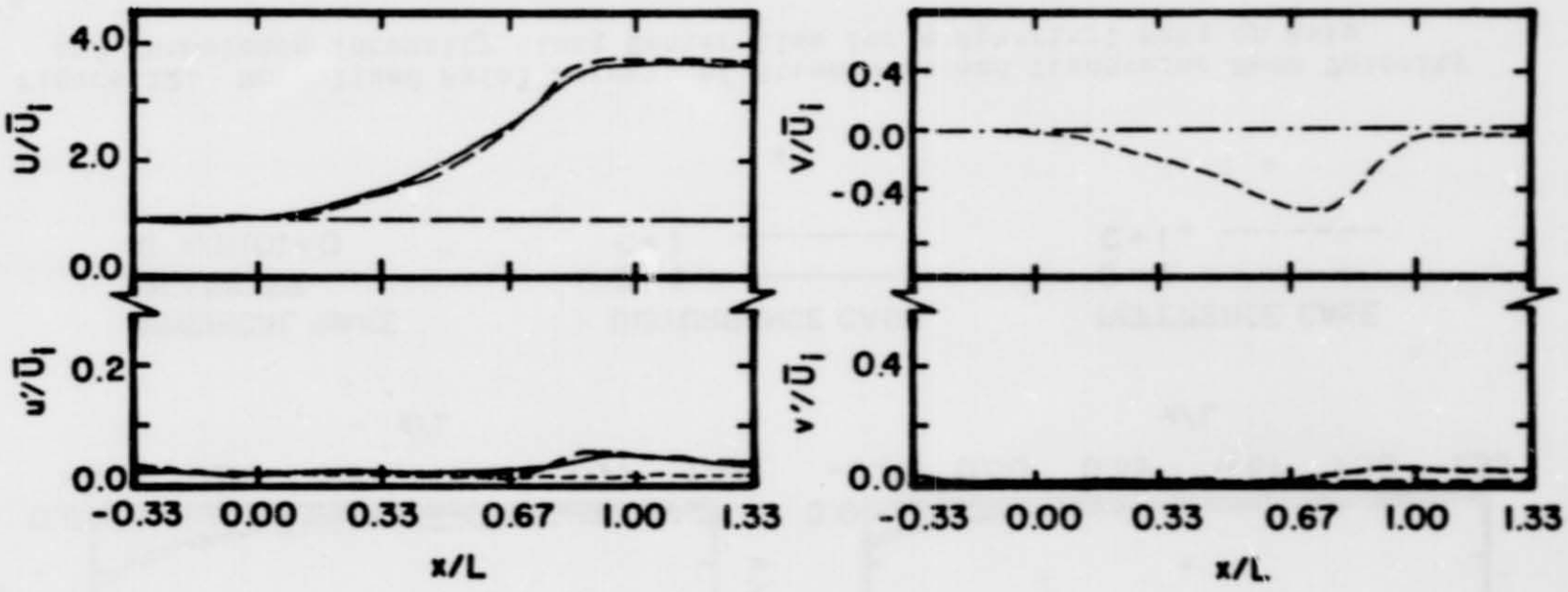

Figure 33. Normalized Axial Surveys of Streamwise and Transverse Mean Velocity and Turbulence Intensity Off Center Line for a Spherical Wake on Axis

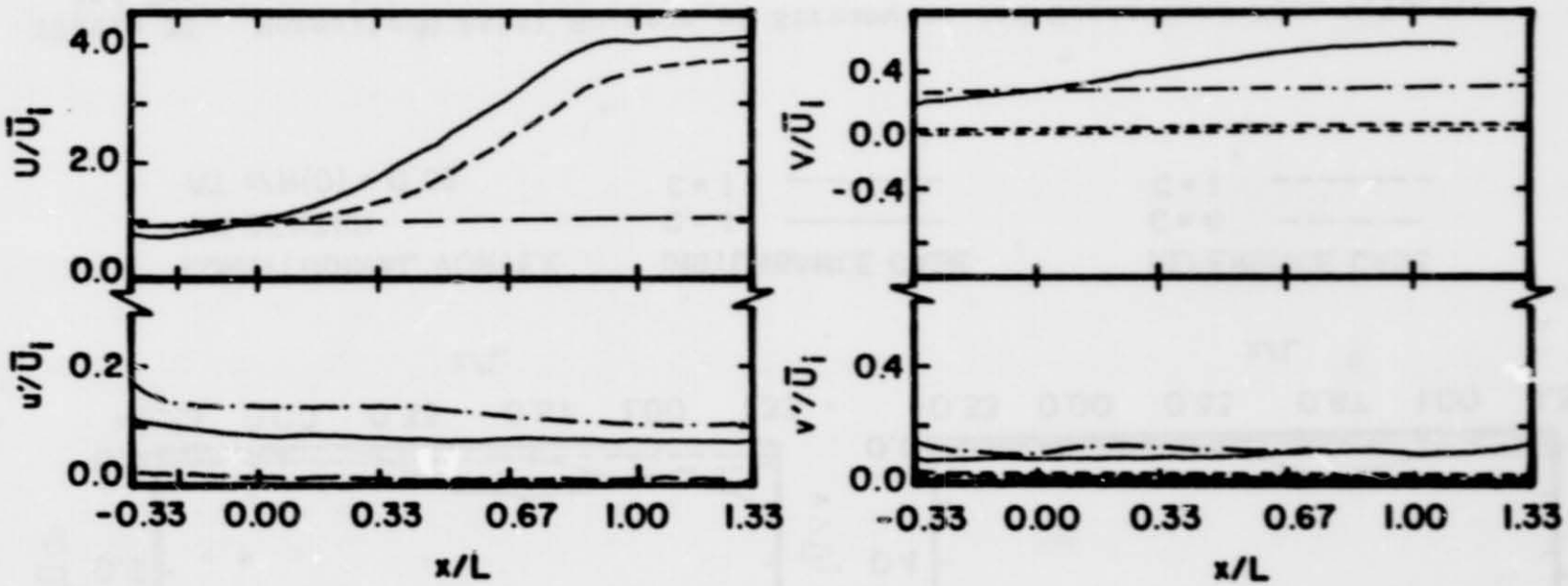

Figure 34. Normalized Axial Surveys of Streamwise and Transverse Mean Velocity and Turbulence Intensity Along Center Line for a Longitudinal Vortex on Axis

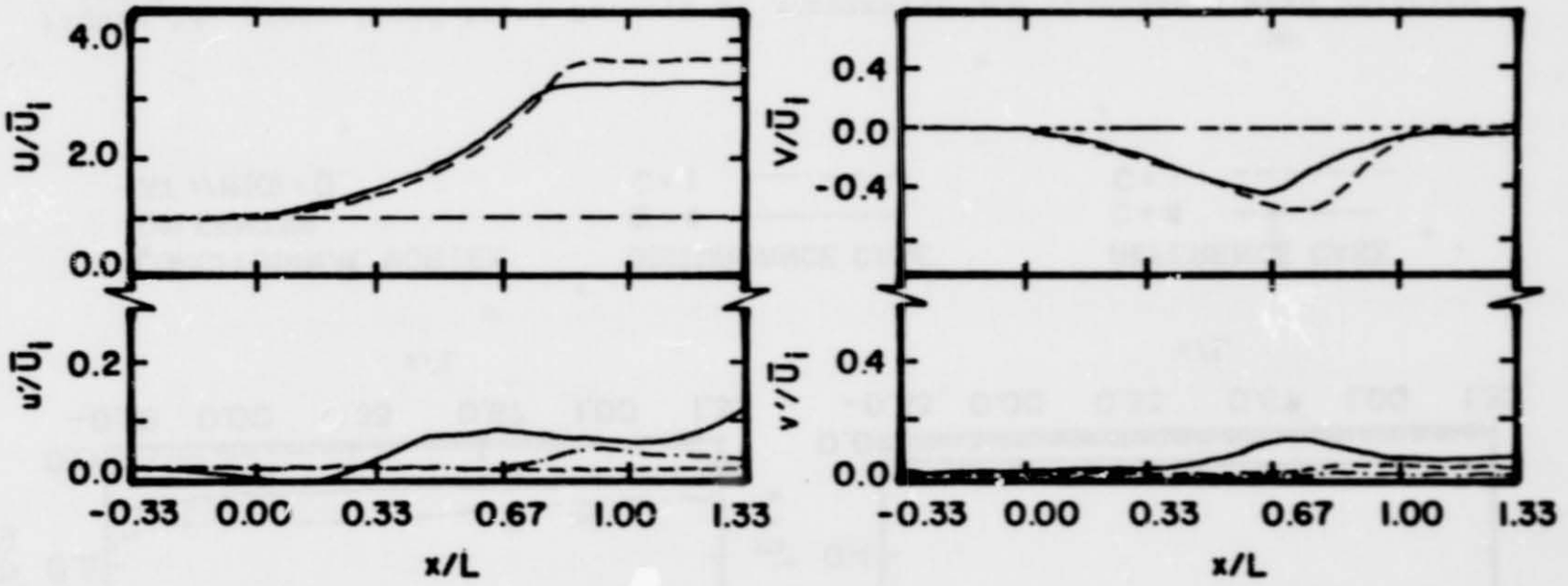

Figure 35. Normalized Axial Surveys of Streamwise and Transverse Mean Velocity and Turbulence Intensity Off Center Line for a Longitudinal Vortex on Axis

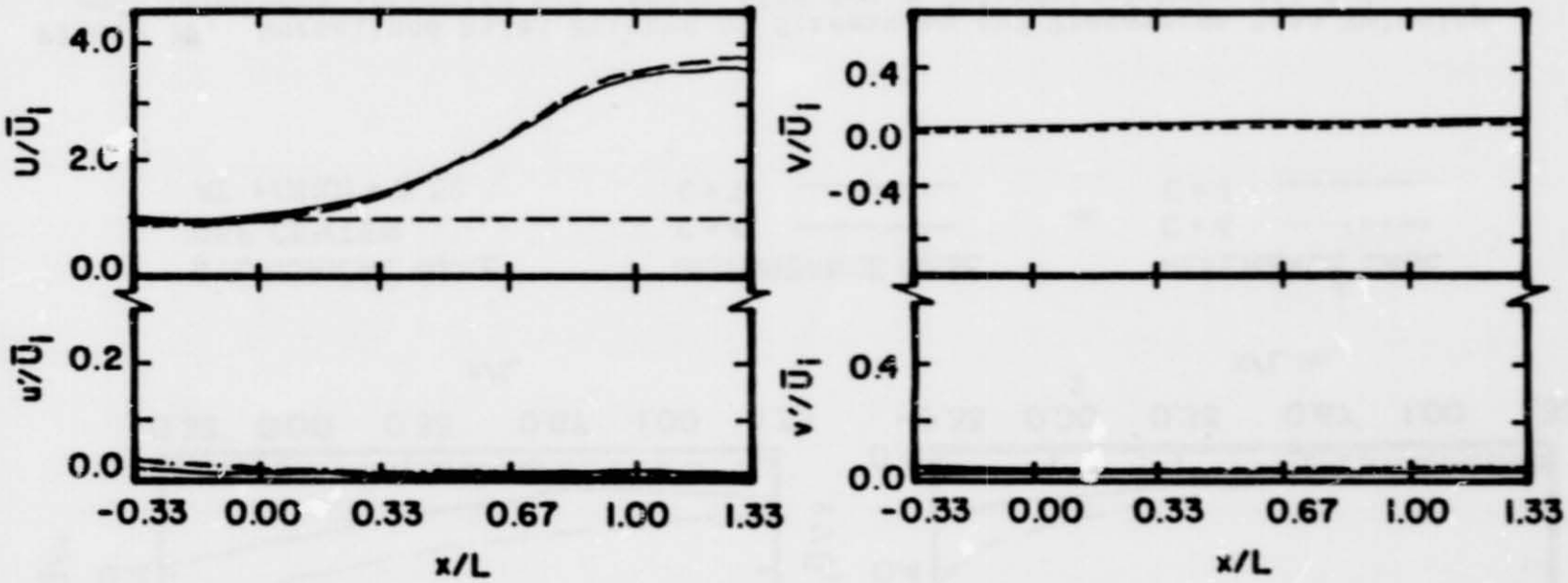

Figure 36. Normalized Axial Surveys of Streamwise and Transverse Mean Velocity and Turbulence Intensity Along Center Line for a Cylindrical Wake Off Axis

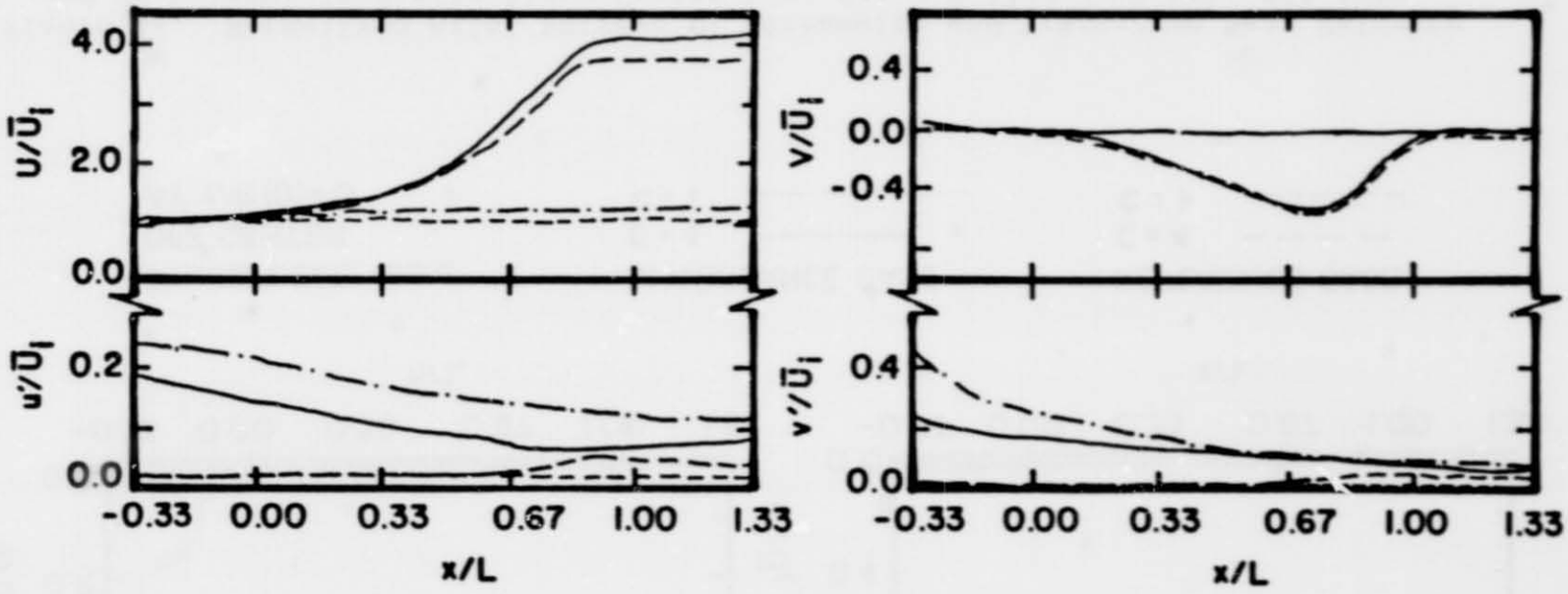

CYLINDRICAL WAKE
OFF CENTER
AT r/R(0) = 0.52

DISTURBANCE CASE
C = 4 ————
C = 1 —·—·—

REFERENCE CASE
C = 4 – – – –
C = 1 -------

Figure 37. Normalized Axial Surveys of Streamwise and Transverse Mean Velocity and Turbulence Intensity Off Center Line for a Cylindrical Wake Off Axis

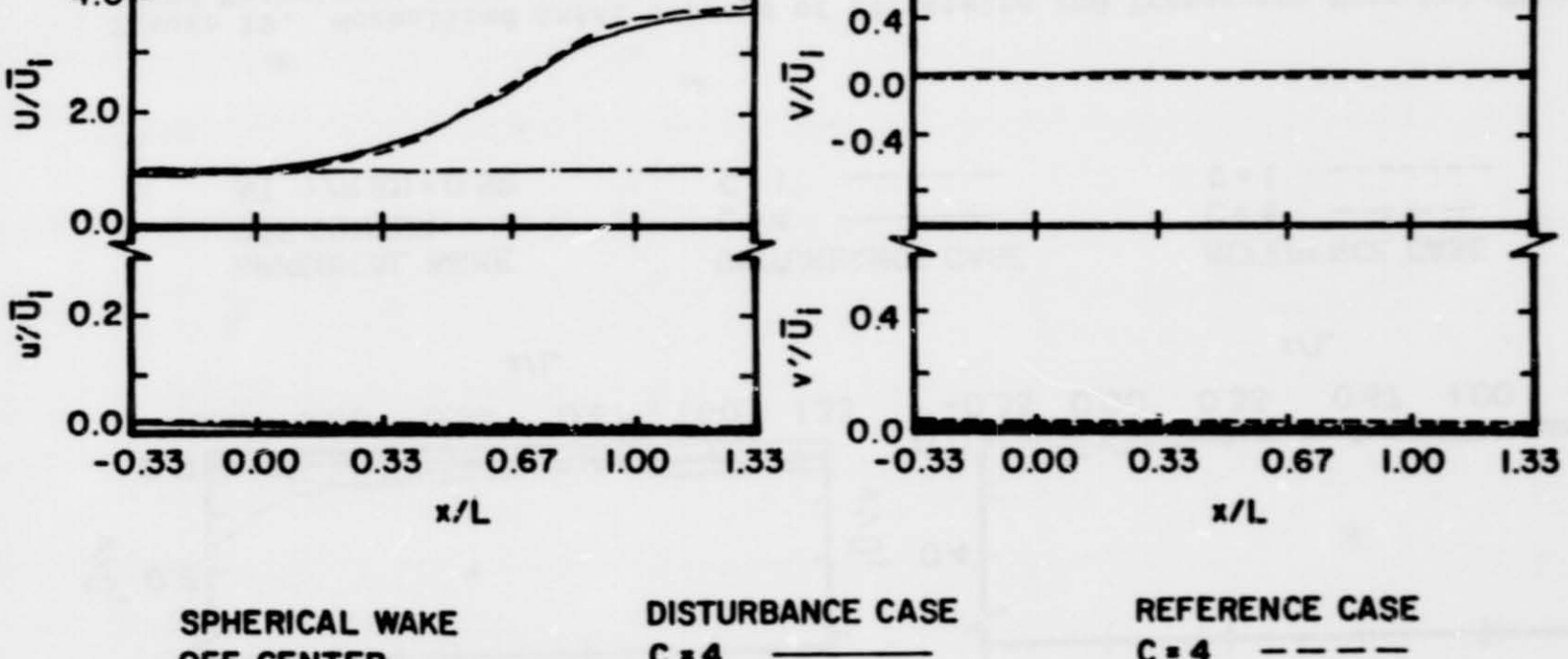

Figure 38. Normalized Axial Surveys of Streamwise and Transverse Mean Velocity and Turbulence Intensity Along Center Line for a Spherical Wake Off Axis

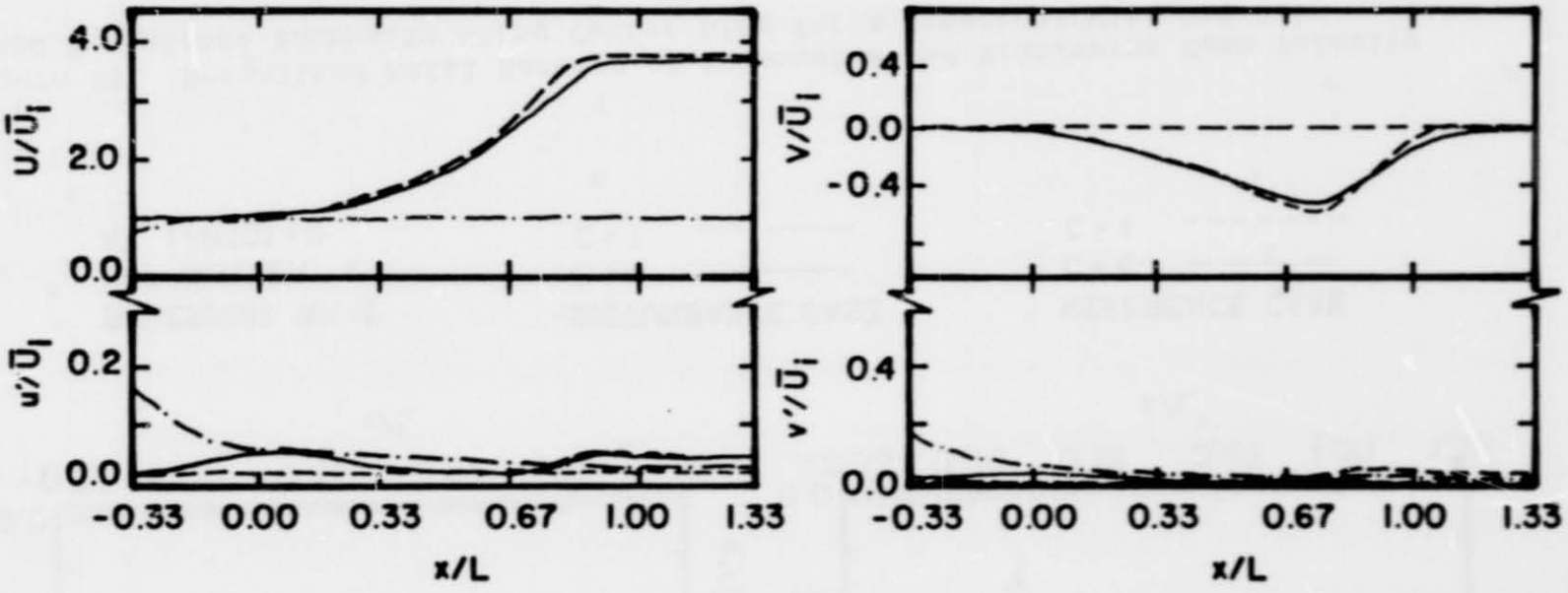

SPHERICAL WAKE
OFF CENTER
AT r/R(0) = 0.52

DISTURBANCE CASE
C = 4 ————
C = 1 —·—·—

REFERENCE CASE
C = 4 – – – –
C = 1 – – – – – –

Figure 39. Normalized Axial Surveys of Streamwise and Transverse Mean Velocity and Turbulence Intensity Off Center Line for a Spherical Wake Off Axis

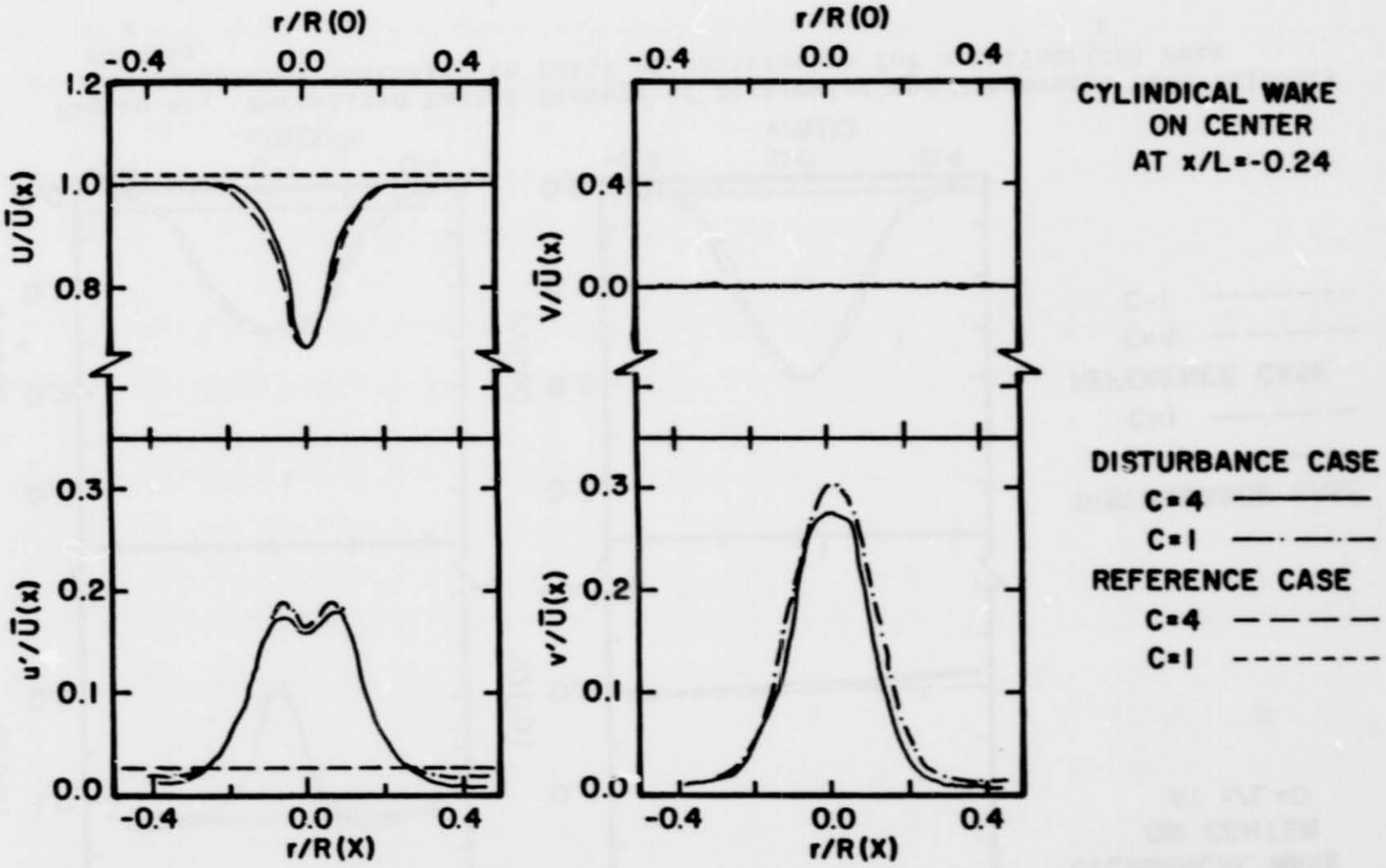

Figure 40. Normalized Radial Surveys of Streamwise and Transverse Mean Velocity and Turbulence Intensity Upstream of Contraction for a Cylindrical Wake on Axis

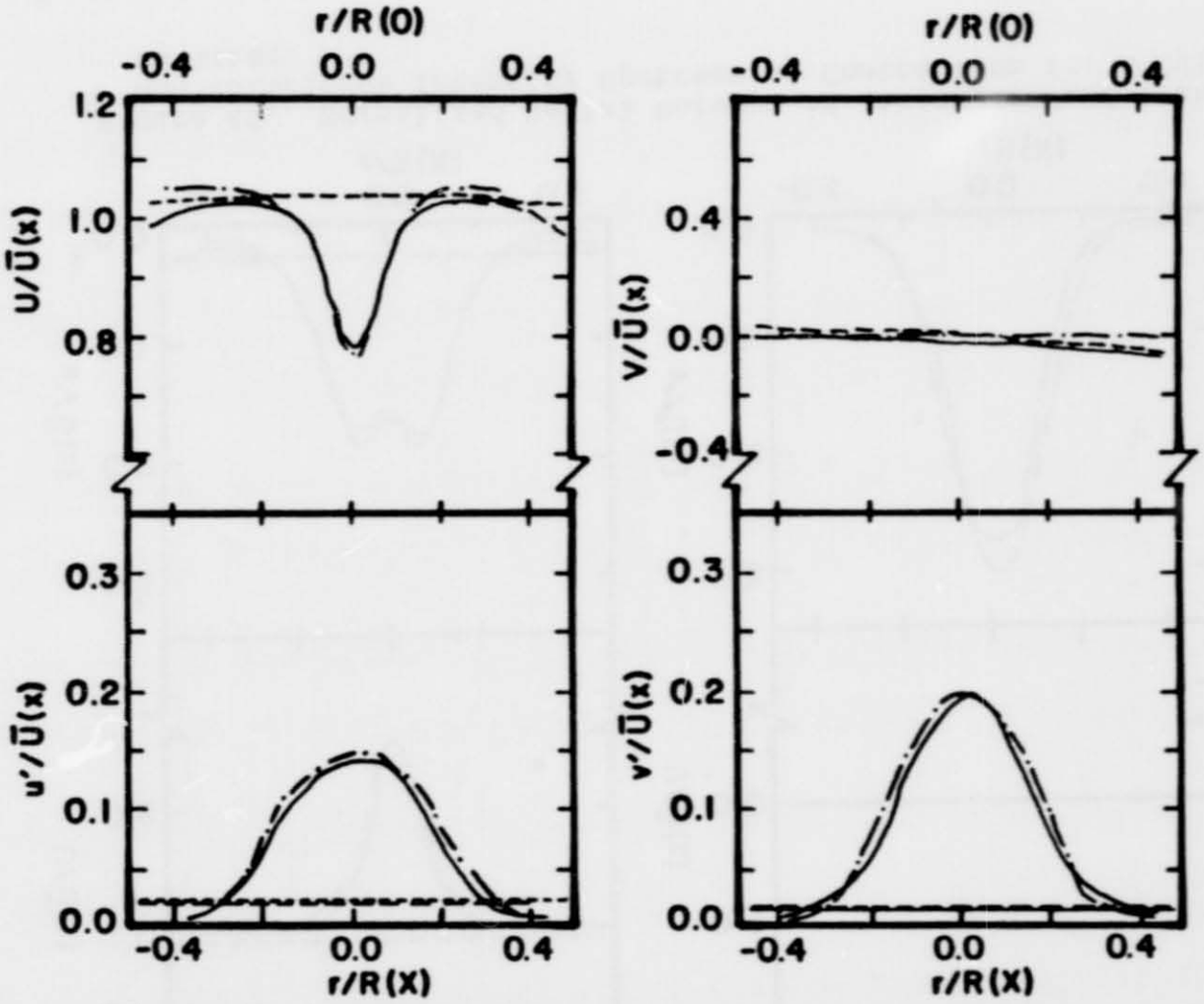

CYLINDRICAL WAKE
ON CENTER
AT x/L=0

DISTURBANCE CASE
C=4
C=1
REFERENCE CASE
C=4
C=1

Figure 41. Normalized Radial Surveys of Streamwise and Transverse Mean Velocity and Turbulence Intensity at Inlet of Contraction for a Cylindrical Wake on Axis

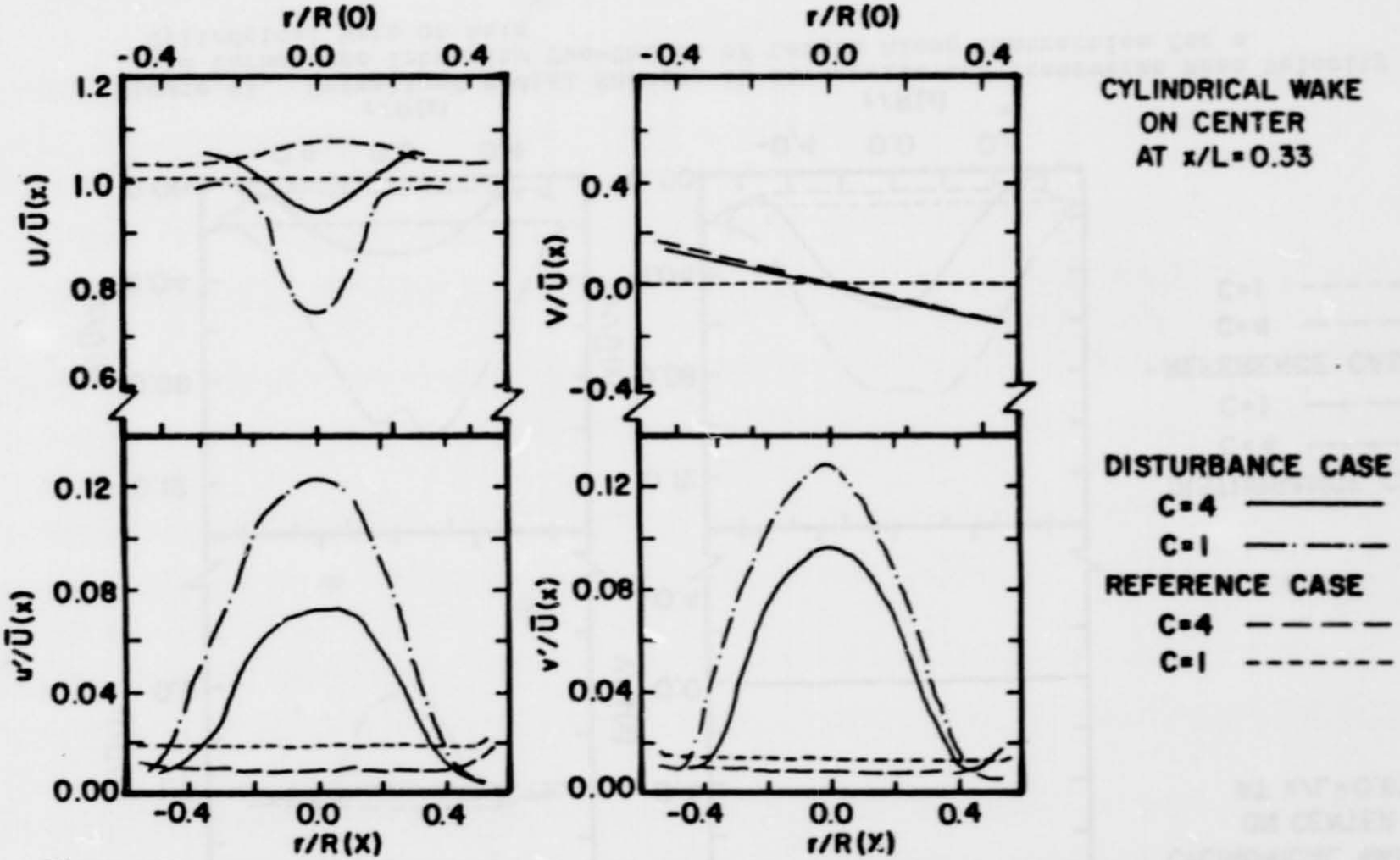

Figure 42. Normalized Radial Surveys of Streamwise and Transverse Mean Velocity and Turbulence Intensity One-Third of Length Along Contraction for a Cylindrical Wake on Axis

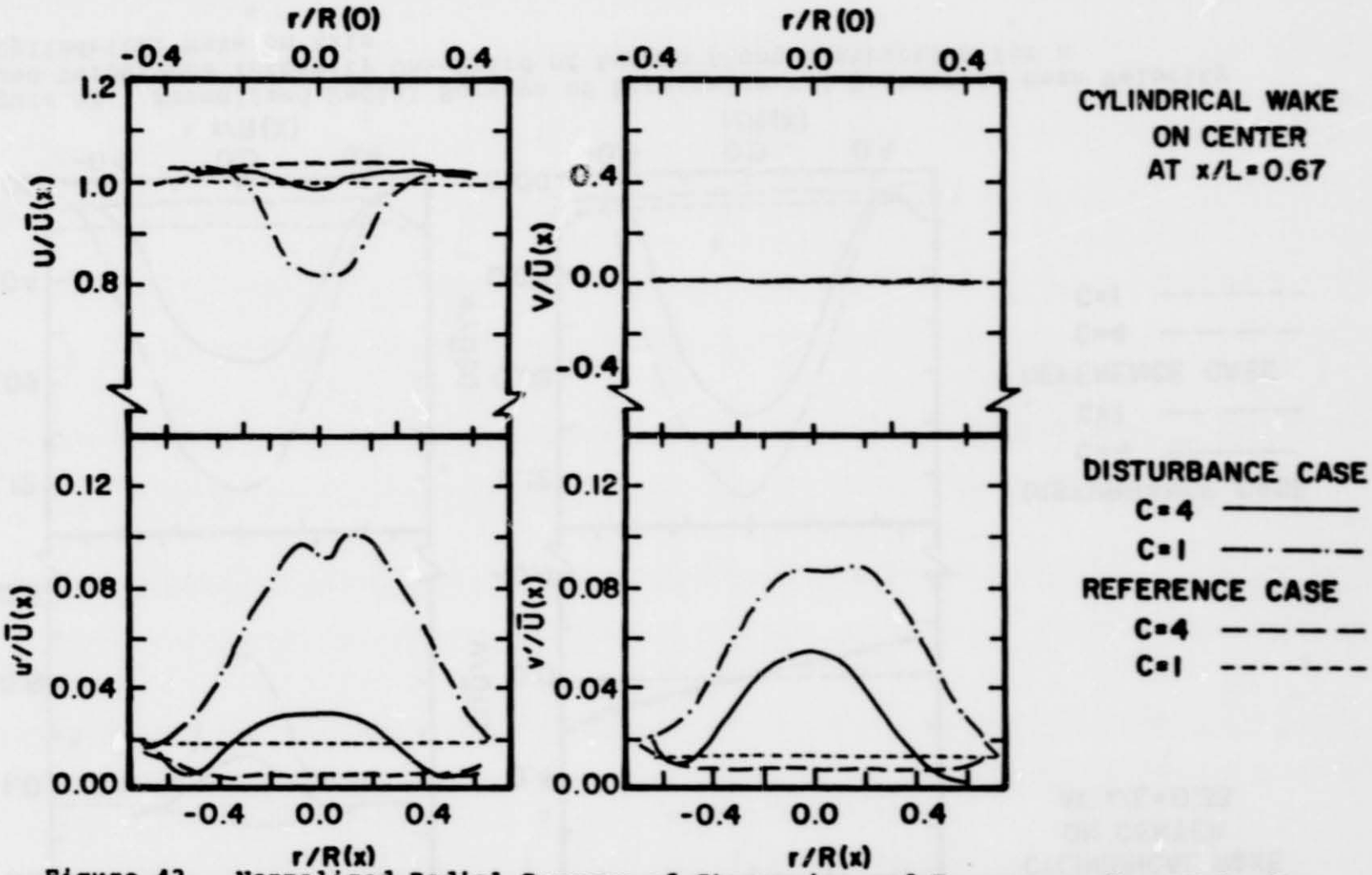

Figure 43. Normalized Radial Surveys of Streamwise and Transverse Mean Velocity and Turbulence Intensity Two-Thirds of Length Along Contraction for a Cylindrical Wake on Axis

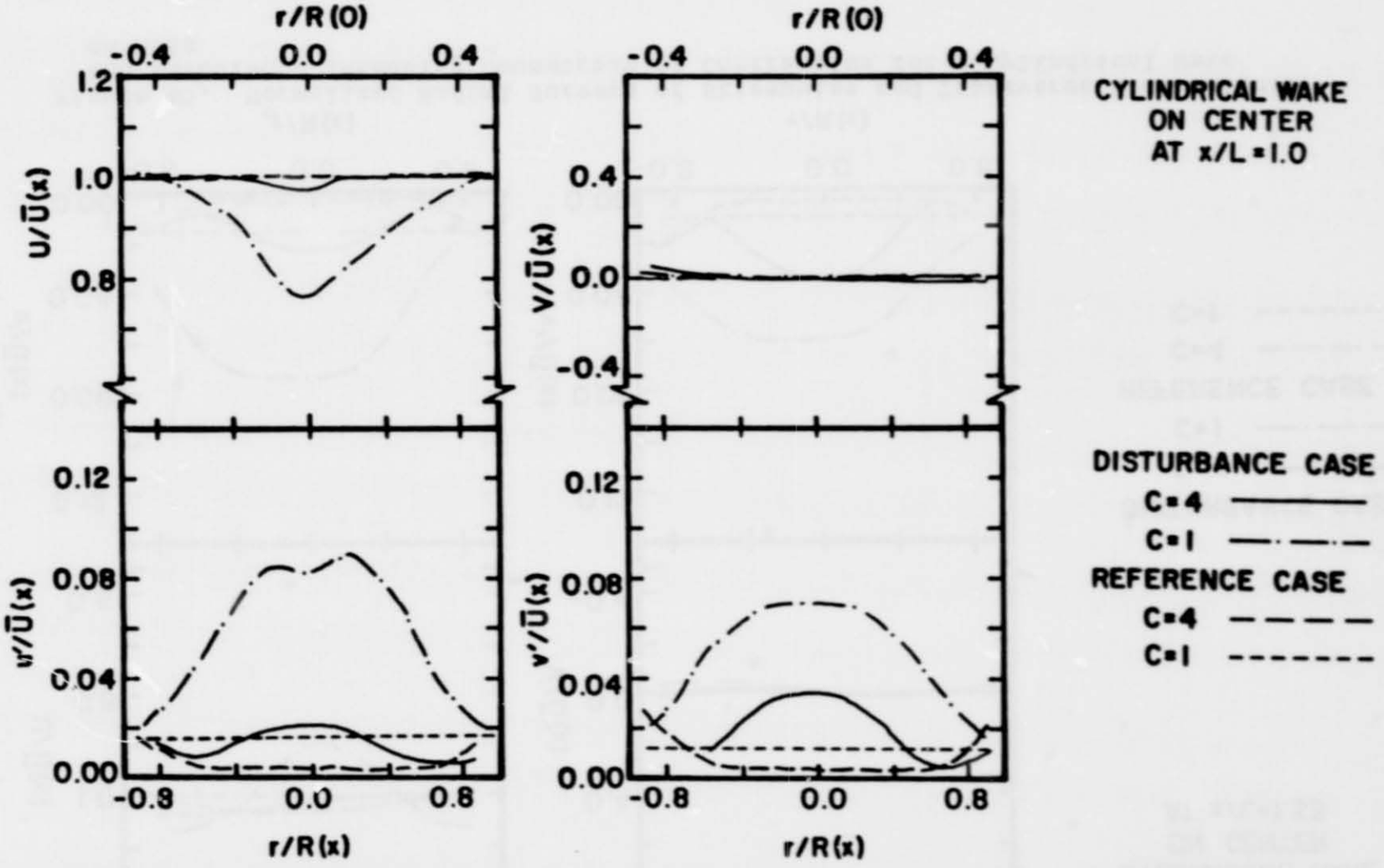

Figure 44. Normalized Radial Surveys of Streamwise and Transverse Mean Velocity and Turbulence Intensity At Exit of Contraction for a Cylindrical Wake on Axis

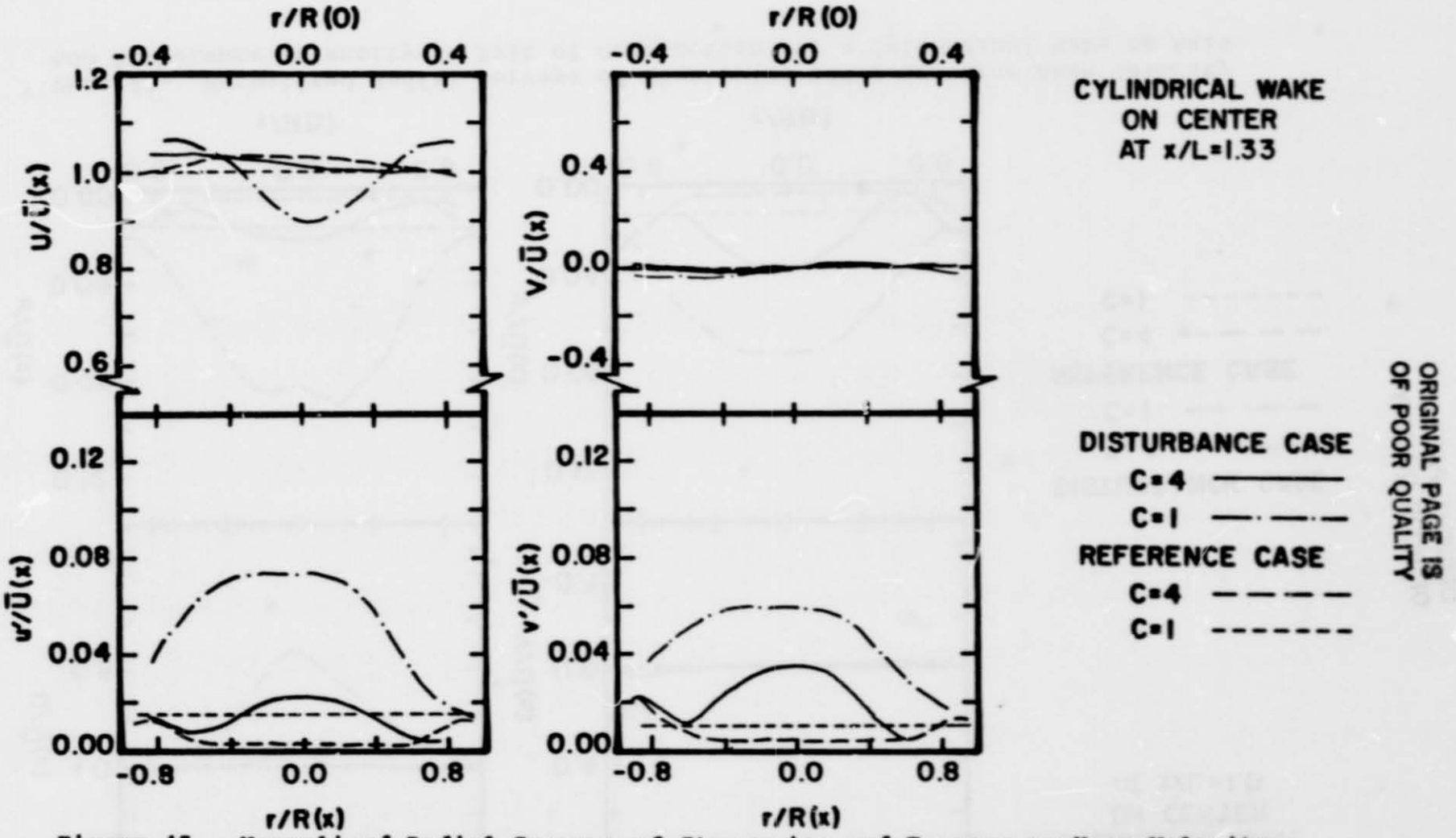

Figure 45. Normalized Radial Surveys of Streamwise and Transverse Mean Velocity and Turbulence Intensity Downstream of Contraction for a Cylindrical Wake on Axis

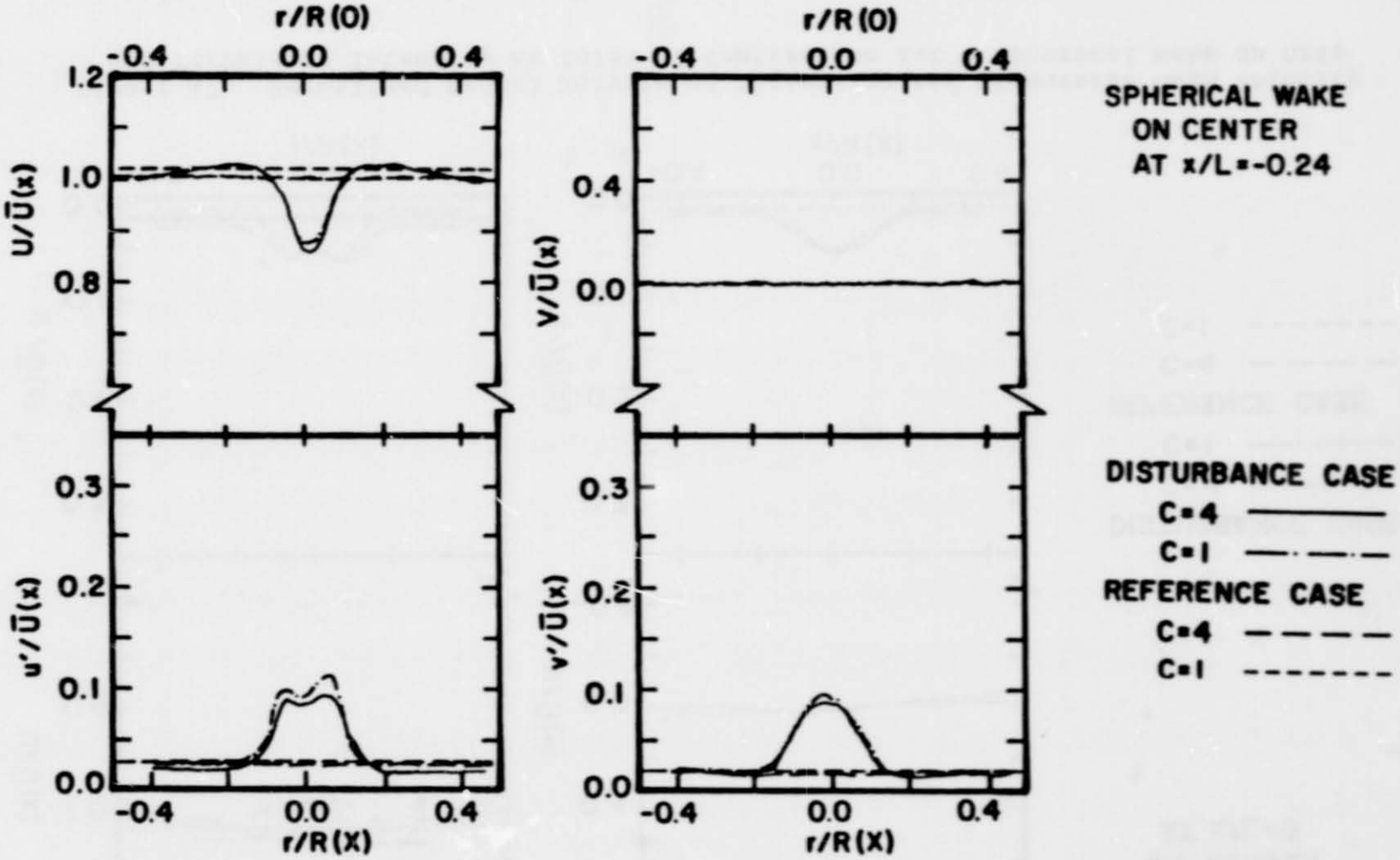

Figure 46. Normalized Radial Surveys of Streamwise and Transverse Mean Velocity and Turbulence Intensity Upstream of Contraction for a Spherical Wake on Axis

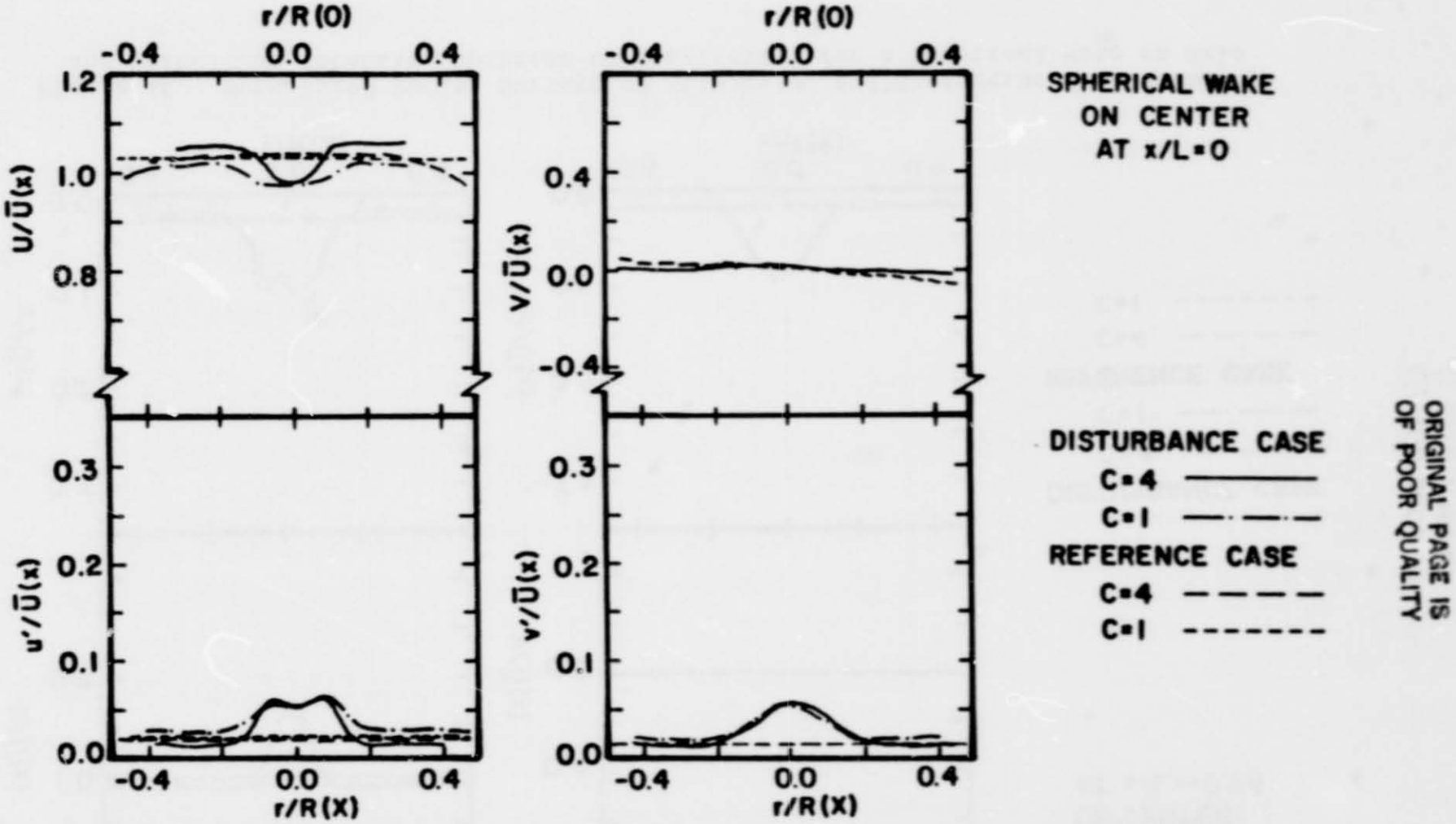

Figure 47. Normalized Radial Surveys of Streamwise and Transverse Mean Velocity and Turbulence Intensity At Inlet of Contraction for a Spherical Wake on Axis

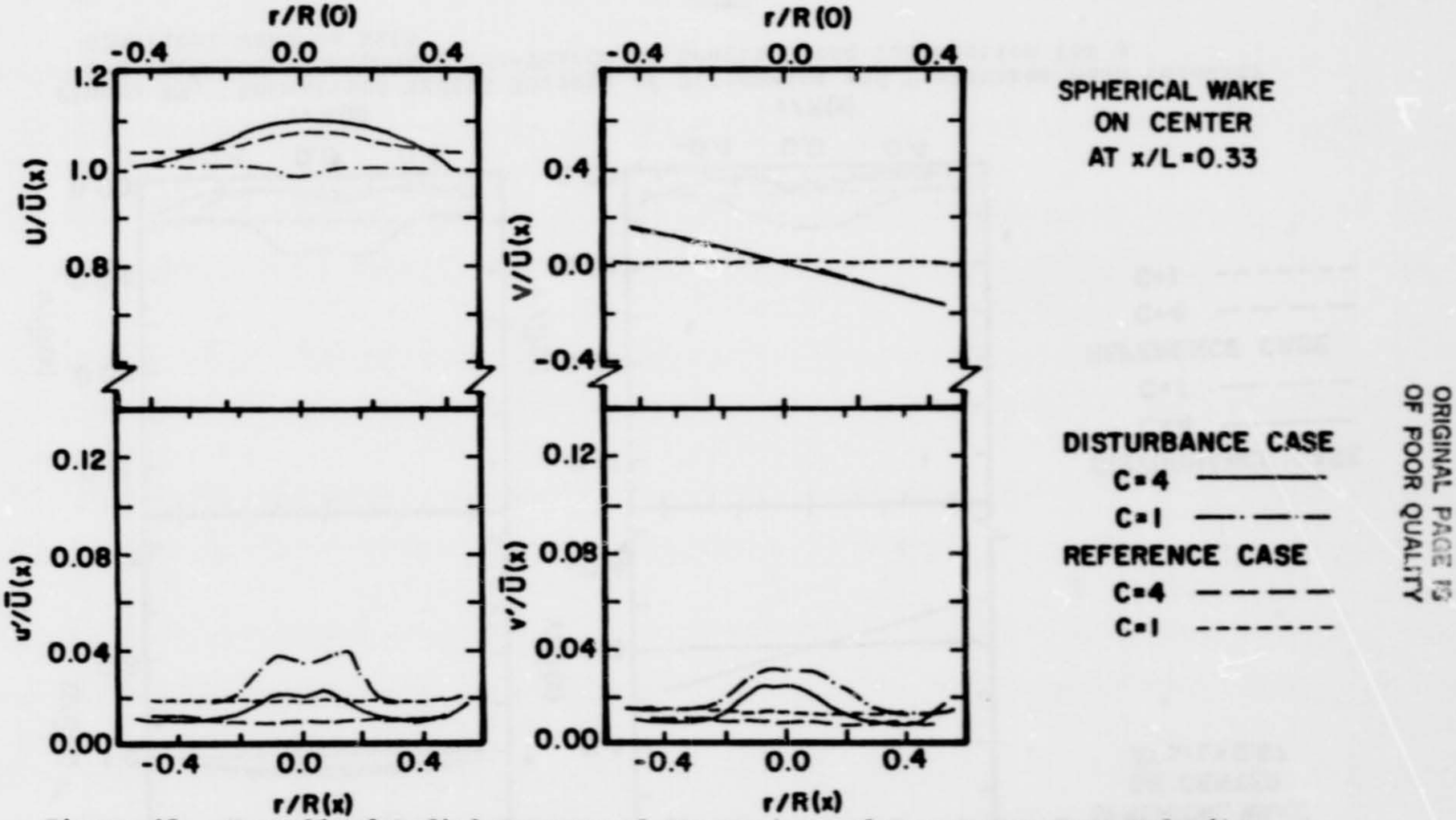

Figure 48. Normalized Radial Surveys of Streamwise and Transverse Mean Velocity and Turbulence Intensity One-Third of Length Along Contraction for a Spherical Wake on Axis

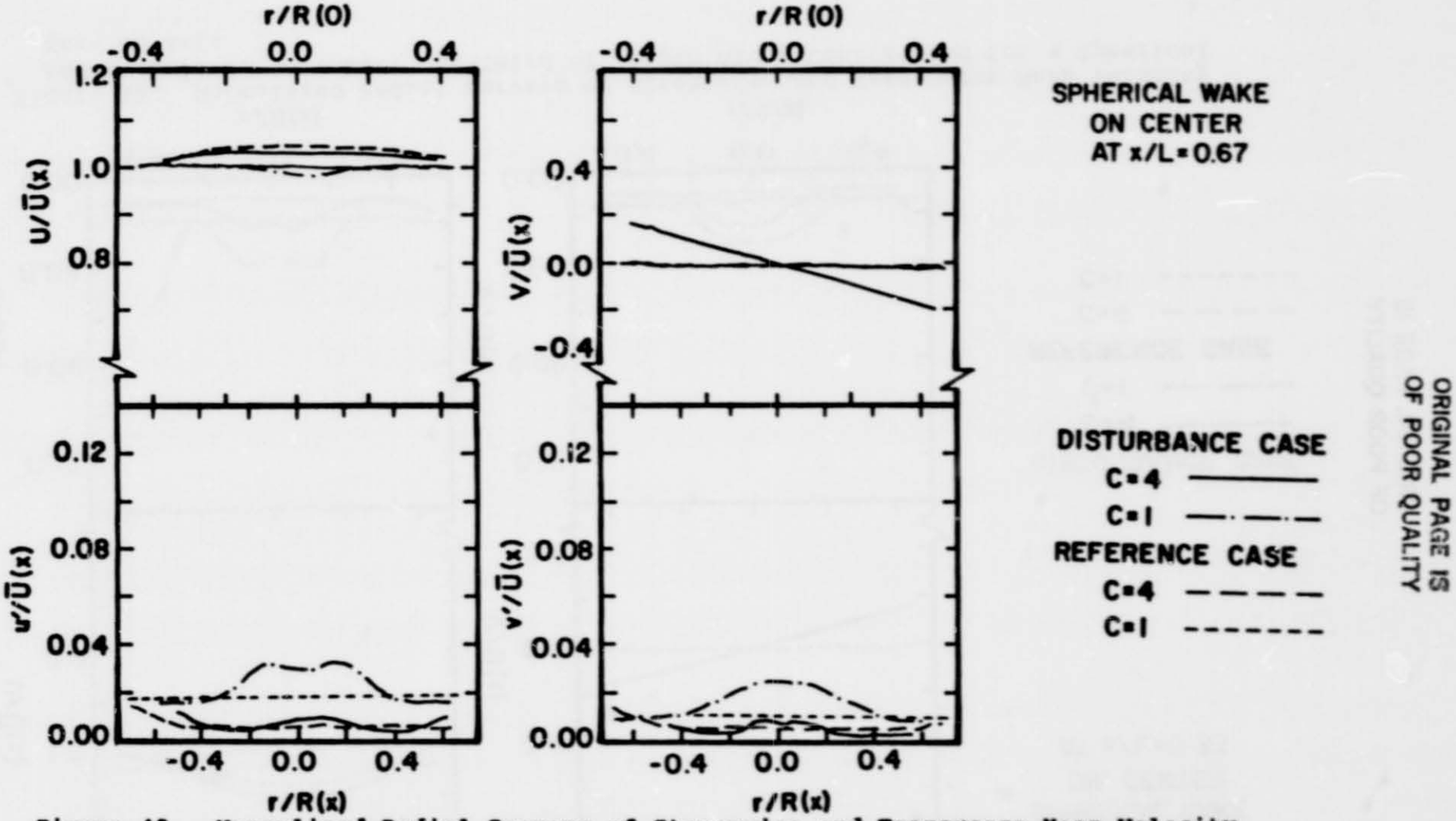

Figure 49. Normalized Radial Surveys of Streamwise and Transverse Mean Velocity and Turbulence Intensity Two-Thirds of Length Along Contraction for a Spherical Wake on Axis

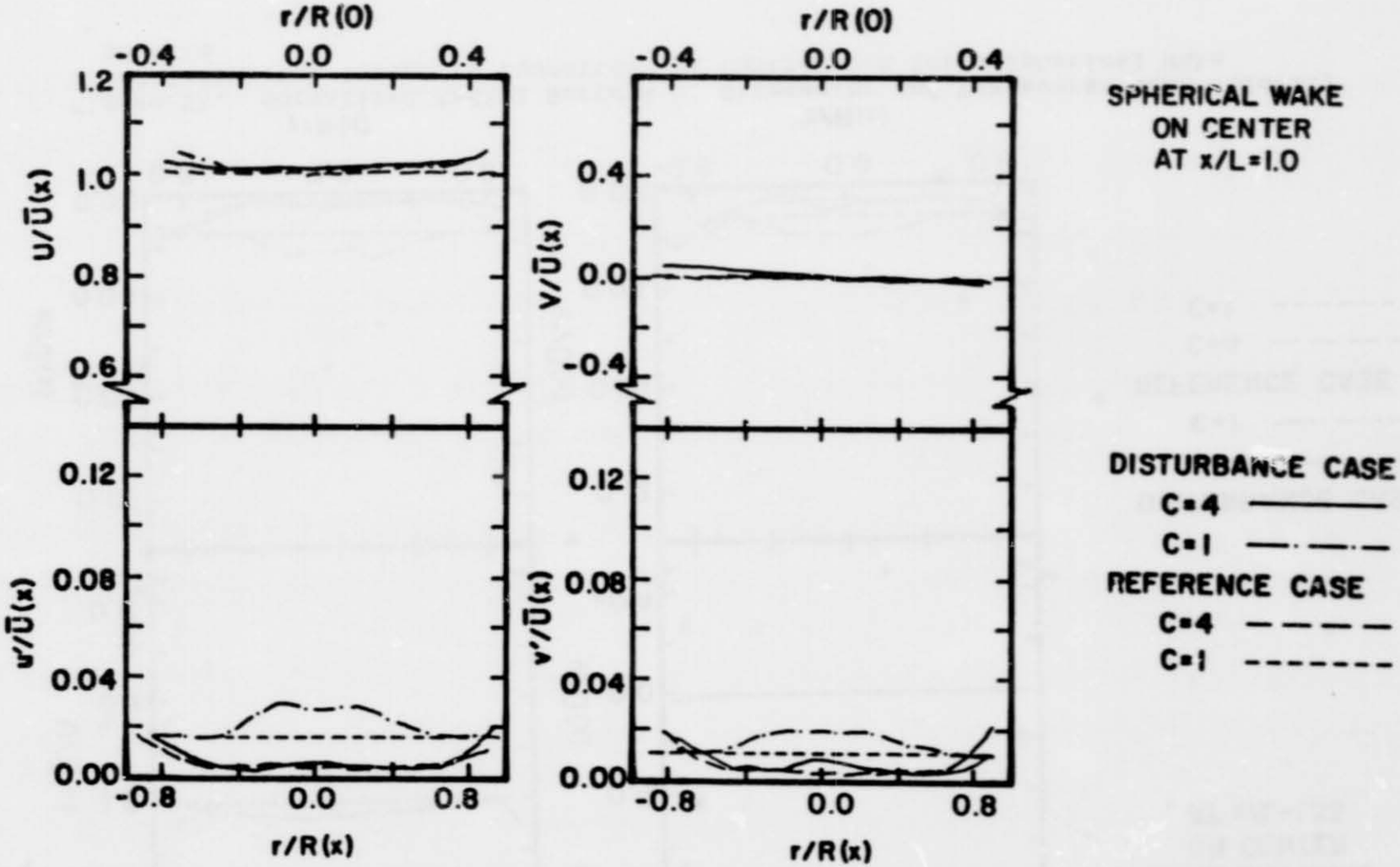

Figure 50. Normalized Radial Surveys of Streamwise and Transverse Mean Velocity and Turbulence Intensity At Exit of Contraction for a Spherical Wake on Axis

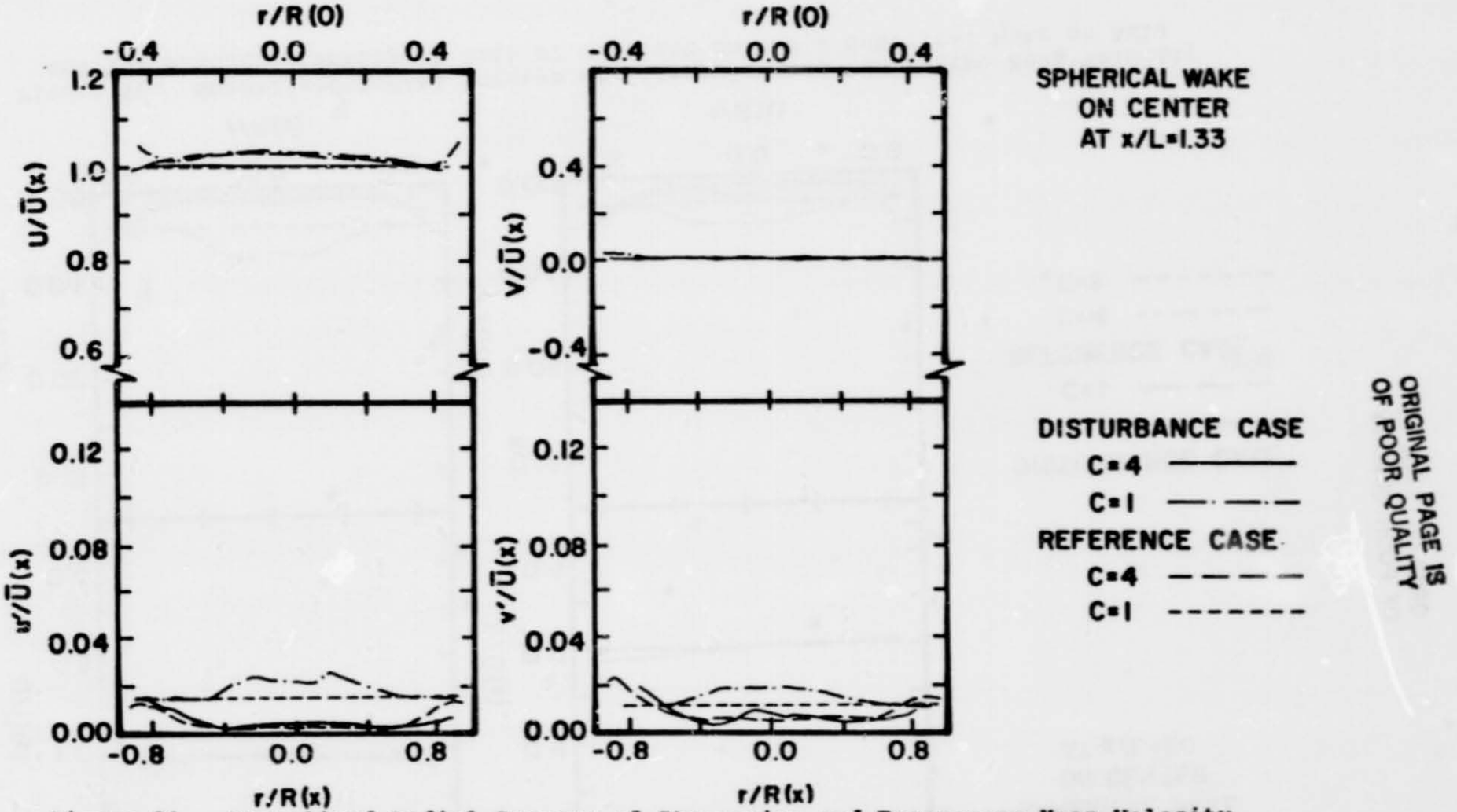

Figure 51. Normalized Radial Surveys of Streamwise and Transverse Mean Velocity and Turbulence Intensity Downstream of Contraction for a Spherical Wake on Axis

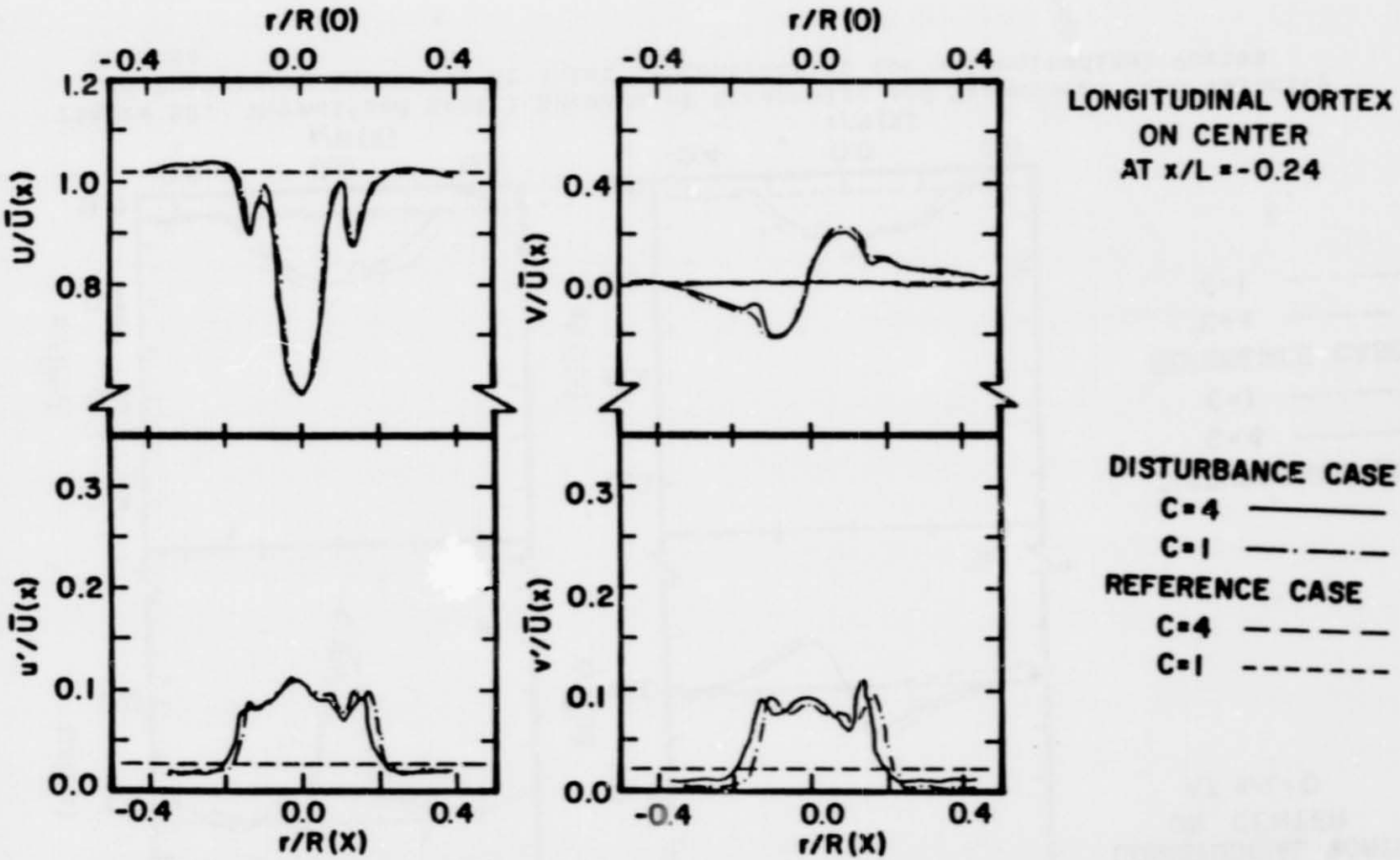

Figure 52. Normalized Radial Surveys of Streamwise and Transverse Mean Velocity and Turbulence Intensity Upstream of Contraction for a Longitudinal Vortex on Axis

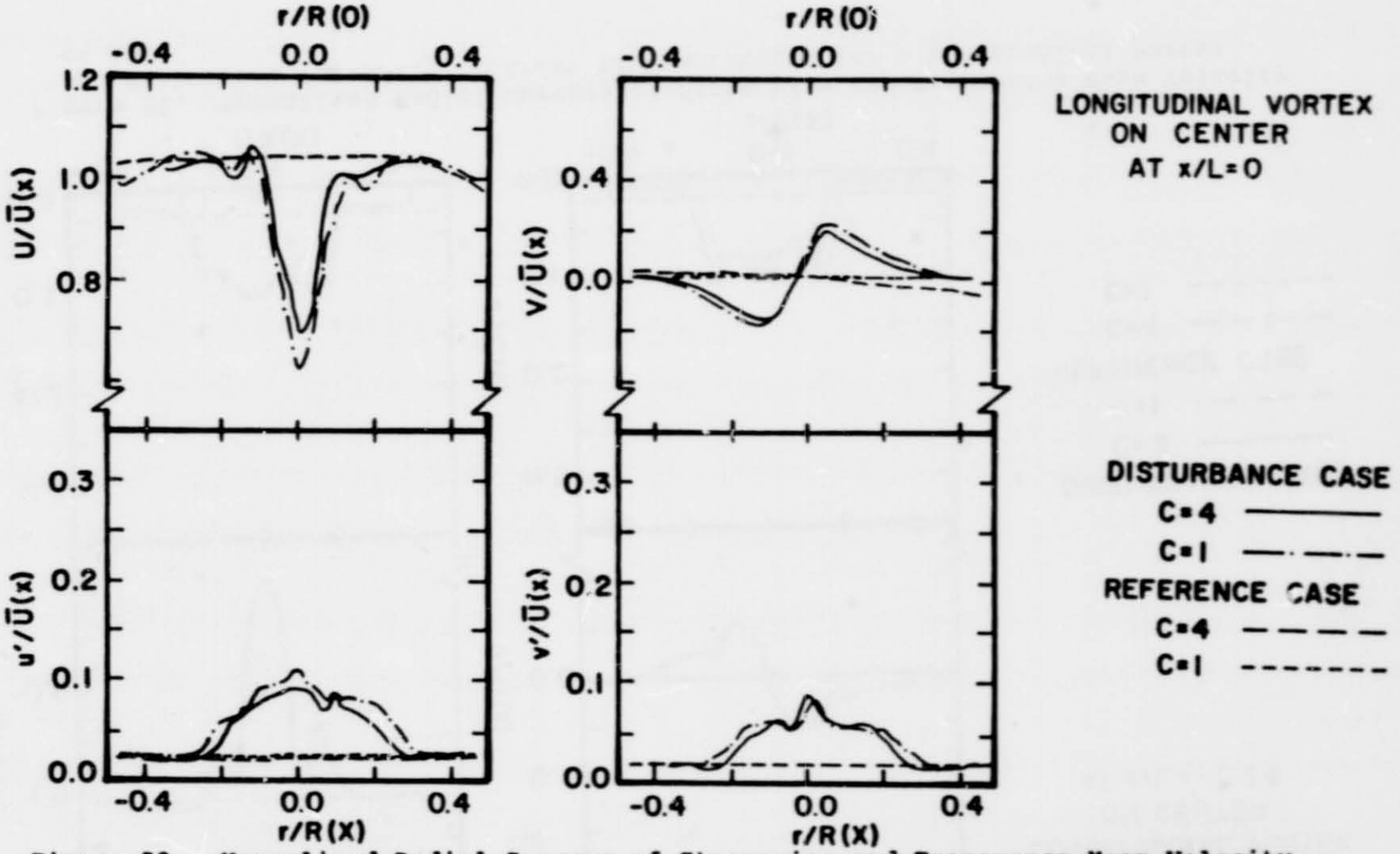

Figure 53. Normalized Radial Surveys of Streamwise and Transverse Mean Velocity and Turbulence Intensity At Inlet of Contraction for a Longitudinal Vortex on Axis

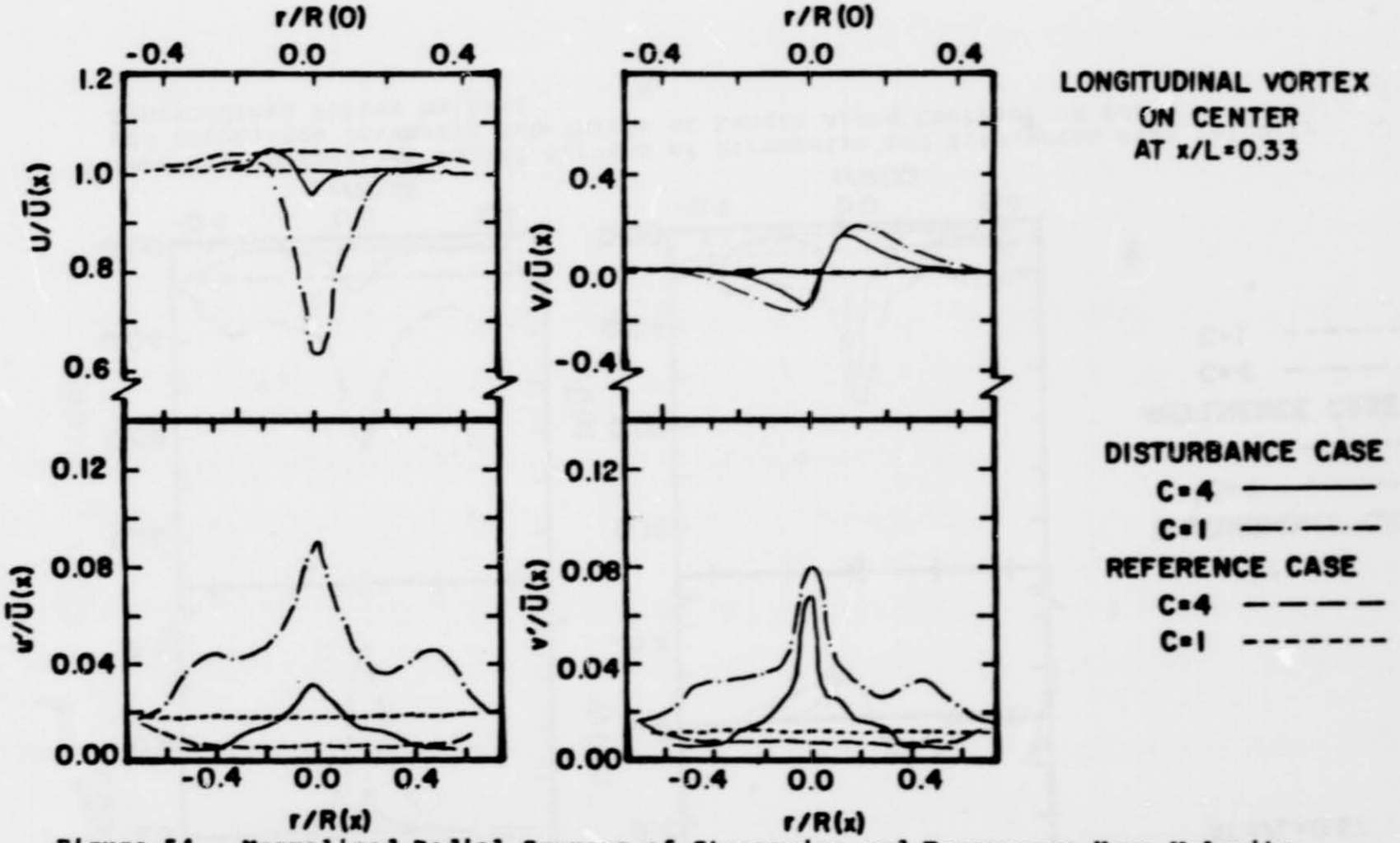

Figure 54. Normalized Radial Surveys of Streamwise and Transverse Mean Velocity and Turbulence Intensity One-Third of Length Along Contraction for a Longitudinal Vortex on Axis

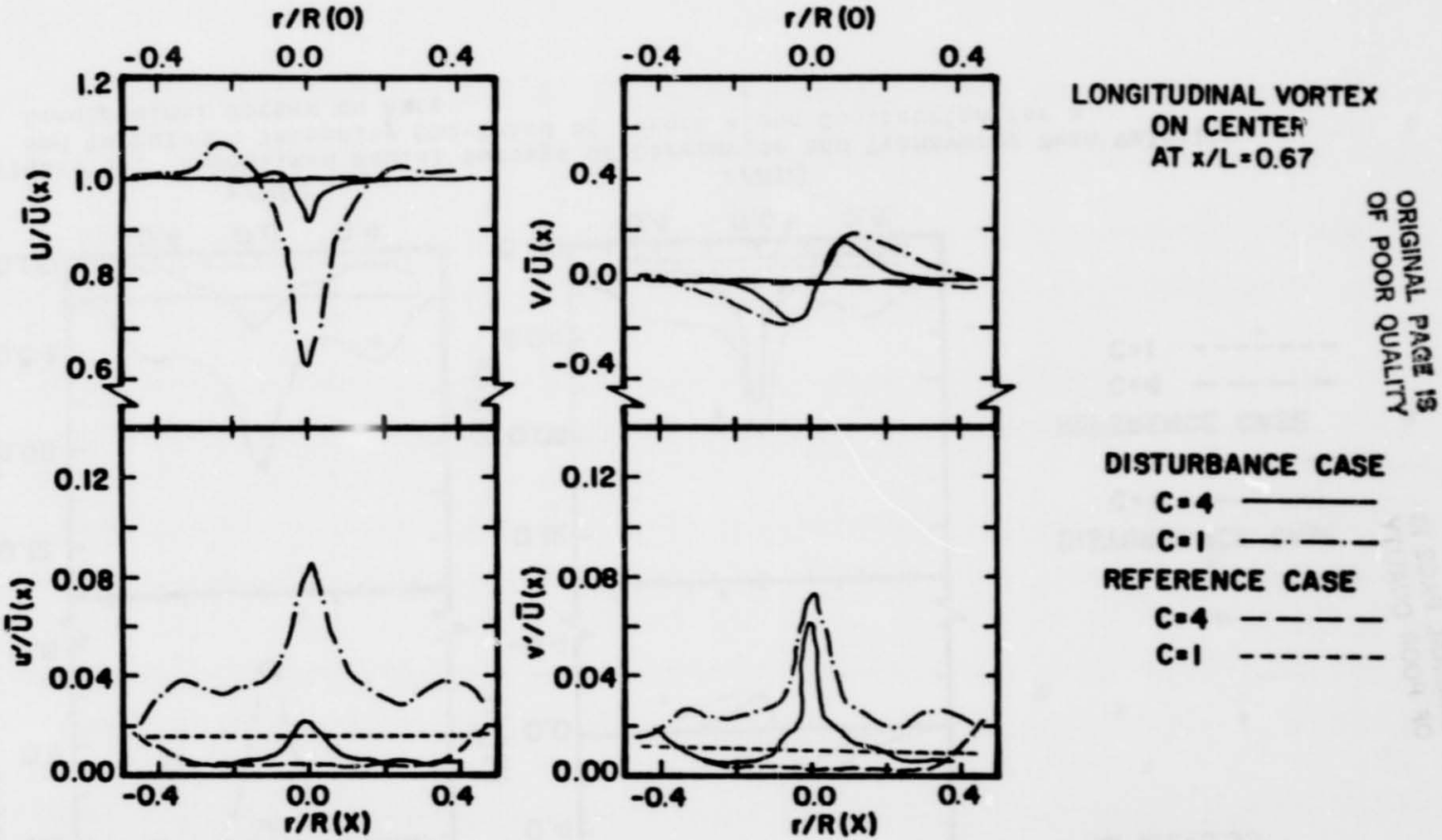

Figure 55. Normalized Radial Surveys of Streamwise and Transverse Mean Velocity and Turbulence Intensity Two-Thirds of Length Along Contraction for a Longitudinal Vortex on Axis

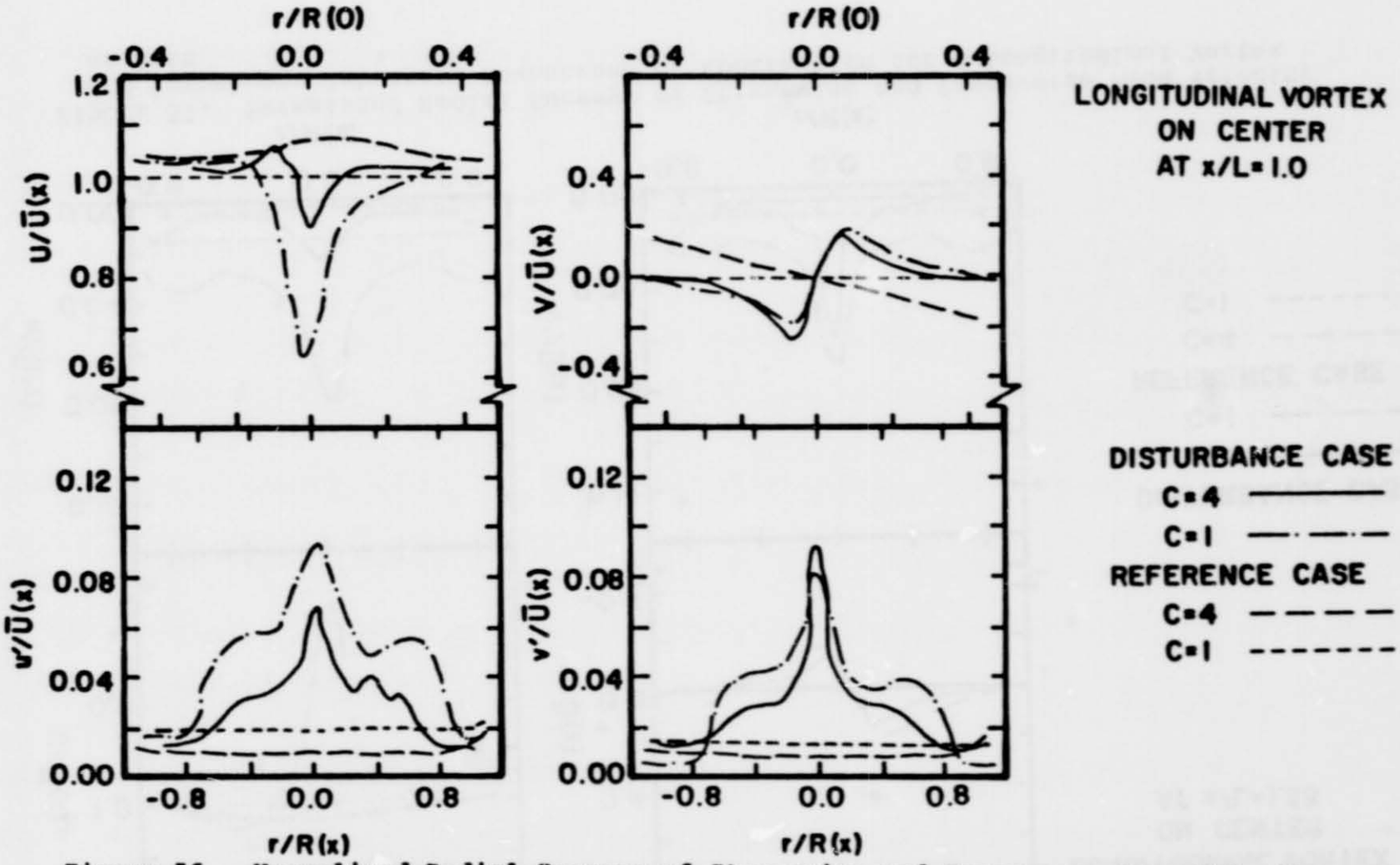

Figure 56. Normalized Radial Surveys of Streamwise and Transverse Mean Velocity and Turbulence Intensity At Exit of Contraction for a Longitudinal Vortex on Axis

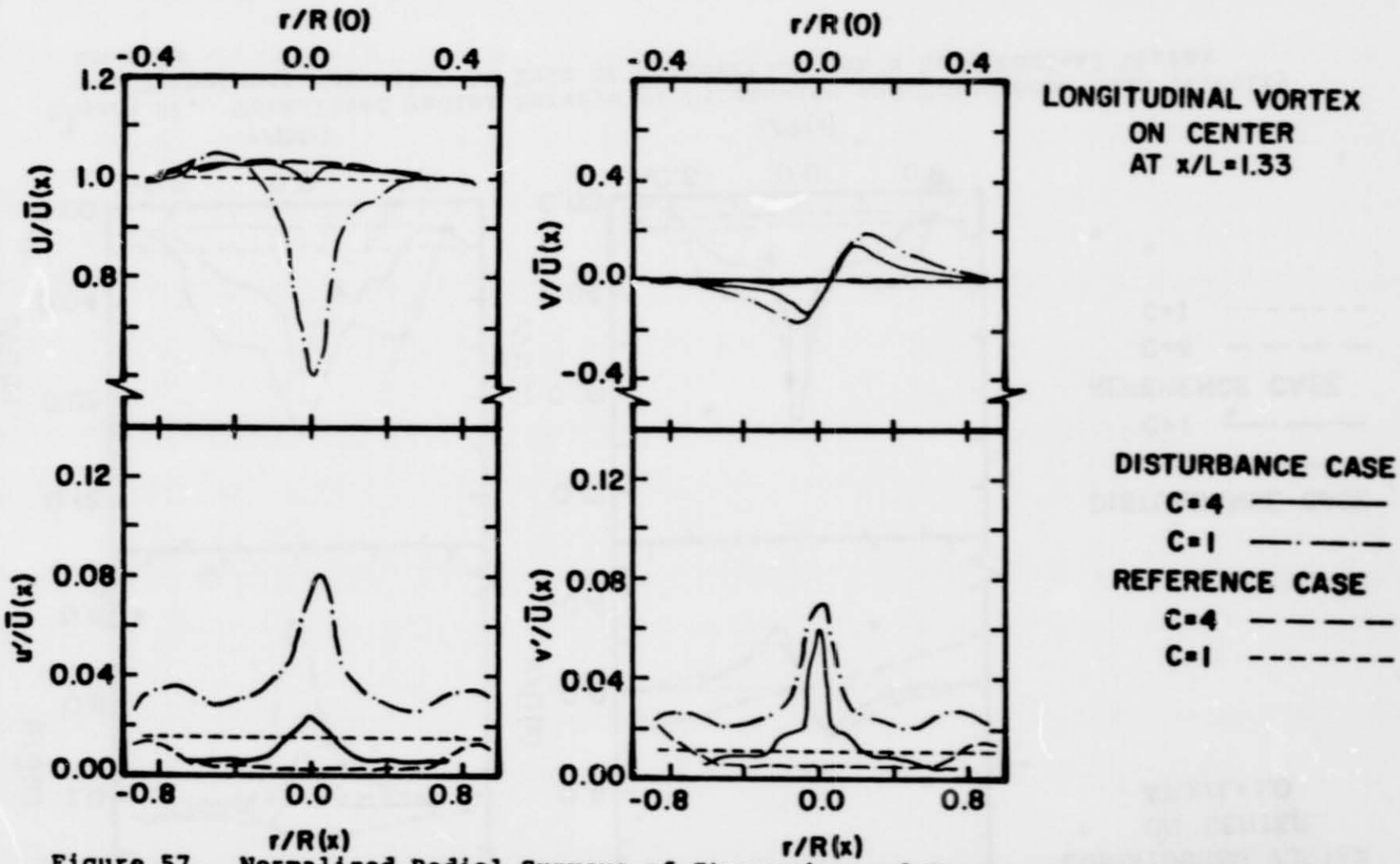

Figure 57. Normalized Radial Surveys of Streamwise and Transverse Mean Velocity and Turbulence Intensity Downstream of Contraction for a Longitudinal Vortex on Axis

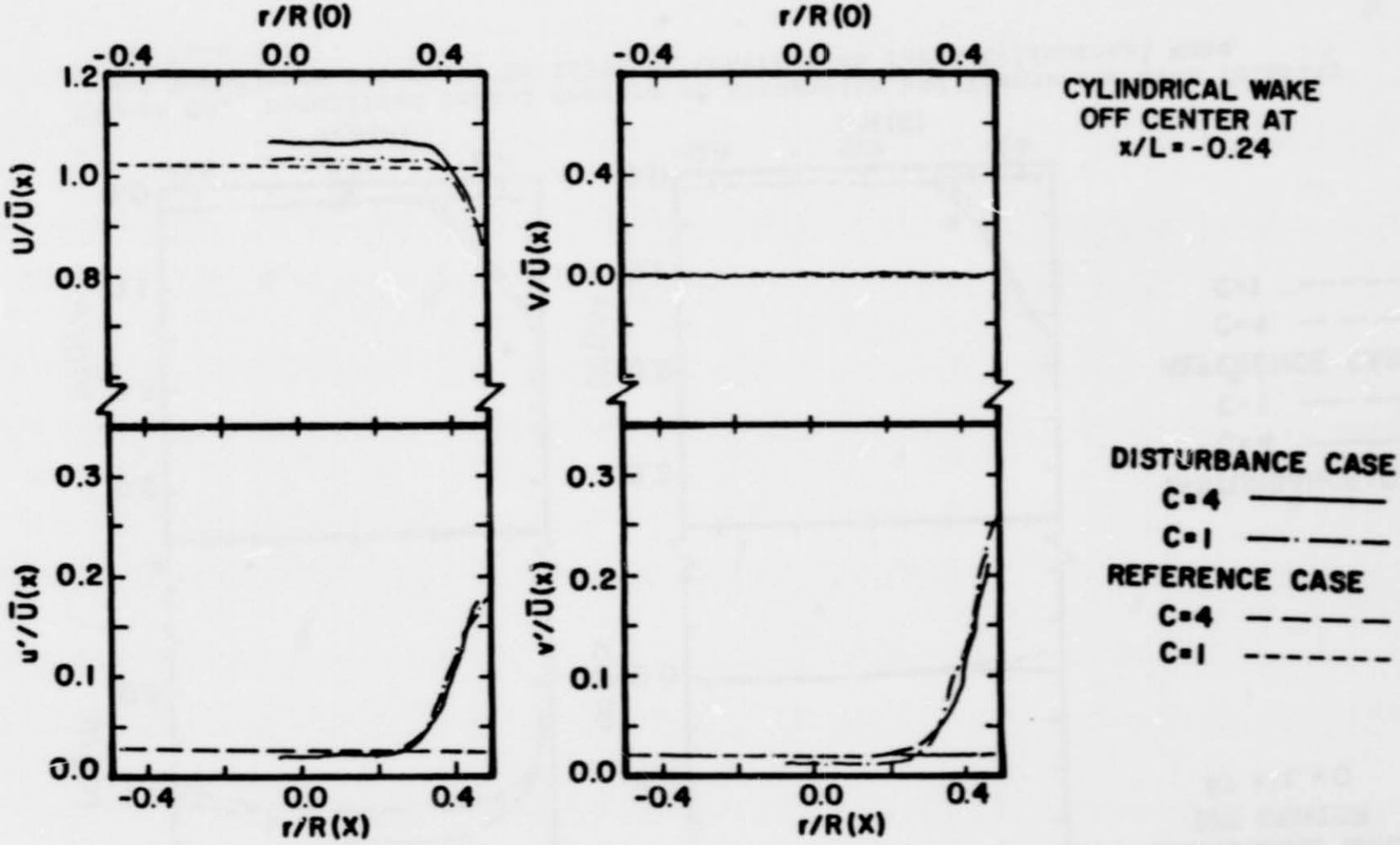

Figure 58. Normalized Radial Surveys of Streamwise and Transverse Mean Velocity and Turbulence Intensity Upstream of Contraction for a Cylindrical Wake off Axis

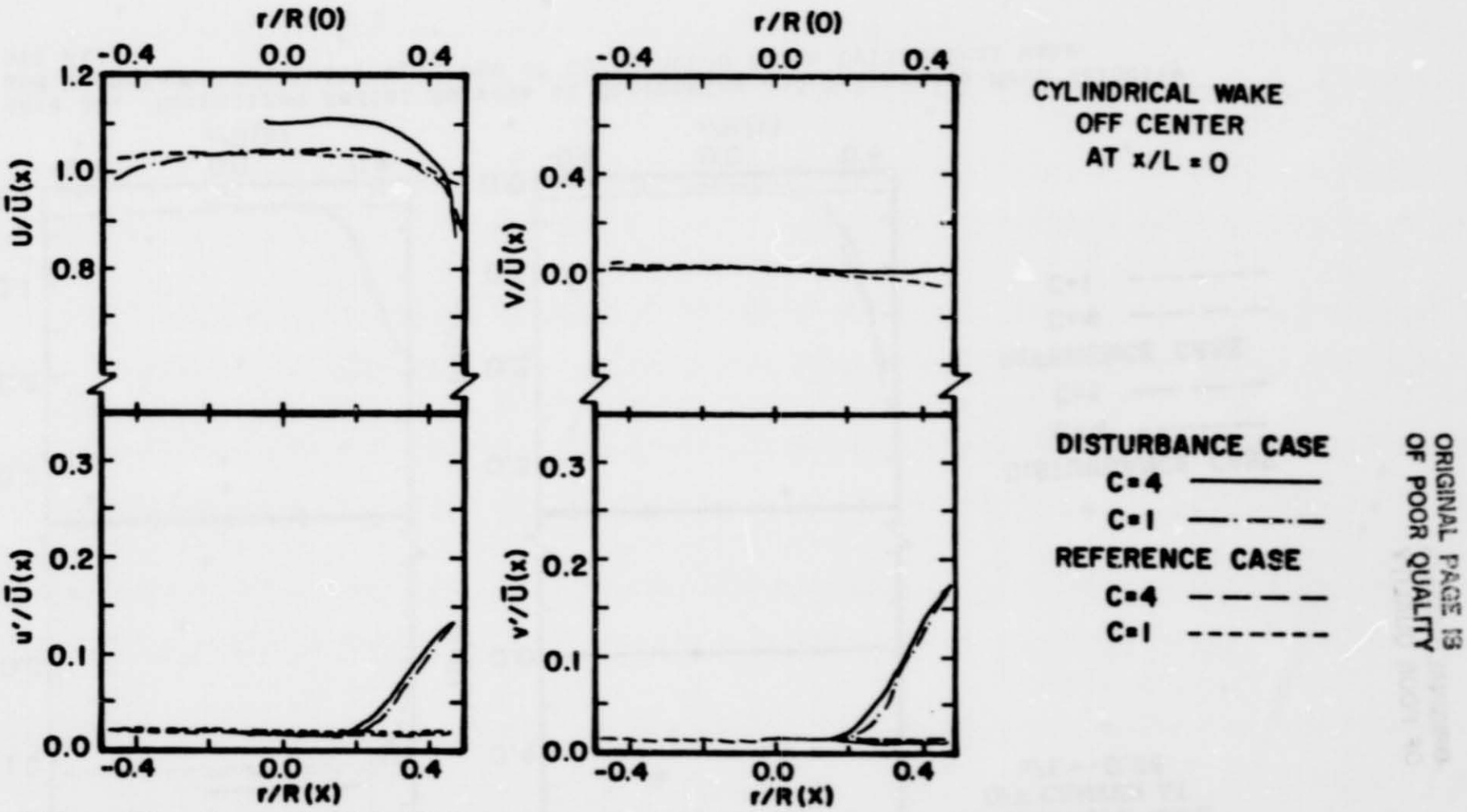

Figure 59. Normalized Radial Surveys of Streamwise and Transverse Mean Velocity and Turbulence Intensity At Inlet of Contraction for a Cylindrical Wake off Axis

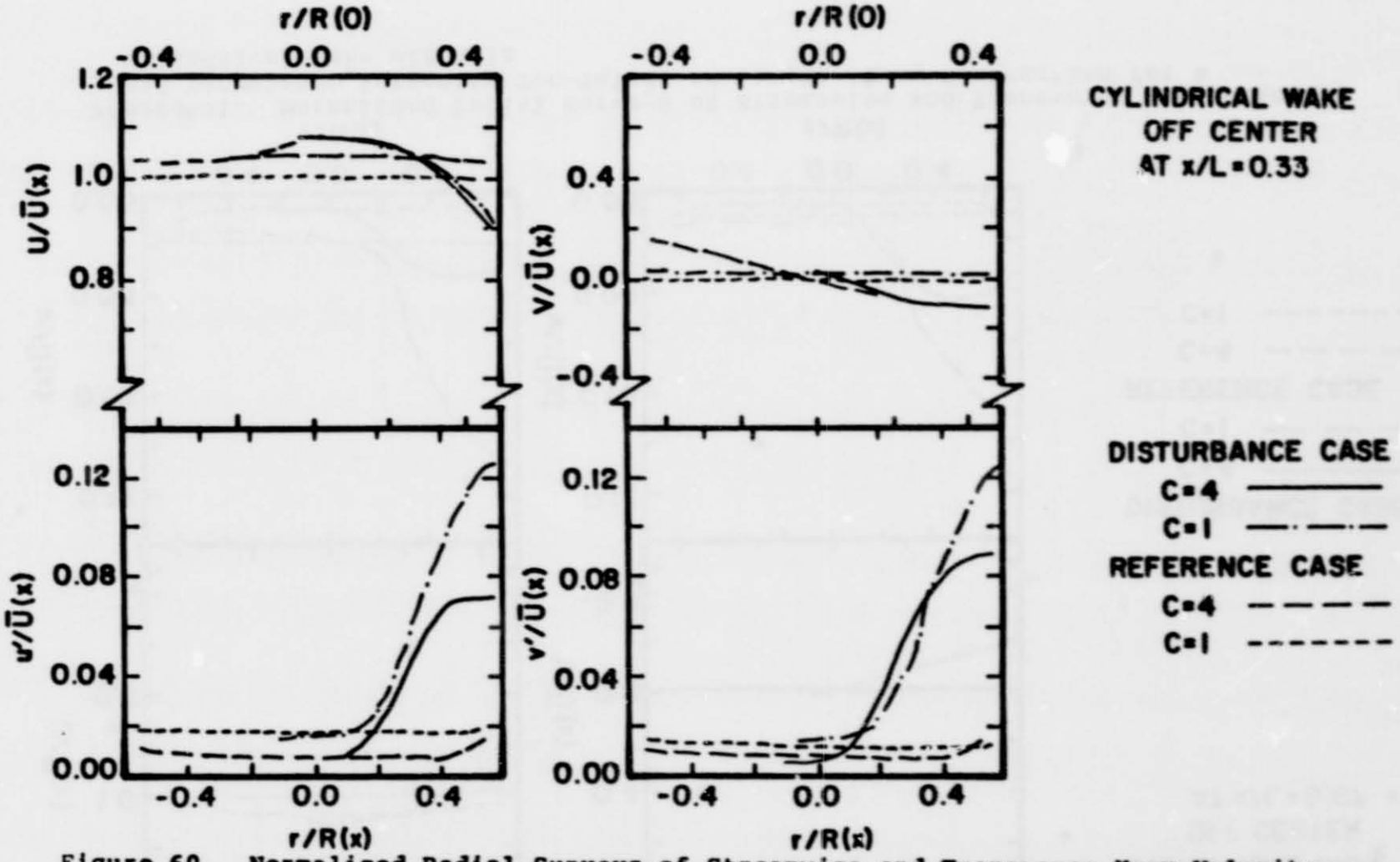

Figure 60. Normalized Radial Surveys of Streamwise and Transverse Mean Velocity and Turbulence Intensity One-Thirds of Length Along Contraction for a Cylindrical Wake off Axis

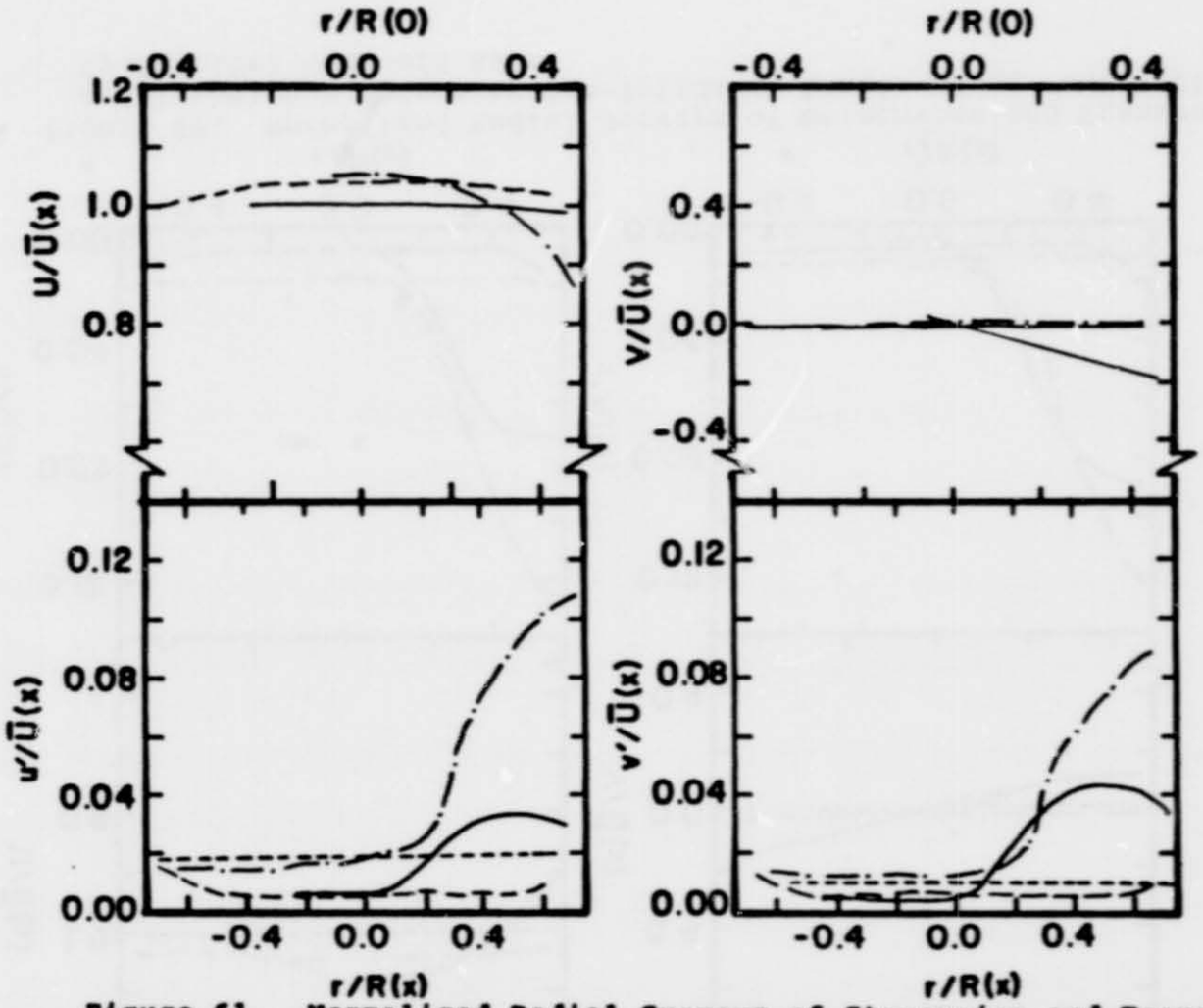

CYLINDRICAL WAKE
OFF CENTER
AT x/L = 0.67

DISTURBANCE CASE
C=4 ———
C=1 —·—·—

REFERENCE CASE
C=4 — — — —
C=1 - - - - - - -

Figure 61. Normalized Radial Surveys of Streamwise and Transverse Mean Velocity and Turbulence Intensity Two-Thirds of Length Along Contraction for a Cylindrical Wake off Axis

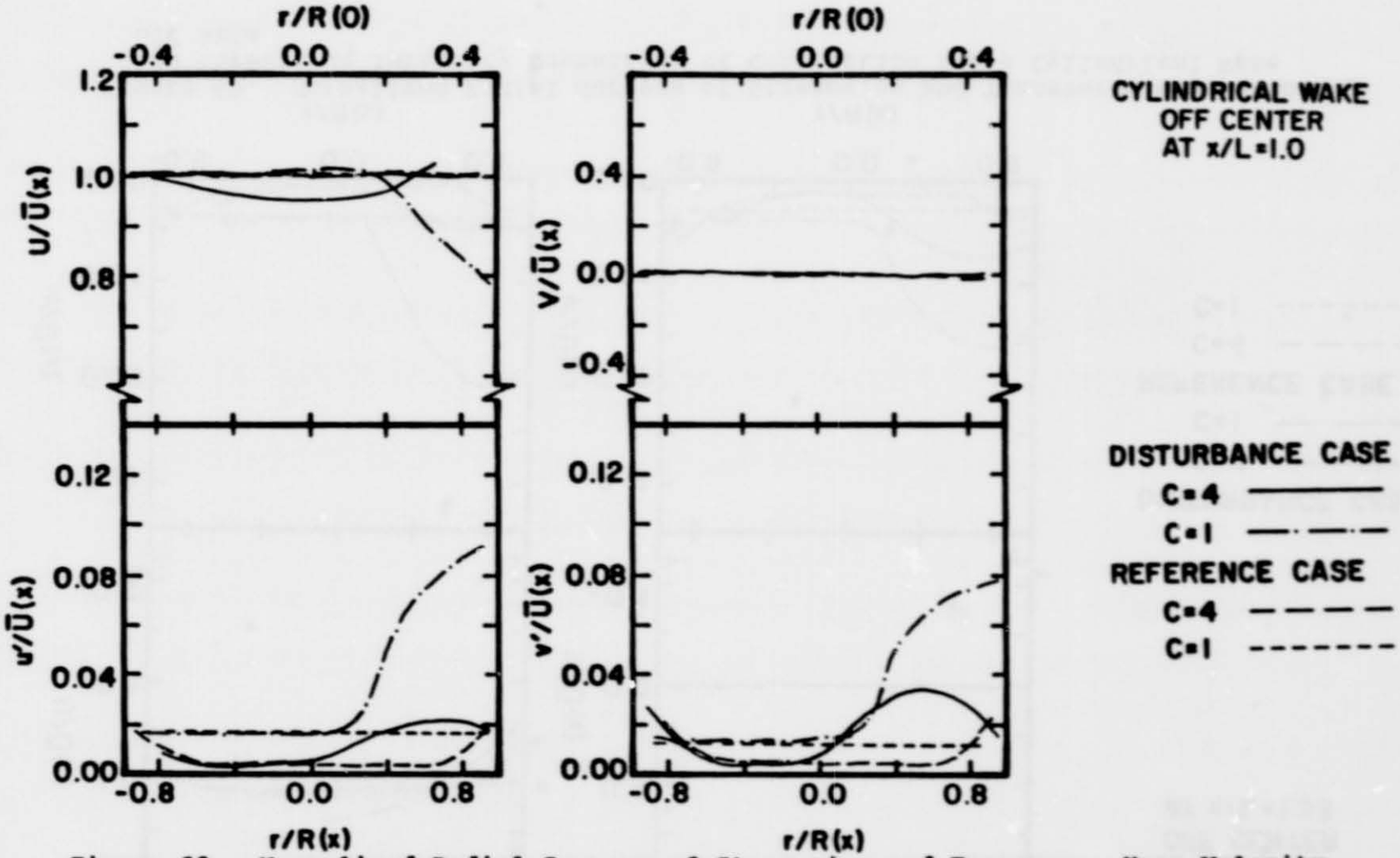

Figure 62. Normalized Radial Surveys of Streamwise and Transverse Mean Velocity and Turbulence Intensity At Exit of Contraction for a Cylindrical Wake off Axis

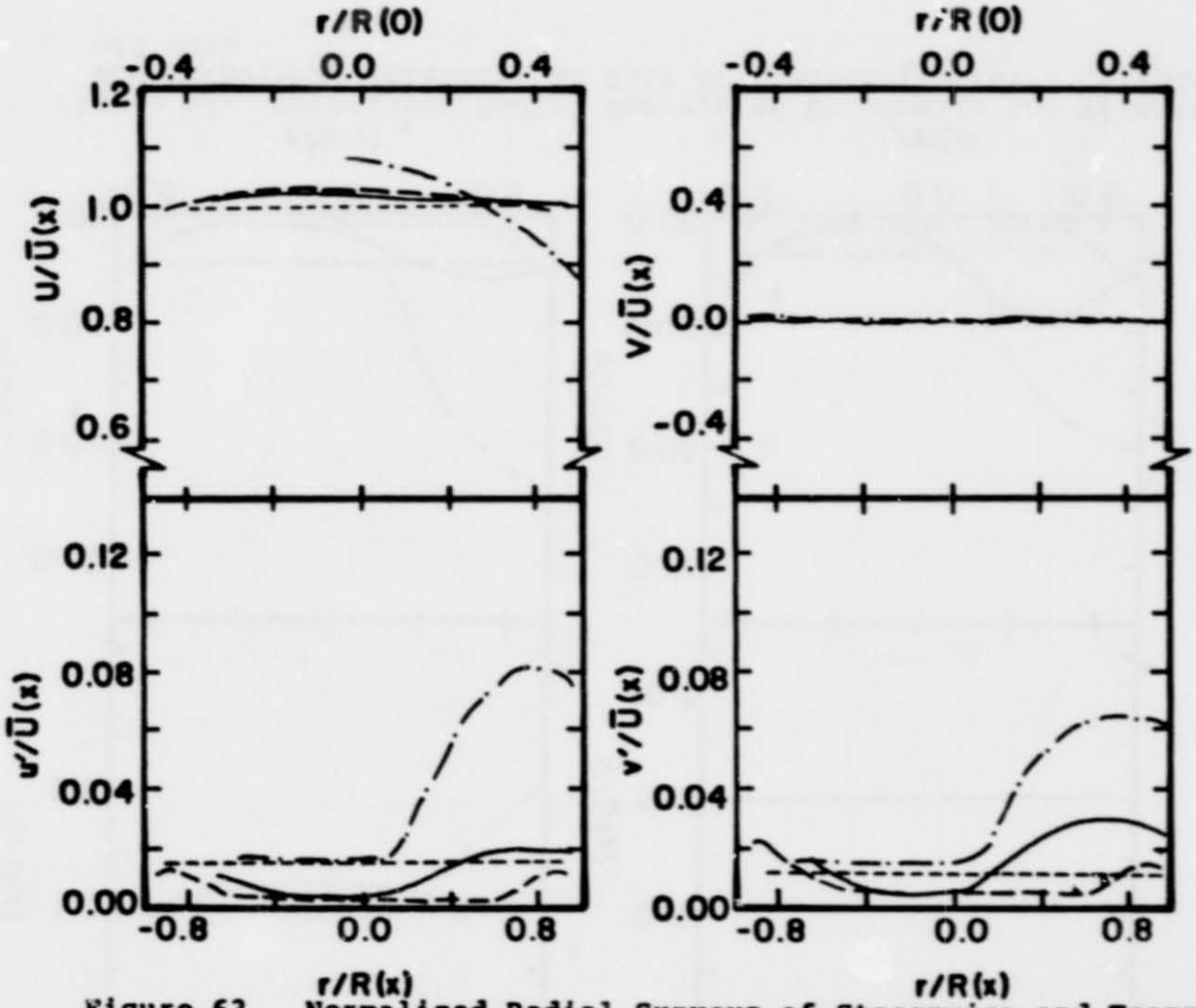

CYLINDRICAL WAKE
OFF CENTER
AT x/L = 1.33

DISTURBANCE CASE
C = 4
C = 1

REFERENCE CASE
C = 4
C = 1

Figure 63. Normalized Radial Surveys of Streamwise and Transverse Mean Velocity and Turbulence Intensity Downstream of Contraction for a Cylindrical Wake off Axis

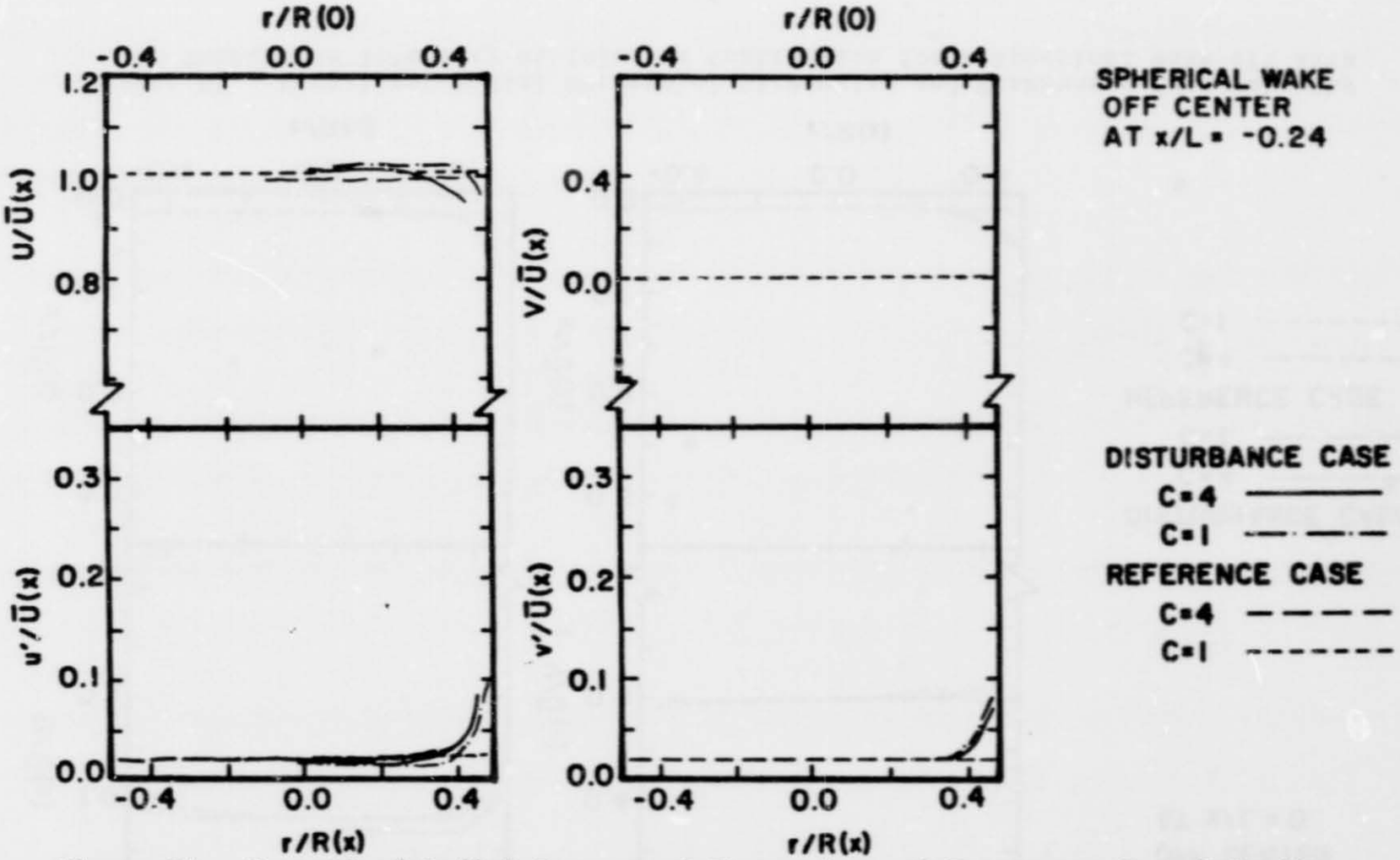

Figure 64. Normalized Radial Surveys of Streamwise and Transverse Mean Velocity and Turbulence Intensity at Upstream of Contraction for a Spherical Wake off Axis

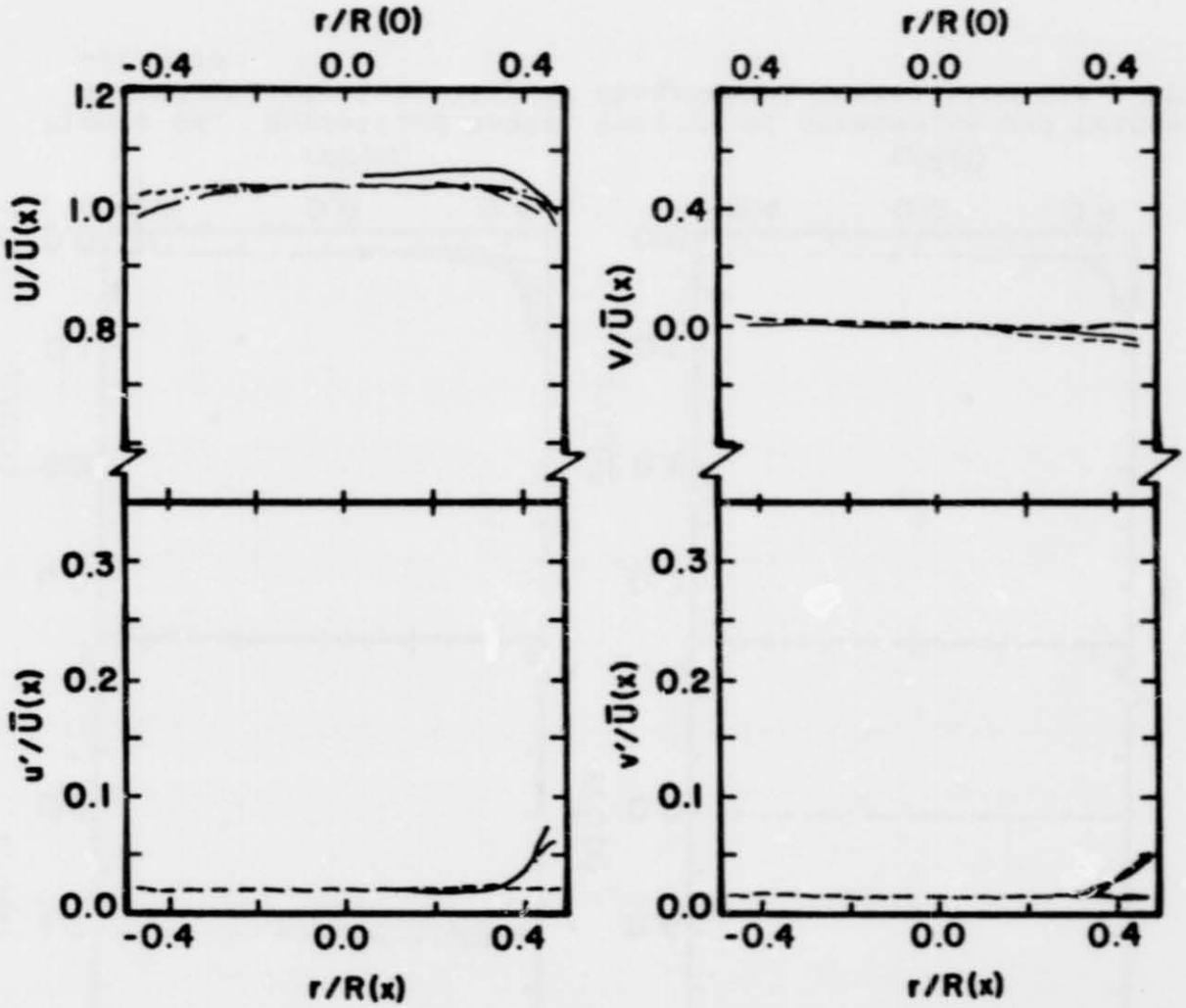

Figure 65. Normalized Radial Surveys of Streamwise and Transverse Mean Velocity and Turbulence Intensity at Inlet of Contraction for a Spherical Wake off Axis

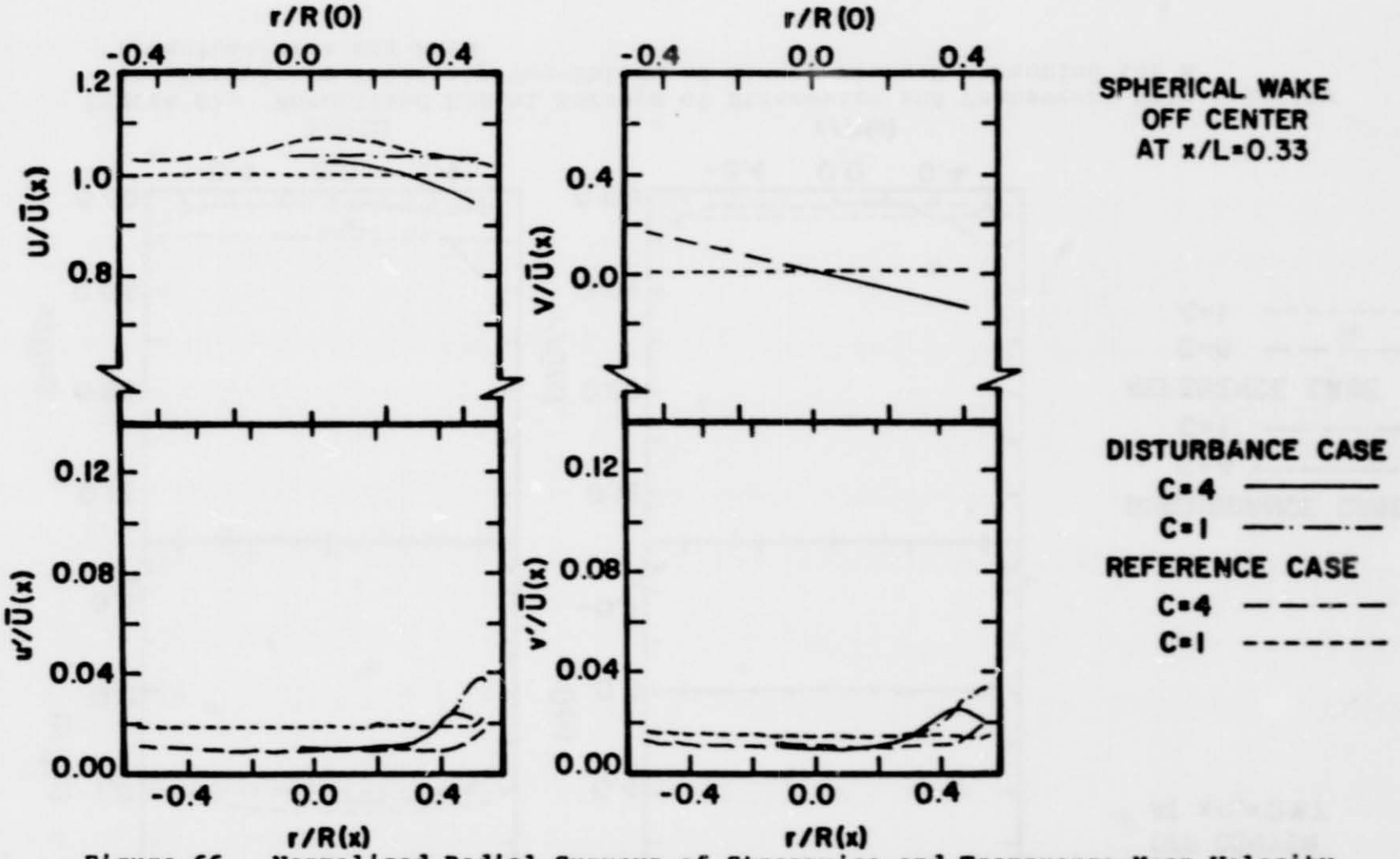

Figure 66. Normalized Radial Surveys of Streamwise and Transverse Mean Velocity and Turbulence Intensity One-Third of Length Along Contraction for a Spherical Wake off Axis

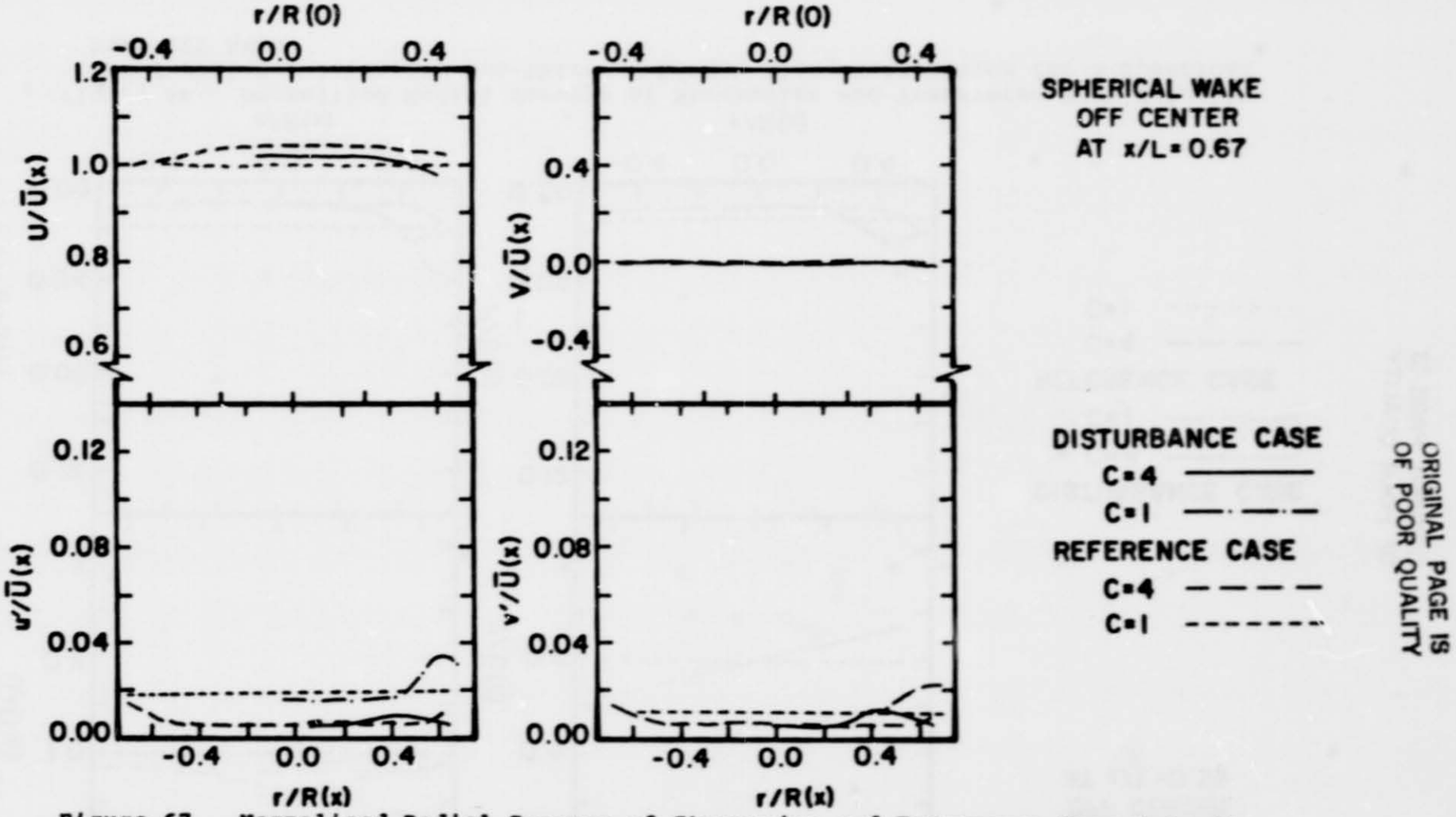

Figure 67. Normalized Radial Surveys of Streamwise and Transverse Mean Velocity and Turbulence Intensity Two-Thirds of Length Along Contraction for a Spherical Wake off Axis

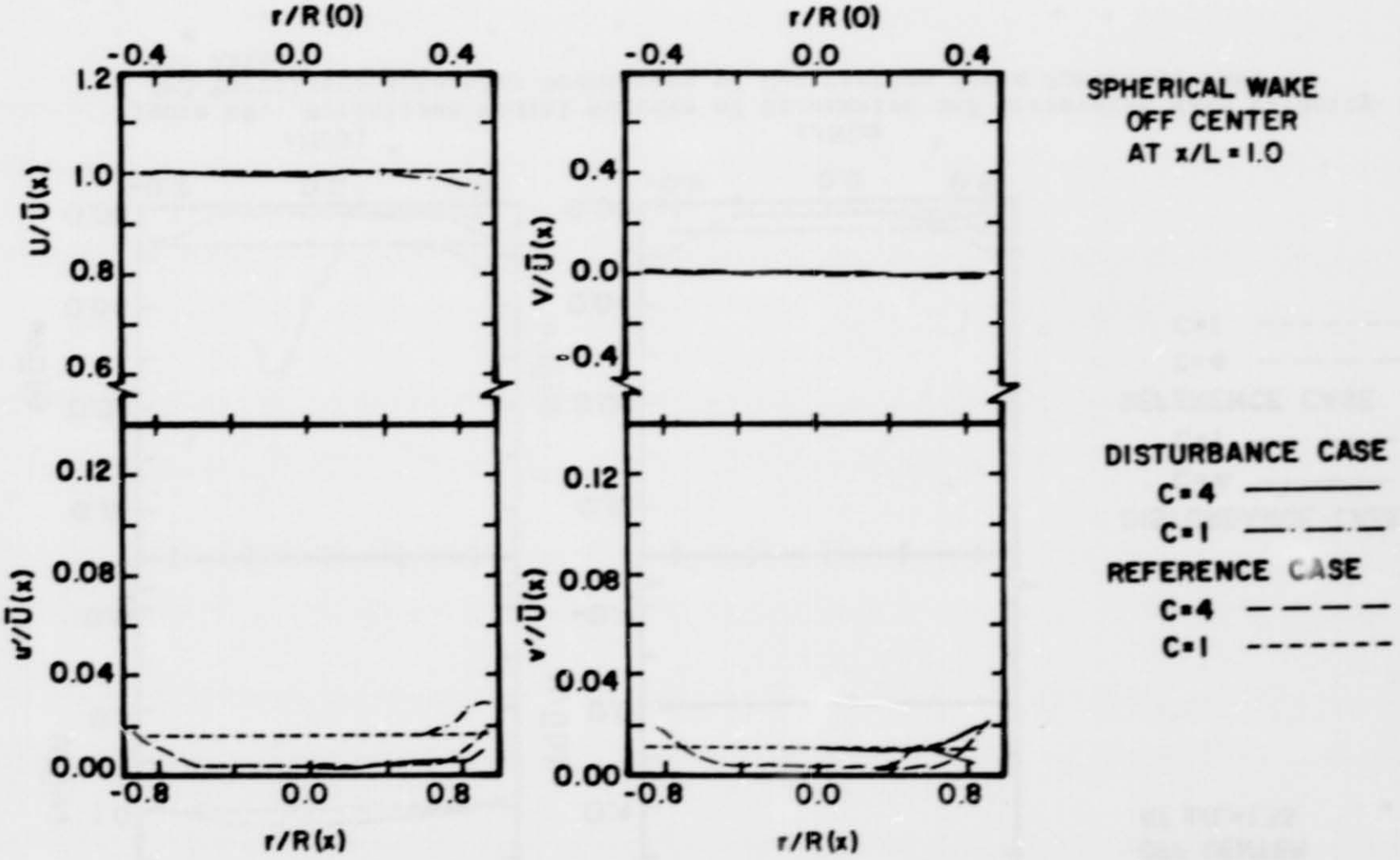

Figure 68. Normalized Radial Surveys of Streamwise and Transverse Mean Velocity and Turbulence Intensity At Exit of Contraction for a Spherical Wake off Axis

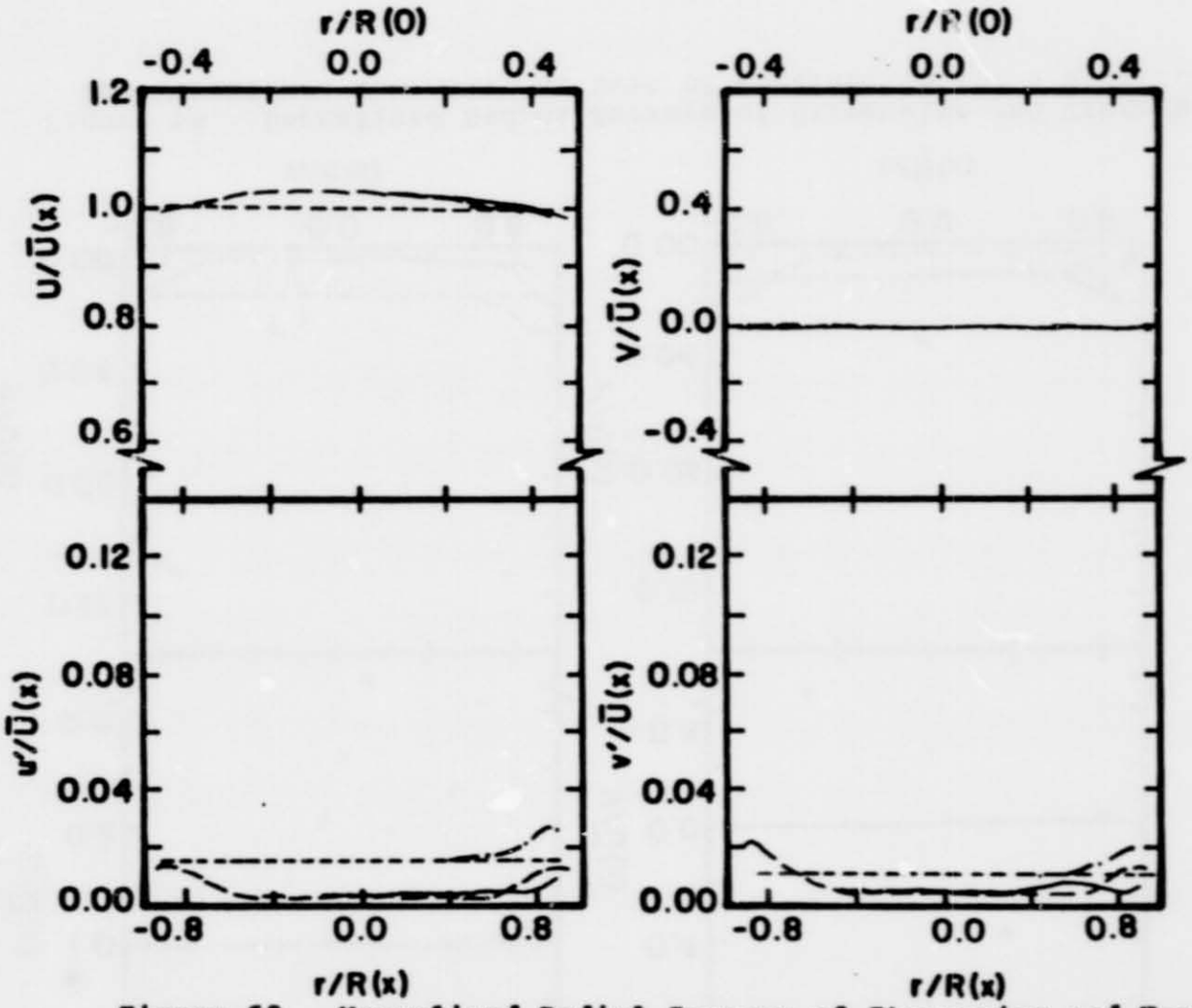

SPHERICAL WAKE
OFF CENTER
AT x/L = 1.33

DISTURBANCE CASE
C = 4
C = 1
REFERENCE CASE
C = 4
C = 1

Figure 69. Normalized Radial Surveys of Streamwise and Transverse Mean Velocity and Turbulence Intensity Downstream of Contraction for a Spherical Wake off Axis

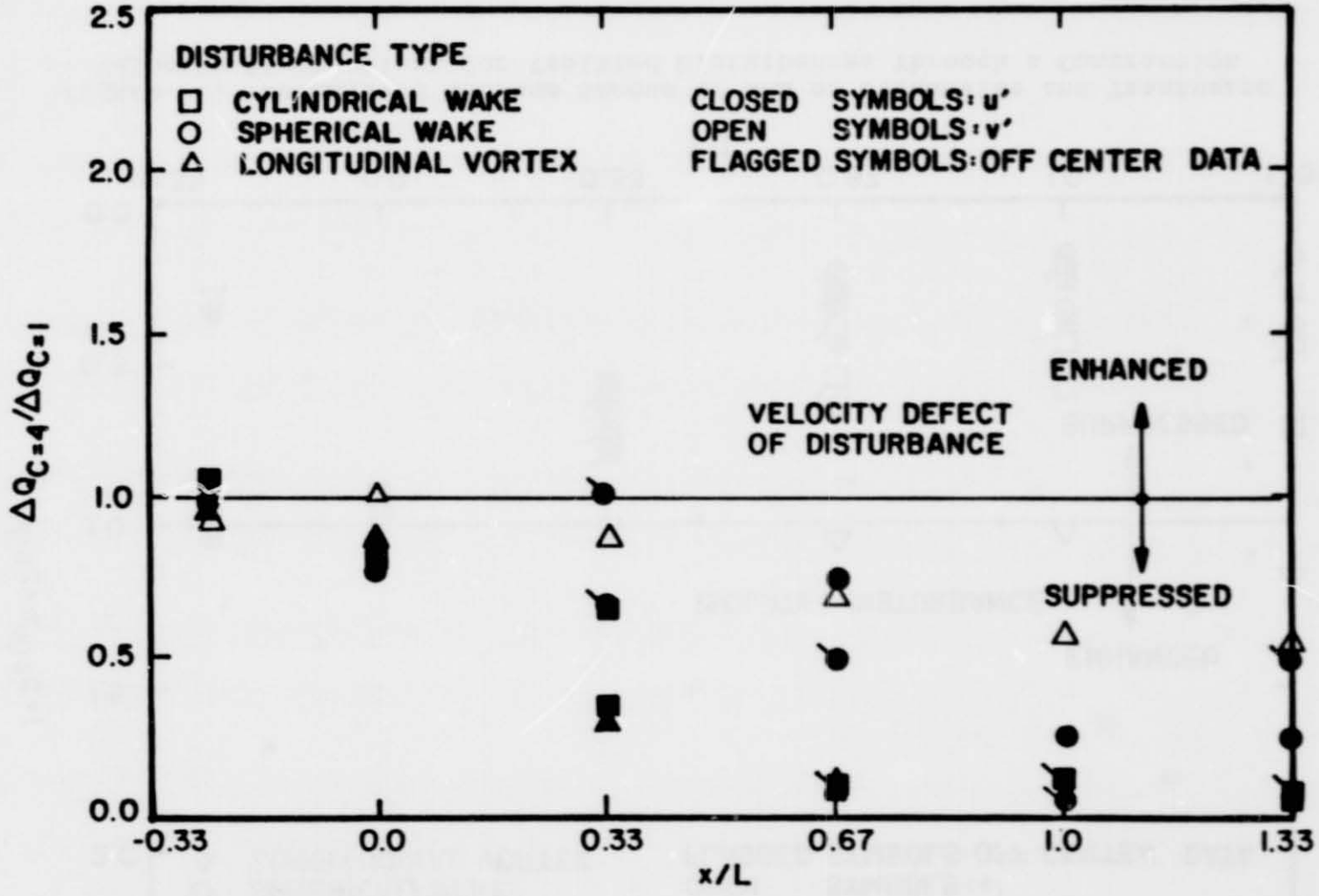

Figure 70. Normalized Mean Streamwise and Transverse Velocity Deficits for Isolated Disturbances Through a Contraction

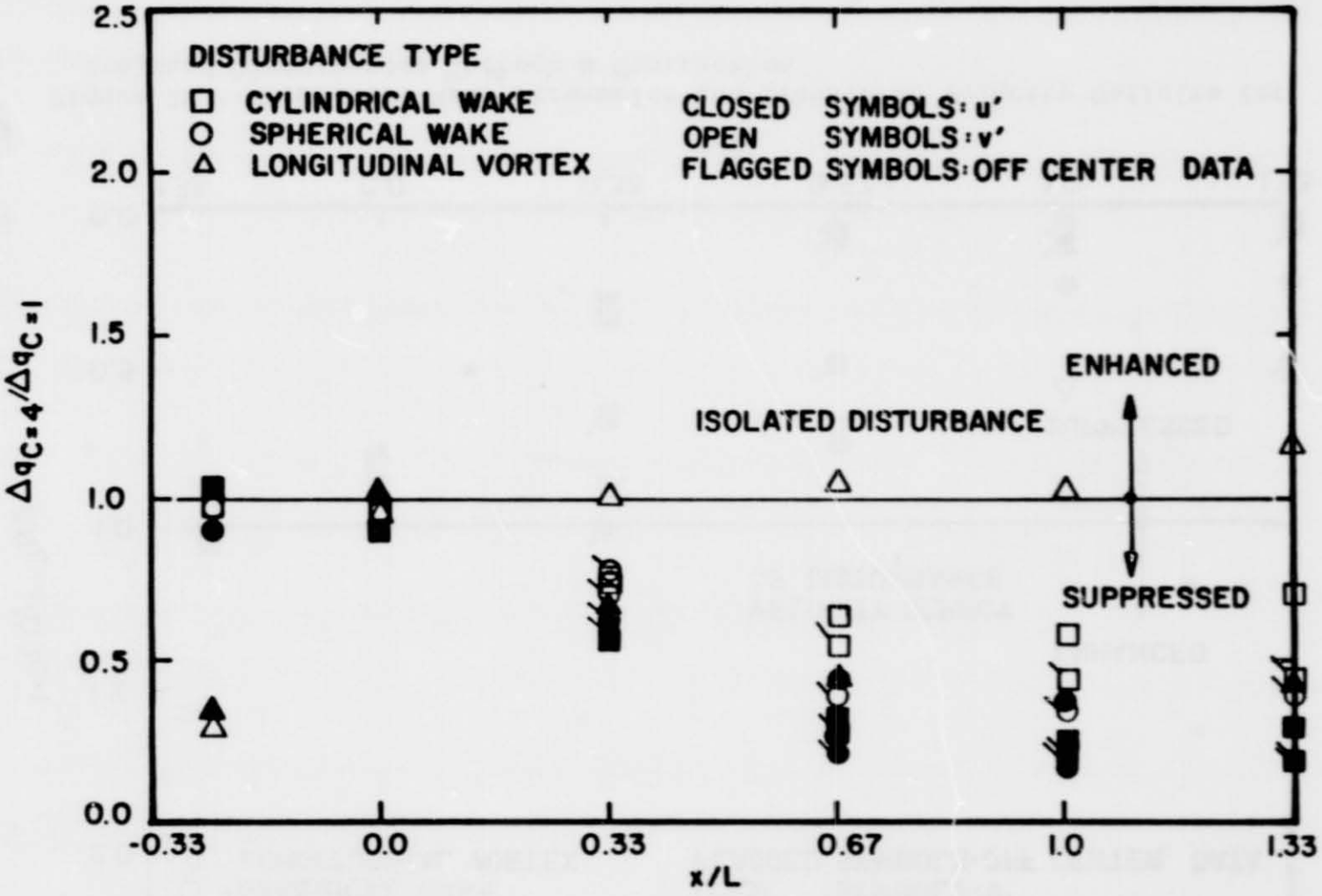

Figure 71. Normalized Maximum Excess of RMS of Streamwise and Transverse Velocity Fluctuations for Isolated Disturbances Through a Contraction

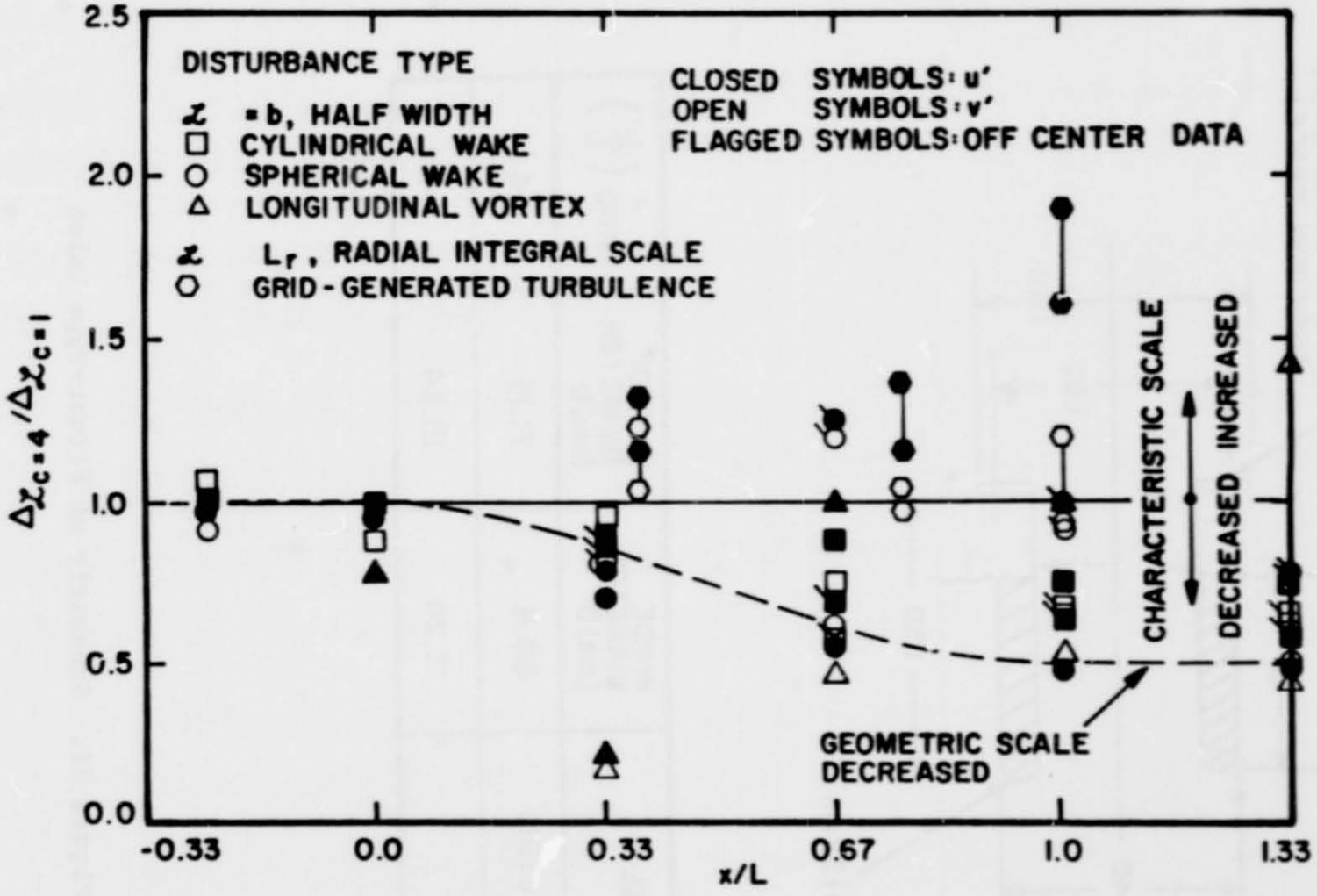

Figure 72. Normalized Characteristic Length Scales Based on Streamwise and Transverse Velocity Fluctuations

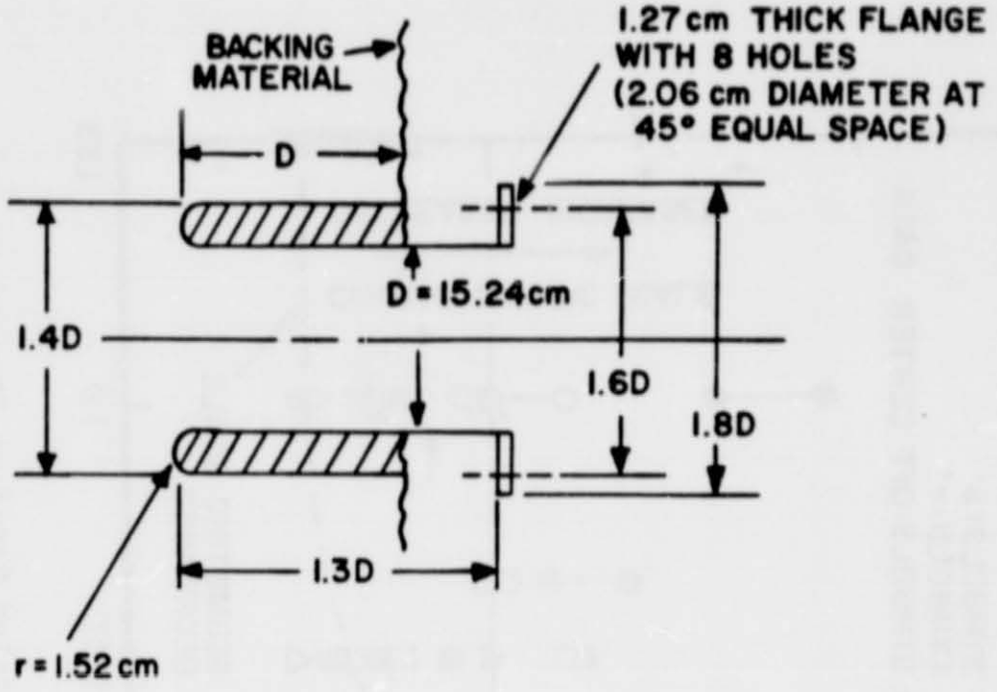

MODEL	INSIDE DIAMETER (cm) D	OUTSIDE DIAMETER (cm) D'	RATIO $\left(\frac{D'}{D}\right)$
NASA-JTDI5	50.8	71.12	1.4
IIT-F_o	15.24	21.34	1.4

Figure 73. Schematic of Flight-Type Inlet

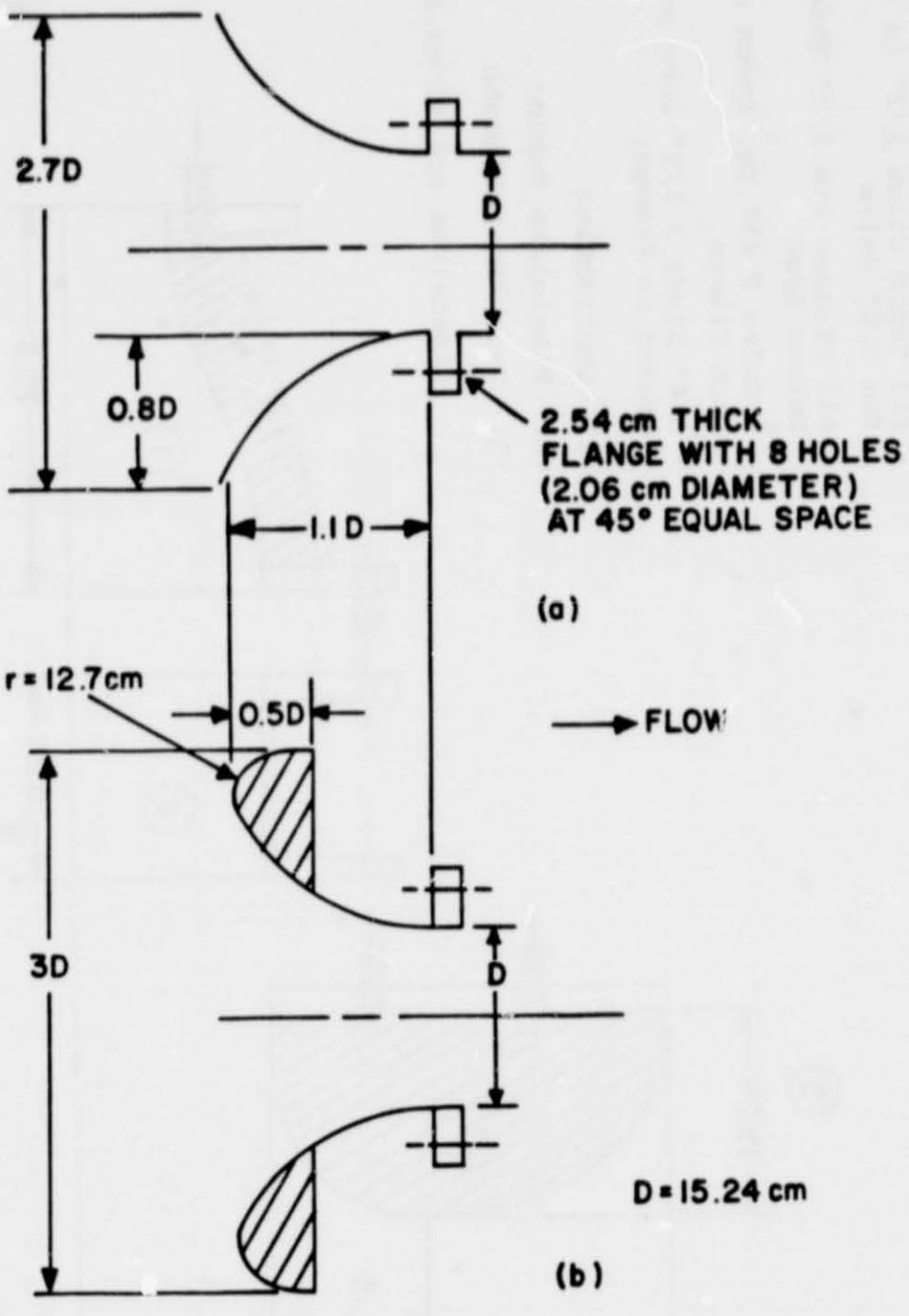

Figure 74. Schematic of Small Bellmouth-Type Inlet With (a) Sharp Edge, and (b) Smooth Edge

- All Holes D = 13/16"
- All Taped Holes 1/2" in Dia. for 3/4" Bolts
- All Flanges are 1/2" Thick Unless Spec.
- 8 Holes @ 45° Eq. Space on Each Flange
- 3/4" Studs 2 1/2" Long are Gluded on Flanges

(1) Contraction

(2) Plexiglass Tubing

(3) Type "D" Bellmouth

Dimensions are given in cm.

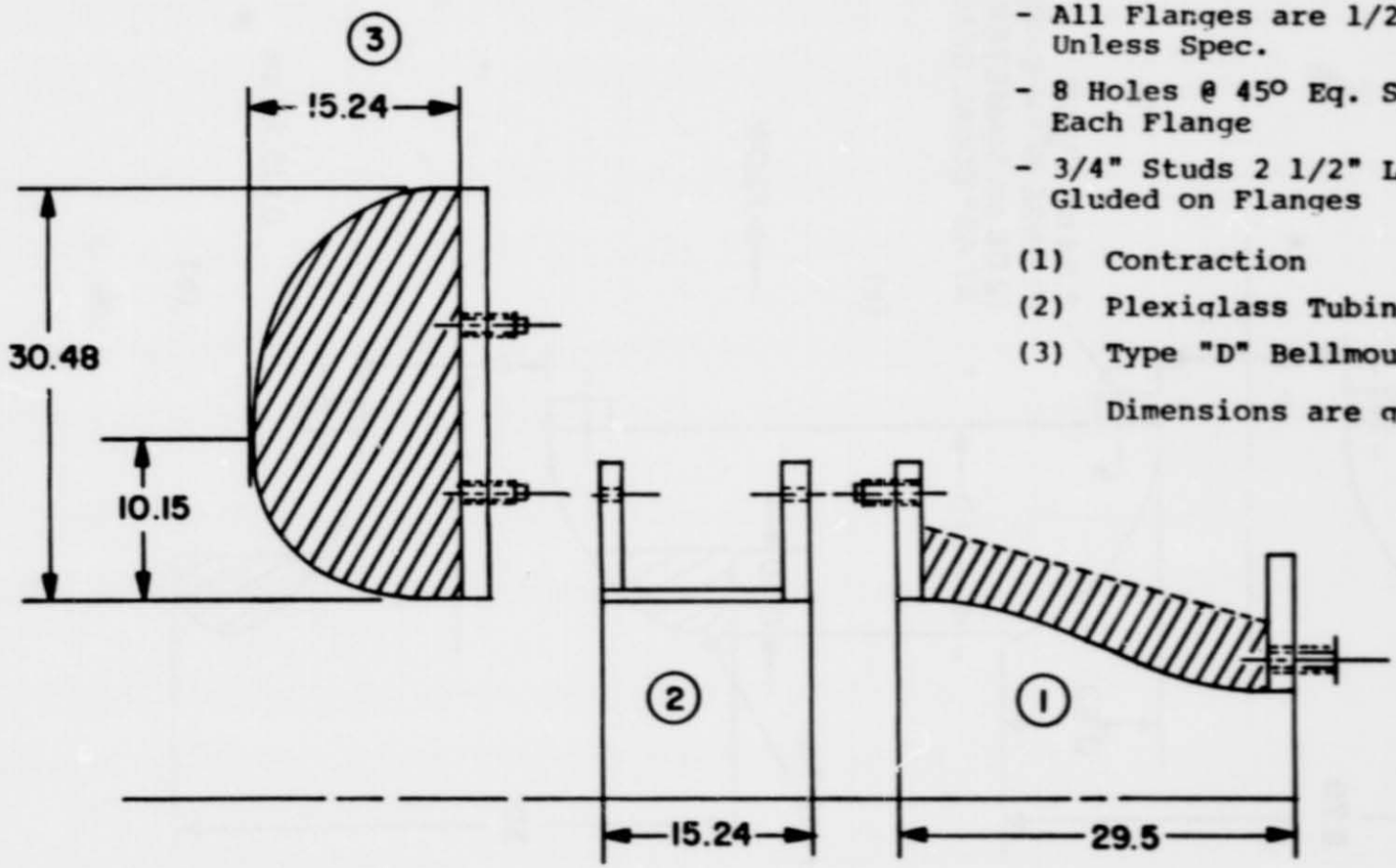

Figure 75. Parts of Large Bellmouth-Type Inlet

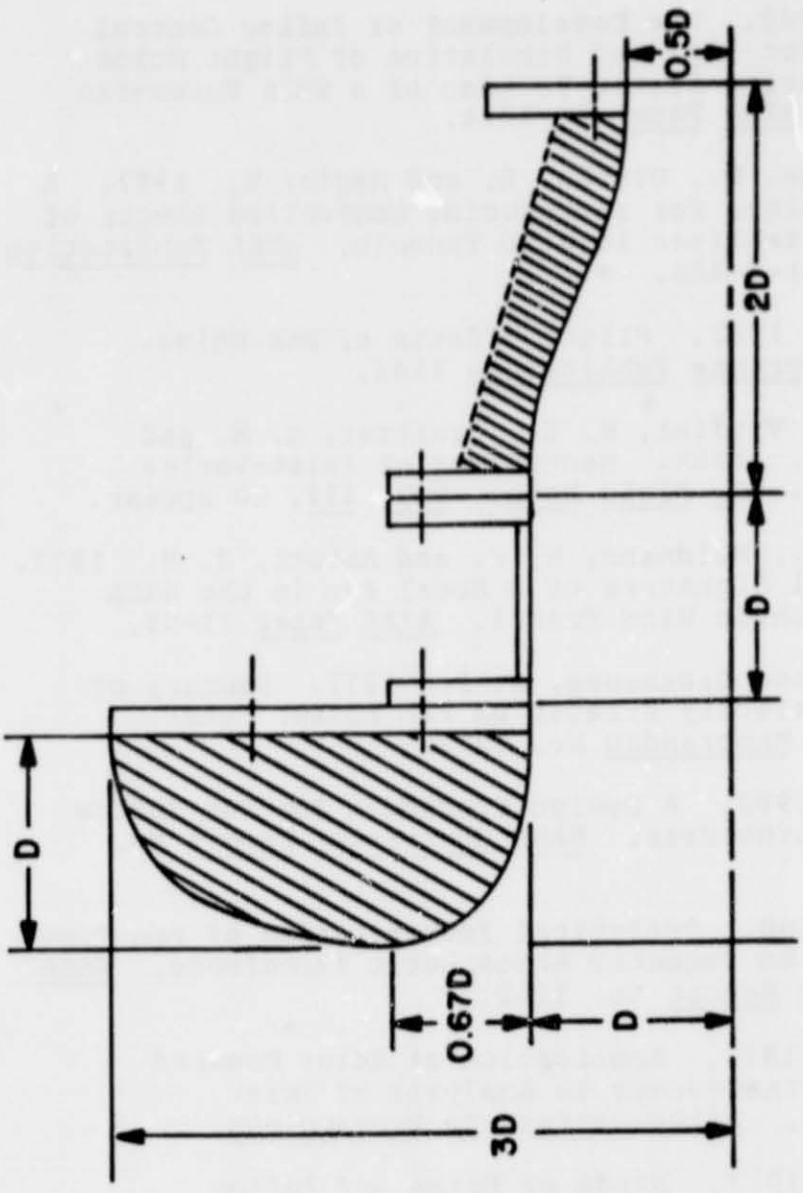

Figure 76. Large Bellmouth-Type Inlet Assembly

BIBLIOGRAPHY

Ahmed, M. A., Wigeland, R. A. and Nagib, H. M. 1976. Generation an Management of Swirling Flows in Confined Streams. IIT Fluids & Heat Transfer Report R76-2.

Atvars, Y. 1980. The Development of Inflow Control Devices for Improved Simulation of Flight Noise Levels during Static Testing of a HBPR Turbo-fan Engine. AIAA Paper 80-1024.

Corke, T., Koga, D., Drubka, R. and Nagib, H. 1977. A New Technique for Introducing Controlled Sheets of Smoke Streaklines in Wind Tunnels. IEEE Publication 77-Ch-1251-8-AES.

Chestnutt, D. 1982. Flight Effects of Fan Noise. NASA Conference Publication 2242.

De Siervi, F., Viguier, H. C., Greitzer, E. M. and Tan, C. S. 1982. Mechanisms of Inlet-Vortex Formation. J. Fluid Mech., Vol. 122, to appear.

Dietrich, D. A., Heidmann, M. F. and Abbott, J. M. 1977. Acoustical Signature of a Model Fan in the NASA Lewis Anechoic Wind Tunnel. AIAA Paper 77-59.

Feiler, C. E. and Groeneweg, J. F. 1977. Summary of Forward Velocity Effects on Fan Noise. NASA Technical Memorandum No. 73722.

Gedge, M. R. 1980. A Design Procedure for Fan Inflow Control Structures. NASA Contractor Report No. 165625.

Ganz, U. W. 1980. Analytical Investigation of Fan Tone Noise Due to Ingested Atmospheric Turbulence. NASA Contractor Report No. 3302.

Hanson, D. B. 1980. Application of Rotor Mounted Pressure Transducers to Analysis of Inlet Turbulence. AGARD Conference Proceedings.

Hanson, D. B. 1977. Study of Noise and Inflow Distortion Sources in the NASA QF-1B Fan Using Measured Blade and Vane Pressures. NASA Contractor Report No. CR-2899.

Kantola, R. A. and Warren R. E. 1979. Reduction of Rotor-Turbulence Interaction Noise in Static Fan Noise Testing. AIAA Paper 79-0656.

Loehrke, R. I. and Nagib, H. M. 1972. Experiments on Management of Free Stream Turbulence. AGARD Report No. 598, AD-749-891.

Loehrke, R. I. and Nagib, H. M. 1976. Control of Free-Stream Turbulence by Means of Honeycombs: A Balance Between Suppression and Generation. J. Fluid Eng., Vol. 98, pp. 342-353.

Marion, A. 1982. On the Design of Contractions and Settling Chambers for Optimal Turbulence Manipulation in Wind Tunnels. M.S. Thesis, Department of Mechanics and Mechanical and Aerospace Engineering, Illinois Institute of Technology.

Marion-Moulin, C. 1982. Interpretation of Two-Probe Turbulence Measurements in An Axisymmetric Contraction. M.S. Thesis, Department of Mechanics and Mechanical and Aerospace Engineering, Illinois Institute of Technology.

Mc Ardle, J. G., Jones, W. L., Heidelberg, L. J. and Homyak, L. 1980. Comparison of Several Inflow Control Devices for Flight Simulation of Fan Ton Noise Using a JT15D-1 Engine. AIAA Paper 81-1025.

Peracchio, A. A., Pratt, and Whitney. 1981. Assessment of Inflow Control Structure Effectiveness and Design System Development. AIAA Paper 81-2048.

Rogers, D. F., Pratt, and Whitney. 1980. Aerodynamics Assessment of Methods to Simulate Flight Inflow Characteristics During Static Engine Testing. AIAA Paper 80-1023.

Shaw, L. M., Woodward, R. P., Glaser, F. W. and Pastoli, B. J. 1977. Inlet Turbulence and Fan Noise Measured in an Anechoic Wind Tunnel and Statically with an Inlet Flow Control Device. AIAA Paper 77-1345.

Tan-atichat, J. 1980. Effects of Axisymmetric Contractions on Turbulence of Various Scales. Ph.D Thesis, Department of Mechanics and Mechanical and Aerospace Engineering, Illinois Institute of Technology. (Also available as NASA Contractor Report 165136).

Tan-atichat, J. and Nagib, H. M. 1981. Optimization of Flow Manipulator Placement Ahead of Wind-Tunnel Contractions. Interim Report, Illinois Institute of Technology.

Tan-atichat, J., Nagib, H. M. and Loehrke, R. I. 1982. Interaction of Free Stream Turbulence With Screen and Perforated Plates: A Balance Between Turbulent Scales. J. Fluid Mech., Vol. 114, pp. 501-528.

Wigeland, R. A., Ahmed, M. and Nagib, A. M. 1978. Vorticity measurements Using Calibrated Vane-Vorticity Indicators and Cross-Wires. AIAA Journal, Vol. 16, No. 12.

Wigeland, R. A., Tan-atichat, J. and Nagib, H. M. 1979. Evaluation of a New Concept for Reducing Free-Stream Turbulence in Wind Tunnels, NASA Contractor Report No. 3196.